(1)

CYCLIC CRACK GROWTH EMANATING AT A ROUND NOTCH CONSIDERING VISCOPLASTICITY

THESIS

Gary L. Chestnut
Captain, USAF

AFIT/GAE/AA/87D-3

DEPARTMENT OF THE AIR FORCE
AIR UNIVERSITY
AIR FORCE INSTITUTE OF TECHNOLOGY
Wright-Patterson Air Force Base, Ohio

AFIT/GAE/AA/87D-3

CYCLIC CRACK GROWTH EMANATING AT A ROUND NOTCH CONSIDERING VISCOPLASTICITY

THESIS

Gary L. Chestnut
Captain, USAF

AFIT/GAE/AA/87D-3

AFIT/GAE/AA/87D-3

CYCLIC CRACK GROWTH EMANATING AT A ROUND NOTCH CONSIDERING VISCOPLASTICITY

THESIS

Presented to the Faculty of the School of Engineering

of the Air Force Institute of Technology

Air University

In Partial Fulfillment of the

Requirements for the Degree of

Master of Science in Aeronautical Engineering

Gary L. Chestnut, B.S.

Captain, USAF

December 1987

Contents

Acknowledgements

I wish to express my gratitude to Dr. A.N. Palazotto for his guidance during this research project. Thanks also go to Dr. T. Nicholas of the Air Force Materials Laboratory for sponsoring this research and Major Joe G. Mercer of Headquarters Air Force Systems Command for providing many helpful suggestions needed to carry out my analysis.

Most of all, I wish to thank my wife, Jan, for her immeasurable support and encouragement during the many long hours required to complete this research project.

Gary L. Chestnut

List of Symbols

$(\dot{})$	Time rate of change
A	Crack length measured from load point for compact tension specimen
A_n	Notch location measured from load point
a	Crack length measured from notch
B	Specimen thickness
[B]	Strain displacement matrix
[D]	Elastic material property matrix
D_o	Bodner material constant
D_2^P	Second invariant of plastic strain rate
E	Elastic modulus
$\{I\}$	Internal force vector
J	J-integral value
J_2	Second invariant of the deviatoric stress
[K]	Elastic stiffness matrix
K_I	Elastic stress intensity
K_{close}	Stress intensity at closure load
K_{max}	Maximum stress intensity
K_{min}	Minimum stress intensity
k_ϵ	Elastic stress concentration factor
k	Strain concentration factor
m	Bodner material constant
n	Bodner material constant
P	Applied load
P_{close}	Load at closure

List of Symbols (Cont'd)

P_{max}	Maximum load
P_{open}	Load at reopening
R	Minimum to maximum load ratio
r	Bodner material constant/Radius of notch
S_{ij}	Deviatoric stress tensor
T_i	Applied surface traction
$\{T\}$	Vector of applied forces
U_i, $\{U\}$	Displacement vector
W	Specimen width/Strain energy density
W_p	Plastic strain energy density
Z	Bodner model state variable
Z_0, Z_1, Z_2	Bodner model constants
$\Delta\epsilon_y$	Crack tip strain range
ΔK	Stress intensity range
ΔK_{eff}	Effective stress intensity range
a	Ratio of crack length to specimen width (A/W)
Γ	J-integral contour path
ϵ_{ij}	Components of total strain
ϵ^e_{ij}	Elastic component of total strain
ϵ^p_{ij}	Plastic component of total strain
ϵ_y	y component of strain
λ	Scalar constant
σ_{ij}	Components of stress tensor
σ_n	Nominal stress
σ_y	y component of stress

List of Figures

List of Figures (Cont'd)

List of Figures (Cont'd)

List of Figures (Cont'd)

Abstract

A finite element investigation was conducted to analyze a crack growing from a round (large radius) notch under cyclic conditions at 1200°F. The results of the finite element analysis were compared to previously published results obtained for a crack emanating from a blunt notch and a single-edge-cracked specimen.

The finite element program used was a two-dimensional materially and geometrically nonlinear finite element code called SNAP. The program has the capability to release fixed nodes to allow crack growth and the ability to simulate crack closure under cyclic conditions. Constitutive equations set forth by Bodner and Partom were used to account for the nonlinear, viscoplastic material behavior exhibited by IN-718 at 1200°F. The load spectrum included loading under a positive load range (R = 0.1) and loading under a negative load range (R = -1.0).

Finite element analysis of a crack growing from a round notch under cyclic loading provided crack opening profile information, opening, and closing loads, stress and strain profiles and plastic zone estimations.

Crack closure develops over a longer distance for the round notch than that for a blunt notch. The elastic stress intensity influence on the round notch was found to be within one radius of the notch. In general, the crack growth trends observed for the round notch agree with those seen in the blunt notch and single-edge-crack specimen.

I. Introduction

Background

Aircraft engine components and structures often operate under conditions severe enough that the designer must ensure that the component or structure has an adequate fatigue life. The United States Air Force has taken steps to ensure that fatigue resistance is considered a primary design criterion by developing the Engine Structural Integrity Program (ENSIP). This program provides an organized approach to the design, analysis, and verification testing of all newly developed aircraft engines (1).

The ENSIP assumes that flaws exist and may be found by means of inspection or by crack growth analysis if the flaw is undetectable by nondestructive inspection (NDI) techniques. This is by no means straightforward, since crack growth analysis comprises both crack initiation as well as crack propagation. For simple geometries, linear elastic fracture mechanics (LEFM) provide a good estimate of remaining useful component life. However, for components in the latter stages of the compressor and turbine, temperatures may reach 1400°F. Thus, crack propagation will be influenced by the superposition of high temperatures and stresses and LEFM crack growth analysis will not provide accurate engine component life determination.

Most fatigue failures originate at some kind of stress concentration or notch. At the roots of notches the stress may exceed the yield stress of the material. The growth of

small cracks (small compared to the notch dimensions) in such regions will be controlled by local notch plasticity. When the crack is propagating in the notch plastic field it becomes incorrect to use LEFM to characterize crack growth. Thus, elastic-plastic or viscoplastic analysis techniques must be used. This study used the finite element method to evaluate crack growth at a round notch using a viscoplastic constitutive law.

Approach

As previously stated, this research concentrated on a crack emanating from a round notched compact tension specimen. The specimen studied was IN-718, a nickel-based superalloy used in the F-100 engine. SNAP, a nonlinear finite element program developed by Brockman (2) was used for this analysis. This finite element program is a two-dimensional plane stress and plane strain code which includes material and geometric nonlinearities. For this study, eight-noded quadratic isoparametric elements were used. SNAP has the ability to release fixed nodes to simulate crack growth and also simulate crack closure under cyclic conditions. In addition, a set of constitutive equations called the Bodner-Partom viscoplastic flow law (3) was used to model the material behavior during load increments. Plastic strains were calculated using an implicit technique developed by Brockman (2) and were incorporated into the finite element model by the residual force method.

The primary goal of the study was to analyze a crack growing from a round notch specimen and compare these results to those obtained for a blunt notch (4) and a single-edge-cracked specimen (5). For comparison to the blunt notch specimen, load was input as a saw-toothed stress-time pattern of constant amplitude with a load ratio of 0.1. Maximum load amplitudes were applied to result in two load levels for which the notch was elastic and plastic. Cyclic load frequency was maintained at 1.0 Hz. For comparison to the single-edge-cracked specimen, the loading was of the same pattern but with a load ratio of -1.0 and for the plastic loading case only.

Literature Review

As stated earlier, the problem of short crack growth at notches is important because most fatigue failures originate at some kind of stress concentration and the period of crack growth through the notch stress field may represent a major part of the total life. Thus, a proper knowledge of short crack growth from notches is essential for accurate predictions of the fatigue life.

Short cracks tend to grow faster than predicted using LEFM principles. Leis (6) observed that LEFM is limited to small scale yielding at the crack tip. The size of the plastic zone is usually much smaller than the crack length. The author found that short cracks have large plastic zones that are generally the same size as the crack length. As a

consequence, the use of LEFM leads to unconservative estimates of the short crack fatigue life. Smith and Miller (7) observed that when a crack emanates from the notch root, it first grows under notch plasticity control and at a decreasing rate because of the falling notch strain field. As the crack reaches the end of the notch plastic zone, it then grows under its own plasticity control.

Several attempts have been made to account for the faster growth of cracks at notches. In general, most provide corrections to the physical crack length to account for the effect of the notch. El Haddad et al. (8) modified the stress intensity range (ΔK) by adding an artificial length, l_o, to the crack length, a:

$$\Delta K = \Delta\sigma / (\pi (a + l_o))^{1/2} \qquad (1.1)$$

where $\Delta\sigma$ is the local stress range. For elastic-plastic solutions, El Haddad et al. (9) proposed using either the J-integral range or a strain-based intensity factor, ΔK_ε, defined as.

$$\Delta K_\varepsilon = E\Delta\varepsilon / (\pi(a + l_o))^{1/2} \qquad (1.2)$$

where E is the elastic modulus, $\Delta\varepsilon$ is the local plastic strain range, and $(a + l_o)$ is the corrected crack length. This formulation gave acceptable results for notched and unnotched geometries.

In recent years, fatigue crack closure, originated by Elber (10), has been used to explain the behavior of cracks growing at notches. Elber found that crack closure occurred

as a consequence of crack tip plasticity. At the tip of a growing fatigue crack, a zone of residual deformation, caused by the plastic zone during increased loading, is left in the wake of the advancing crack tip. When the fatigue load decreases, this residual deformation causes the crack to close. According to this concept, the crack cannot propagate while it is closed. Thus ΔK is replaced by ΔK_{eff} and is defined as:

$$\Delta K_{eff} = K_{max} - K_{cl} \tag{1.3}$$

where K_{max} is the maximum stress intensity and K_{cl} is the stress intensity value for which the crack tip closes (or opens) during the loading cycle. Newman (11) performed an elastic-plastic finite element analysis of cracks growing from notches. He used spring elements along the crack to satisfy changing boundary conditions. He found that K_{cl} can explain, in terms of ΔK_{eff}, the non-LEFM behavior of short cracks growing at notches. Nicholas, Palazotto and Bednarz (5) performed a numerical analysis which modeled the plasticity induced closure of a short crack emanating from a single-edge-cracked specimen. They used a two-dimensional plane stress/plane strain viscoplastic finite element code called VISCO, which was originally developed by Hinnerichs (12). They examined crack growth and crack closure for TI-6246 at room temperature for stress values of approximately .60 and .90 material yield strength at load ratios of -1.0 and 0.1. Finite element results included displacements along the crack surface, stress-strain values immediately in

front of the crack tip, stress profiles ahead of the crack tip, plastic strains behind, as well as in front of, the crack tip and crack closure information.

Mercer (4) performed a viscoplastic finite element analysis of a crack growing from a blunt notch under cyclic loading conditions at 1200°F. The two-dimensional finite element code called SNAP was modified by Mercer to include the capability to simulate crack closure by the addition of springs to the nodes along the crack line. This method is similar to the one used by Newman (11). He examined crack growth and crack closure for IN-718 at elastic and plastic loading for a load ratio of 0.1. The finite element analysis provided crack tip stress and strain, plasticity induced closure effects and crack opening profile information.

The review of the literature indicates that the behavior of cracks is not completely understood and additional research needs to be done. In addition, numerical methods, especially finite element analyses, can be used to provide helpful information in predicting the behavior of cracks at notches.

II. Theory

Linear Elastic Fracture Mechanics (LEFM)

Linear elastic fracture mechanics relates the stress field and displacements near a crack tip to the stress applied to the component for various crack geometries. The difference between one cracked component and another lies in the magnitude of the stress field parameter, K_I, defined as the mode I (opening or tensile mode) stress intensity factor. In essence, the whole stress field at the crack tip is known when the stress intensity solution is known (13). The stress intensity parameter has been discussed explicitly in fracture mechanics literature (13,14), and thus will not be elaborated upon herein. However, the following stress intensity factors for some of the more well-known specimen geometries are given:

Center Cracked Plate (14):

$$K_I = \sigma(\pi a)^{1/2}(\sec \frac{\pi a}{W})^{1/2} \qquad (2.1)$$

where σ is the notch stress, a is the crack length measured from edge of notch, and W is the specimen width.

Single Edge Notched Plate (13):

$$K_I = 1.12\ \sigma(\pi a)^{1/2} \qquad (2.2)$$

where σ is the notch stress and a is the crack length measured from edge of notch. This equation is only valid for small cracks.

Compact Tension Specimen (15):

$$K_I = \frac{P}{BW^{1/2}} \cdot f\left(\frac{a}{W}\right) \tag{2.3}$$

where

$$f\left(\frac{a}{W}\right) = (2+\alpha)\,\frac{[0.866 + 4.64\alpha - 13.32\alpha^2 + 14.72\alpha^3 - 5.6\alpha^4]}{(1-\alpha)^{3/2}}$$

P is the applied load, B the specimen thickness, W the specimen width and $\alpha = \frac{A}{W}$ where A is measured from point of load application. This solution is valid for $\frac{A}{W} \geq 0.2$.

Bodner-Partom Constitutive Law

The Bodner-Partom flow law accounts for viscoplastic behavior as well as rate sensitivity and strain hardening effects (3). Work has been previously presented on the ramifications of this law (16), but for completeness, basic concepts and equations are presented. After initial yielding the material behavior will be partly elastic and partly plastic. During any increment of stress, the changes of strain are assumed to be separable into elastic and plastic components such that

$$\dot{\varepsilon}_{ij} = \dot{\varepsilon}^e_{ij} + \dot{\varepsilon}^p_{ij} \tag{2.4}$$

The plastic strain rate can be expressed in the form of the Prandtl-Reuss equation of classical plasticity as

$$\dot{\varepsilon}^p_{ij} = \lambda S_{ij} \tag{2.5}$$

where λ is the proportionality constant called plastic multiplier and S_{ij} is the deviatoric stress tensor. The form of λ depends on the flow law used. Bodner expressed λ as a function of the deviatoric stress tensor and the plastic strain rate tensor and can be written as

$$\lambda^2 = \frac{D_2^p}{J_2} \tag{2.6}$$

where $D_2^p = 1/2\ \dot{\varepsilon}_{ij}^p \dot{\varepsilon}_{ij}^p$ and is called the second invariant of the plastic strain rate tensor and $J_2 = 1/2\ S_{ij}S_{ij}$ is called the second invariant of the deviatoric stress tensor.

Bodner and Partom expressed D_2^p as

$$D_2^p = D_o^2 \exp\left[-\left(\frac{Z^2}{3J_2}\right)^n \left(\frac{n+1}{n}\right)\right] \tag{2.7}$$

where D_o is the limiting value of plastic strain rate in shear, Z is the measure of material hardening, and n is a rate sensitivity parameter. Z depends on the deformation history of the material and is assumed to be a function of the plastic work, Wp, such that

$$Z = Z_1 + (Z_0 - Z_1) \exp\left(-\frac{mW_p}{Z_o}\right) \tag{2.8}$$

where Z_1 and Z_o are the material's maximum and initial value of hardness respectively, and m is a constant that controls the rate of work hardening.

Generally, the plastic work is expressed as

$$W_p = \int S_{ij}\ \dot{\varepsilon}_{ij}^p\ dt \tag{2.9}$$

However, to account for the thermal recovery of hardening at high temperature, the plastic work must be redefined as

$$Wp = \int S_{ij} \dot{\epsilon}^{p}_{ij} dt + \int \frac{\dot{Z}rec}{m(Z_1 - Z)} dt \qquad (2.10)$$

where the rate of thermal recovery is defined as

$$\dot{Z}rec = - AZ_1 \left(\frac{Z - Z_2}{Z_1} \right)^r \qquad (2.11)$$

and Z_2 is the value of Z that gives the minimum expected value of hardening at a given temperature. A and r are material constants chosen to match creep test data.

The constants used for IN 718 as determined by Beaman (17) are:

$D_0 = 10^6 \text{ sec}^{-1}$

$Z_0 = 235.3$ Ksi

$Z_1 = 260.3$ Ksi

$Z_2 = 104.1$ Ksi

$n = 3.0$

$m = 2.875 \text{ Ksi}^{-1}$

$A = 1.5 \times 10^{-3} \text{ sec}^{-1}$

$r = 7.0$

Viscoplastic Solution Procedure

Bodner-Partom Solution

SNAP employs a semi-implicit technique to solve the Bodner equations. Plastic strains are calculated based upon a semi-implicit scheme which averages the strain rates at the beginning and end of each increment (2). Initial estimates of conditions at the end of the increment are obtained

using Euler extrapolation. This scheme is summarized as follows:

1. Initial values for stress, plastic strain, plastic work, Z, and the strain increment for the load step are input into the Bodner routine.

2. The following Bodner-Partom equations are solved for this increment:

$$J_2^{i-1} = 1/2\left\{S_{ij}\right\}^{i-1}\left\{S_{ij}\right\}^{i-1} \tag{2.12}$$

$$Z^i = Z_1 - (Z_1 - Z_o)\exp\left(\frac{-mWp^{i-1}}{Z_o}\right) \tag{2.13}$$

$$\left(D_2^p\right)^i = D_o^2 \exp\left[-\left(\frac{(Z_1)^2}{(3J_2^{i-1})}\right)^n\left(\frac{n+1}{n}\right)\right] \tag{2.14}$$

$$\left\{\dot{\varepsilon}_{ij}^p\right\} = \left(\frac{(D_2p)^i}{J_2^{i-1}}\right)^{1/2}\left\{S_{ij}\right\}^{i-1} \tag{2.15}$$

$$\left\{d\varepsilon_{ij}^p\right\}^i = \left\{\dot{\varepsilon}_{ij}^p\right\}^i dt^i \tag{2.16}$$

$$\dot{Z}rec^i = -AZ_1\left(\frac{Z^i - Z_2}{Z_1}\right)^r \tag{2.17}$$

$$Wp^i = Wp^{i-1} + \left\{S_{ij}\right\}^{i-1}\left\{d\varepsilon_{ij}^p\right\}^i + \frac{\dot{Z}_{rec}dt^i}{m(Z_1 - Z^i)} \tag{2.18}$$

3. New estimates of stresses, plastic strains, plastic work, and Z are calculated using an average of rates. As

described by Owen and Hinton (18), the plastic strain rate is:

$$\left\{d\varepsilon_{ij}^{p}\right\}^{i} = dt^{i}\left[(1-\theta)\left\{\dot{\varepsilon}_{ij}^{p}\right\}^{i-1} + \theta\left\{\dot{\varepsilon}_{ij}^{p}\right\}^{i}\right] \qquad (2.19)$$

where in the semi-implicit case $\theta = 1/2$.

4. The difference in stress values from steps (2) and (3) are calculated. If the difference is within a prescribed tolerance, the solution for this increment is complete and the next increment begins. If the difference is not within the allowable tolerance, a convergence loop is entered.

Solution Procedure

The overall solution procedure employed in SNAP is the residual force method. The residual force method uses the elastic stiffness matrix during the entire analysis and incorporates plasticity effects by including a plastic load vector. The residual force method has the following form:

$$[K]\{U\}^{i} = \{T\}^{i} + \{I\}^{i-1} \qquad (2.20)$$

where [K] is the constant elastic stiffness matrix, $\{U\}^{i}$ are the nodal displacements vector, $\{T\}^{i}$ is the applied load vector, and $\{I\}^{i-1}$ is the element internal force vector developed by the accumulation of plastic deformation. The superscript i reflects the current increment. The visco-plastic solution for a typical time step using the residual force method proceeds as follows:

1. Compute the current time

$$t^{i} = dt^{i} + t^{i-1} \qquad (2.21)$$

2. Calculate the plastic strain rate using the Bodner model relations

$$\left\{\dot{\varepsilon}^{p}_{ij}\right\}^{i} = \left(\frac{(D_2 p)^i}{J_2^{i-1}}\right)^{1/2} \left\{S_{ij}\right\}^{i-1} \tag{2.22}$$

3. Compute the plastic strain using the semi-implicit scheme

$$\left\{d\varepsilon^{p}_{ij}\right\}^{i} = \left[(1-\theta)\left\{\dot{\varepsilon}^{p}_{ij}\right\}^{i-1} + \theta\left\{\dot{\varepsilon}^{p}_{ij}\right\}^{i}\right] dt^{i} \tag{2.23}$$

where $\theta = 1/2$ for the semi-implicit technique. For $\theta = 0$, we get the Euler integration scheme (fully explicit) and for $\theta = 1$ we get the fully implicit scheme.

4. The plastic load vector is computed by

$$\{I\}^{i-1} = \int_{VOL} [B][D] \left\{\varepsilon^{p}_{ij}\right\}^{i} dVOL \tag{2.24}$$

where [B] is the strain-displacement matrix and [D] is the elastic material property matrix.

5. Compute the current external load vector

$$\{T\}^{i} = \{\dot{T}\}^{i}\, dt^{i} + \{T\}^{i-1} \tag{2.25}$$

where $\dot{T}$ is the known force rate vector.

6. Compute the nodal displacements using Gaussian elimination techniques

$$\{U\}^{i} = [K]^{-1} \left(\{T\}^{i} + \{I\}^{i-1}\right) \tag{2.26}$$

7. Compute the total strain from the strain-displacement relationship

$$\{\varepsilon_{ij}\}^{i} = [B]\{U\}^{i} \tag{2.27}$$

8. Compute the current stress

$$\left\{\sigma_{ij}\right\}_i = [D]\left(\left\{\varepsilon_{ij}\right\}_i - \left\{\varepsilon_{ij}^{p}\right\}_i\right) \tag{2.28}$$

9. The particular time step is determined when the differences in stress values discussed earlier are within a set tolerance. If convergence is not obtained within 40 iterations, the time step is halved and steps 1-9 are repeated for this particular time step. If, after 10 successive time step reductions, convergence is not achieved, the problem solution is stopped.

Crack Closure and Growth

Crack growth and closure were implemented by Mercer (4) into the SNAP program by the addition of "springs" to the boundary node along the crack line. This method is similar to that used by Newman (19). The spring stiffness for each node was related to the boundary condition of that respective node. If the spring was made very stiff the node was considered fixed and if the node was free the stiffness was set equal to zero.

For the nodes lying along the crack line, a flag for each node behind and ahead of the crack tip was monitored. A positive value indicated a fixed node and a negative value meant the node was free. During each load increment, the nodal displacements along the crack line were also monitored to determine whether the node had closed (negative displacement) or opened (positive displacement). If the node had closed, the flag was set equal to a positive value and the

spring stiffness was set to 1000 times the maximum diagonal entry in the structure stiffness matrix and the stiffness matrix was updated to account for the changing boundary conditions. If the node had opened, the flag was set equal to a negative value and the spring stiffness was set equal to zero and the stiffness matrix was recalculated. This procedure of adding or deleting spring stiffnesses to the structural stiffness matrix had the advantage that the global stiffness matrix did not have to be reformulated and decomposed whenever the crack opened or closed (4).

Crack growth was accomplished by releasing nodes when a user-defined criterion such as stress or load was exceeded. The selected method released an element with every cycle of loading at 98 percent load for R = 0.1, where R is the minimum to maximum load ratio. For R = -1.0, an element was released with every cycle of loading at 98 percent of the stress. These methods allowed for full recovery of crack tip plastic strain in each cycle, and no convergence problems were encountered (4).

J-Integral

The elastic stress intensity factor can be determined for crack problems by using finite element methods including the J-integral, compliances, and extrapolation of the stress and displacement fields near the crack. The J-integral technique seems to provide the best results (4); thus, the J-integral concept was used in this study.

The J-integral concept is based upon an energy balance approach. The concept was introduced by Rice (20). For an elastic case, J is equivalent to the energy release rate G (13). The J-integral formula represents an energy influx across an arbitrary boundary Γ around the crack tip and is defined as:

$$J = \int_{\Gamma} \left[W dy - T_i \frac{\partial U_i}{\partial x} ds \right] \tag{2.29}$$

where W is the strain energy density, T_i is the traction vector, and U_i is the displacement vector along the contour. Obtaining solutions for the J-integral in actual specimens is difficult. It is generally necessary to use finite element techniques. Mercer (4) describes in detail how the actual J-integral numerics were computed using the SNAP finite element program.

III. Results and Discussion

A viscoplastic analysis of a crack growing from a compact tension specimen with a round notch was investigated using the SNAP finite element program. A specimen consisting of IN-718 at 1200° was modeled under cyclic conditions at two load levels with a load ratio of 0.1. The specimen was also analyzed under plastic loading with a load ratio of -1.0. Both elastic and viscoplastic analyses were performed on an uncracked specimen considering a plane stress approach. A viscoplastic analysis was performed for a crack growing from an initial length of 0.0 inches to a final crack length of 0.024 inches.

Data obtained from the finite element model analysis included an elastic stress intensity solution, crack opening displacements, opening and closure loads, stress values in front of the crack tip, and plastic strains along, as well as in front of, the crack tip. These values are compared to data obtained for a crack emanating from a blunt notch and a single-edge-cracked specimen.

Compact Tension Finite Element Modeling

The compact tension specimen had a round notch with a radius of .197 inches. The specimen geometry is shown in Figure 3.1. Due to symmetry, only half of the specimen was modeled. The model used the eight-noded quadratic isoparametric elements.

The overall finite element model is shown in Figure 3.2. The refined elements used in the neighborhood of the crack, along with a typical Gauss point location, are shown in Figure 3.3. This refinement is identical to that used by Mercer (4) for a blunt notch (r = 0.47 in). The number of elements near the crack tip and the degree of model refinement represented a trade-off between the amount of crack growth required and the computer storage space available, as well as the computer time required to carry out the simulation. The model with crack tip refinements had about 1000 degrees of freedom, 490 nodes, and 140 elements. The crack tip elements were 0.002 inch square.

Mercer (4) performed an extensive series of validation tests using the SNAP program. These tests include: a) V-notched elastic-plastic tension problem as described by Yamada (21), b) center-cracked panel analysis as reported by Hinnerichs (12) and Henkel (22), and c) compact tension specimen analysis as examined by Wilson (23). The SNAP program was found to provide satisfactory results for all of the above problems. Since acceptable accuracy was shown by Mercer using the SNAP program, no extensive accuracy tests were carried out for the round notch study. However, a validation run was performed for the round notch uncracked specimen and SNAP gave acceptable results as will be seen in the following section.

Uncracked Specimen Elastic Analysis

Irregularities in a component, such as holes and notches, will have high localized stresses and may also provide possible sites for fatigue in a cyclic-loaded component. These high localized stresses are called stress concentrations and they provide useful information regarding the irregularity's stress distribution and are usually expressed in terms of a stress concentration factor. This factor was determined for the round notch condition using the finite element method and was then compared to previously published compact tension stress concentration results.

The finite element model was monotonically loaded to 0.5 Kips using linear elastic material properties. The elastic stress concentration factor, k, is defined as the ratio between the maximum stress and the nominal stress in a notched sample and can be calculated by:

$$k = \frac{\sigma_y}{\sigma_n} \qquad (3.1)$$

where σ_y is the calculated stress at the notch and σ_n is the applied nominal stress at the notch. The nominal stress for the specimen considered in Figure 3.1 is defined by Wilson (24) as:

$$\sigma_n = \frac{P}{B} \frac{1}{(W-A_n)} \left[1 + 3 \frac{(W + A_n)}{(W - An)} \right]$$

where P is the applied load, B is the specimen thickness, W

is the specimen width, and A_n is the distance from load point to notch location. The calculated stress concentration factor for the round notch was 2.18. As shown in Figure 3.4, the round notch stress concentration factor result agrees with that reported by Wilson (24). Wilson's results are for a compact tension specimen with three different notch shapes. Figure 3.4 is drawn to show how the round notch result compares to Wilson's notch shapes. The symbol, $\bar{R}$, is a nondimensional notch radius and is defined as:

$$\bar{R} = \frac{r}{W-A_n} \tag{3.3}$$

where r is the notch radius, W is the specimen width and A_n is the distance from load point to notch location. The stress concentration factor obtained by Mercer (4) for a blunt notch (r = .047") was 4.29. The difference between the k values is obvious; the round notch has a lower maximum notch stress than that of a blunt notch.

Uncracked Specimen Viscoplastic Analysis

In order to determine which loads will be used in this study, we must first determine if the load to be applied is an elastic or plastic load. This can be accomplished by evaluating the stress concentration factor and by observing if the applied load produced any plastic strain. Both of these methods can be evaluated using the finite element model.

The finite element model was monotonically loaded to 2.0 Kips in one second using the previously described Bodner model. The stress concentration factor is defined by equation (3.1). A strain concentration factor, as described by Wilson (24), can be defined as:

$$K_\varepsilon = \frac{\varepsilon_y}{\overline{\varepsilon_n}} = \frac{E\,\varepsilon_y}{\overline{\sigma_n}} \qquad (3.4)$$

where E is the elastic modulus, ε_y is the calculated strain obtained from the finite element program, and σ_n is the nominal stress from equation (3.2). If the stresses and strains are elastic, the stress concentration factor and the strain concentration factor will be equal. The stress and strain concentration factors are shown in Figure 3.5 as a function of the load level. The stress and strain concentration are the same up to loads equal to 1.2 Kips, thus there was no plastic deformation at the notch up to this load level. However, for loads greater than 1.2 Kips, the effect of plasticity at the notch is observed. The strain intensity increases due to the plastic strain increasing, while the stress intensity decreases since the notch is no longer elastic.

The plastic strain at each element Gauss point was observed and the 0.1% plastic strain location obtained by interpolation. This plastic strain value was the same value used by Mercer (4). The size of the plastic zone as defined by $\varepsilon_{yp} \geq 0.1\%$ is shown in Figure 3.6. The loads selected for crack growth analysis, at a load ratio of 0.1, were 1.148

Kips and 1.55 Kips. We see that for the lower load, there is no notch plasticity while at the higher load the notch plasticity was 0.013 inches. The load selection criteria used for this study were similar to those used by Mercer (4). The lower load was an elastic load, while the higher load produced significant notch plasticity. It should be noted that the lower load chosen for this study coincided with Mercer's plastic load for the blunt notch study. By choosing these two load levels, crack growth could be observed under two different cases: one within the elastic notch influence and one within the plastic notch influence.

The model was subjected to a cyclic load condition to examine the response at the notch for these selected load levels. The load ratio used was R = 0.0. At P = 1.148 Kips, we see that the material stays within the elastic regime as shown in Figure 3.7. However, at P = 1.55 Kips, we see plastic deformation during the initial cycle, but subsequent cycle response was elastic. The stress profiles ahead of the notch at 100% and zero load are shown in Figure 3.8 and Figure 3.9 for the elastic and plastic load levels, respectively. We can see that for maximum loading, the material starts out in tension near the notch and goes into compression away from the notch. This observation is due to the "bending" effect taking place as the compact tension specimen is being loaded as shown diagrammatically in the inset in Figures 3.8 and 3.9. For the plastic load, we see that the material goes into compression when the load is

reduced. This observation tells us that a local negative R ratio is seen for an applied load ratio of 0.0.

Elastic Stress Intensity Calculation

As discussed earlier, the elastic stress intensity is a commonly used parameter to characterize linear elastic fracture mechanics. The stress intensity factor incorporates geometrical terms as well as the stress level. The elastic stress intensity for a crack growing from a round notch was determined from the finite element model. The finite element results were compared with the compact tension specimen long crack solution to determine the effect of notch influence. The solutions are based on an elastic load of 1.148 Kips and the elastic constitutive model in SNAP was used.

First, we must establish bounds on the elastic stress intensity solution. This was established by using the compact tension solution for long cracks and edge crack approximations for short cracks. The compact tension solution is given by earlier equation (2.3) from ASTM standard E-647-83 (15). This equation is valid for $\frac{A}{W} \geq 0.2$. This solution is shown as the slightly inclined curve in Figure 3.10. A small crack in a notch acts like an edge crack in a plate under a far field stress equal to the concentrated stress at the notch. The edge crack solution for small cracks is defined by equation (2.2). Observing that the magnitude of the stress decreases away from the notch, we

use the finite element model stress (σ_y) corresponding to a given crack size in place of the value at the notch (σ) in equation (2.2). The edge crack solution is shown as the bottom curve in Figure 3.10 with the notch stress profile (σ_y) shown diagrammatically in the inset figure. We expect to see the actual elastic stress intensity solution for the round notch to approximate the edge crack solution for short cracks and approach the compact tension solution as the crack size increases.

For the finite element solution, an elastic analysis was performed for crack lengths up to .200 inches using the finite element model. The J-integral was used to evaluate the stress intensity solution. The J-integral was calculated over four paths as shown in Figure 3.11. The J integral equation is given by equation (2.29). In the elastic case, J is equal to the energy release rate and is related to the stress intensity by the following equation:

$$K_I = (EJ)^{1/2} \text{ for plane stress} \qquad (3.5)$$

The stress intensity values calculated for the round notch is shown in Figure 3.12. These values were averaged over the J integral paths. Figure 3.12 shows the round notch elastic stress intensity to approximate the edge crack solution for short cracks and approach the compact tension specimen solution for long cracks. We can also see that the notch influence on the stress intensity lies within one radius of the notch (approximately 0.2 inches). This phenomenon was also seen in Mercer's blunt notch study. Thus,

given a certain notch geometry, we can state that the notch influence for that particular geometry should lie within one radius of the notch.

Crack Growth Analysis

A crack growing from the round notch of the compact tension specimen was modeled using the finite element model. Cracks up to 0.024 inches were analyzed under cyclic loading conditions. Two cases of loading were studied. The first case consisted of two load levels, P = 1.148 and P = 1.55 Kips, and a load ratio of 0.1. The second case was subjected to a plastic load level (P = 1.55 Kips) and a load ratio of -1.0. These R-ratios give a good representation of the stress levels which may be seen in the life cycle of a component. These load spectra are shown in Figure 3.13. Both cases had a loading frequency of one Hz and a constant crack growth rate. The following results apply for the R = 0.1 case only.

Crack Opening Displacements

Figures 3.14 and 3.15 show the crack opening profiles for crack lengths of 0.010, 0.016 and 0.024 inches at loads of 1.148 Kips and 1.55 Kips, respectively. We see that the displacemnts behind the crack tip for the plastic load case (Figure 3.15) are approximately 1.33 times greater than those for the elastic load case (Figure 3.14) for the three crack lengths. Figures 3.16 and 3.17 show the crack profiles at partial loads for a crack which has grown from

0.0 inches to a final length of 0.024 inches at loads of 1.148 Kips and 1.55 Kips, respectively. The cracks initially close at the crack tip, but as the load is reduced, the crack closes at a distance other than at the crack tip location. As the crack grows, a zone of plastic deformation is left in the wake of the growing crack. This plastic deformation causes the shape of the profiles seen in Figures 3.14-3.17 to become concave downward and also cause closure as the load is reduced as seen in Figures 3.16 and 3.17. We again see that even at partial loading, the displacements behind the crack tip are greater for the plastic load case (Figure 3.17) than those seen for the elastic load case (Figure 3.16). The shapes and trends of Figures 3.14 through 3.17 are also seen in Mercer's (4) blunt notch study.

Crack opening displacements at a point .002 inches behind the crack tip were monitored as the crack was grown and are shown in Figure 3.18 for the two different load levels. The displacements shown are at 100% load. The displacements gradually increase as the crack grows and seem to be reaching a constant value for the lower load case. This observation for the round notch differs from that seen by Mercer (4). For the blunt notch, the displacements reached an initial peak value early on for the two load levels, then approached a constant displacement as the crack continued to grow. Thus, the round notch geometry seems to have an influence on the results as expected.

Crack Closure

Crack closure due to the formation of the plastic wake during crack growth is seen in Figures 3.19 and 3.20 for the two respective loads. P_{open} is the opening load which corresponds to the load at which the last node separates or opens. P_{close} is the closure load which corresponds to the load at which the node closes and exhibits a negative displacement. The closure and opening loads are normalized with respect to the maximum load (PMAX). At the lower load (Figure 3.19), we see that the crack had to grow at least 0.010 inches before closure was seen at that location. For the higher load (Figure 3.20), the crack had to grow 0.008 inches before closure was seen at that location. This "delayed" crack closure can be attributed to the round notch geometry condition. Since the round notch has a lower notch stress value than that of a blunt notch, the associated plastic deformation develops slower than that for the blunt notch. Thus, the crack must grow long enough, as observed in Figures 3.19 and 3.20, so that the formation of a plastic wake will develop and allow crack closure. Mercer observed some "delayed" closure for his elastic load case but not for his plastic load case. The opening and closing loads gradually increase as the crack grows. This trend was also seen by Mercer.

Opening and closing loads can be converted to opening and closing stress intensities by the following equations:

$$K_{close} = K_{max} \ (P_{close}/P_{max}) \quad (3.6)$$

$$K_{open} = K_{max} \ (P_{open}/P_{max}) \quad (3.7)$$

The values for K_{max} were obtained from the previously described elastic stress intensity solution. Figures 3.21 and 3.22 show the opening and closing stress intensities for the two load levels plotted versus the maximum stress intensity. The stress intensities linearly increase with K_{max}. This observation was also seen in the blunt notch study (4) and the single-edge-cracked work (5). One interesting point regarding Figures 3.21 and 3.22 is that at the higher applied load the stress intensity at closure is lower than that for the elastic load at the same K_{max} level. This phenomenon was also seen in the single-edge-cracked specimen, as shown in Figure 3.23, and the blunt notch crack closure studies. Thus, if a parameter such as $\Delta K_{eff} = K_{max} - K_{close}$ is a driver of crack growth, the higher load would result in a larger effective stress intensity range than the lower load at the same maximum applied stress intensity.

Stress Intensity Ranges

As stated earlier, the crack growth rate may be governed by a ΔK_{eff} parameter. Thus, we need to evaluate the influence of the stress level on the growth rate of the round notch crack. This is best done by evaluating the stress intensity ranges for the two applied loads.

For an applied load of 1.148 Kips, Figure 3.24 shows the maximum stress intensity, minimum stress intensity, and

stress intensity at closure for a crack grown to 0.024 inches. The minimum stress intensity is taken as 10% of the maximum stress intensity. From this figure we can define a corresponding stress intensity range (ΔK) and an effective stress intensity range (ΔK_{eff}) by the following equations:

$$\Delta K = K_{max} - K_{min} \tag{3.8}$$

$$\Delta K_{eff} = K_{max} - K_{close} \text{ (or } K_{open}) \tag{3.9}$$

These ranges are shown in Figure 3.25. We see that over the 0.024-inch crack growth range, ΔK increases by 124%, but ΔK_{eff} changes only 19%.

At the higher load of 1.55 Kips, we see the values of K_{max} , K_{min}, and K_{close} in Figure 3.26. Figure 3.27 shows the corresponding ΔK and ΔK_{eff} values. In Figure 3.27, K increases by 123%, while ΔK_{eff} changes by 22%.

We observe that ΔK_{eff} is greater at the higher load level (Figure 3.27) since K_{close} (or K_{open}) is smaller at a common value of K_{max} of approximately 32 $K_{si}\sqrt{in}$ as seen in Figures 3.21 and 3.22. Thus, we can say that the crack effect at the round notch should be more pronounced at the higher load level than the lower one. This observation was also seen in the single-edge-crack work (5) and can be seen in Figure 3.23.

Stresses and Strains

The stresses and strains at and ahead of the crack tip were monitored. The values at the crack tip actually refer to the values calculated at the element integration point

closest to the crack tip. For the eight-noded quadratic elements, this point is located approximately 0.0004 inches from the crack tip.

The stress response at the crack tip ranged between full tensile and compressive yielding for both load cases and is shown in Figure 3.28 for the higher load case. This results in a crack tip R ratio of approximately -1.0.

The crack tip strains were found to increase similarly to that seen for the maximum elastic stress intensity as shown in Figures 3.29 and 3.30 for the two load cases. As expected, the maximum strains are greater for the higher load level than for the lower load level. These trends were also seen by Mercer (4).

The stress profiles ahead of the crack tip for crack lengths of .010, .016, and .024 inches are shown in Figures 3.31-3.34 at 100% and 10% loading for the respective load cases. In Figure 3.31, we see that the stress levels remain constant for a short period near the notch, but steadily decrease as the crack grows away from the notch. For the 10% load condition (Figure 3.32), we see that the stresses dramatically increase to a peak value and then gradually decrease to a constant value. The plastic zone extent is shown in Figure 3.32 and is approximately the same size as the three respective crack sizes. This is typical of short crack behavior. At the higher load level (Figure 3.33), we see that the stress levels remain constant similar to Figure 3.31 but for a longer duration. The stresses

remain constant as the crack grows within the notch plastic zone and starts to decrease once the crack grows beyond this plastic region. In Figure 3.34, we again see that the crack tip plastic zone extent for the three crack lengths are approximately the same size as the cracks. Figure 3.34 is similar in shape to Figure 3.32, but the plastic zone extent is more pronounced in Figure 3.34 due to the plastic load condition.

The strain profiles ahead of the crack tip for crack lengths of .010, .016, and .024 inches are shown in Figures 3.35-3.38 at 100% and 10% loading for the two load cases. At the lower load (Figure 3.35), we see that the strains are greatest at the crack tip and gradually decrease away from the notch. As the strain decreases, it approaches a constant value for the three different crack sizes. The plastic zone extent is shown in Figure 3.35 and is approximately the same size as the respective crack length. As stated earlier, this phenomenon is typical of short crack behavior. Figure 3.36 shows the strain profile ahead of the crack tip at 10% load for the elastic load case. The shape is similar to Figure 3.35 but at lower strain levels. At the higher load level (Figure 3.37), we see the expected result of the strain values being greater for the higher load than for the lower load. As the crack grows out of the crack tip plastic zone, we see that the strain values are approximately the same for the high load case and the low load case. We also see the same phenomenon

noticed in Figure 3.35 regarding the plastic zone extent. Figure 3.38 shows the strain profile at 10% load for the plastic load case. The curve is again similar in shape to the previous strain profiles. The strain values are slightly higher than those seen in Figure 3.36, as expected.

A comparison of plastic strain profiles can be seen from Figures 3.39 and 3.40 for the two load cases. The higher load induces significantly more plasticity than the lower load. For a crack length of .024 inches, Figure 3.41 shows the accumulated plastic strain ahead of, as well as behind, the crack tip is greater for the higher load case than the lower load case. As the crack tip grows, a region of plasticity or plastic wake is formed. This region is produced between the original crack tip location and its current position. Ahead of the crack tip, we see from Figure 3.41 that the amount of plastic strain appears to be less than that behind the crack tip. Thus, the formation of the plastic wake along the crack surface seems to restrict the amount of plasticity ahead of the crack tip. In Figure 3.41, the plastic wake increases dramatically behind the crack tip for the two load level cases and the amount of plastic strain seems to vary directly in relation to the magnitude of the load applied. The plastic zone size for the .024-inch crack is seen to be approximately .025 inches for plastic strains greater than 0.5%. The spikes observed in the curves are attributed to numerical inaccuracies within the finite element program due to a plastic strain

singularity effect at the crack tip; at this point the theory of small displacement is no longer valid.

The stress and strain trends observed for cracks growing from a round notch specimen were similar to those seen in the blunt notch work (as shown in Figures 3.42 and 3.43) and the single-edge-crack specimen (as shown in Figure 3.44). Both of these studies centered on short crack growth analysis.

Negative R-Ratio Results

The results and discussion in this section are derived from the compact tension specimen loaded at the higher load level and with a load ratio of -1.0. The results for the negative load ratio can be broken down into three major areas:

a. Crack opening displacements at and behind the crack tip.

b. Opening and closure load information during crack growth.

c. Profiles of stress and plastic strain ahead of the crack tip.

Crack opening profiles for crack lengths of .010, .016, and .024 inches are shown in Figure 3.45 for the higher load case. The curves for the negative load ratio case are similar to those for the positive load ratio case (Figure 3.15), but we see that the displacements behind the crack tip for the three crack lengths are approximately 1.5 times greater

for the negative load ratio than for the positive load ratio condition.

Crack opening displacements at a point .002 inches behind the crack tip are observed in Figure 3.46. These displacements are approximately three times greater than those seen in the positive load ratio case (Figure 3.18).

Crack opening and closure loads were examined for a point .002 inches behind the crack tip. These loads are shown in Figure 3.47 for which crack closure and opening occurred for the negative load ratio condition. We see that for the plastic load the crack closes immediately. However, for the positive load ratio case with the same loading (Figure 3.20), the crack had to grow .008 inches before closure was seen at that location. Thus, crack closure develops quicker for R = -1 than for R = 0.1 for the same load value. The closure loads decrease gradually with increasing crack extension and the opening loads approach a constant value as the crack grows.

Opening and closure stress intensities are shown in Figure 3.48 for the plastic loading case. The closing and opening stress intensities are defined by equations (3.6) and (3.7), respectively. The values for the opening stress intensity remain relatively constant while the closure stress intensity values decrease steadily with increasing crack growth. These opening and closure load trends, for a crack growing from a round notch with a negative load ratio,

are similar to those seen in the single-edge-cracked specimen work (5), as shown in Figure 3.49.

The stress profiles ahead of the crack tip at 100% and -100% load for crack lengths of .010, .016, and .024 inches are shown in Figures 3.50 and 3.51, respectively. For the negative load ratio case at 100% load (Figure 3.50), we see results that are similar to those found in the positive load ratio case at 100% load (Figure 3.33). At the full compressive load (Figure 3.51), we see the stress values remain relatively constant, then gradually decrease.

The plastic strain profile ahead of the crack tip for the negative load ratio case is seen in Figure 3.52. The accumulated plastic strain ahead of, as well as behind, the crack tip for a crack length of .024 inches is shown in Figure 3.53 for the plastic load case. We see that the plastic strains behind and ahead of the crack tip are smaller for the negative load ratio than those seen for the positive load ratio case (Figure 3.41) at the same load (P = 1.55 Kips). This indicates that there is a severe compression developed in the plastic wake under fully reversed loading and these compressive forces have restricted the size of the plastic wake in the region directly behind the crack tip. This phenomenon was also observed in the single-edge-cracked work (5), as seen in Figure 3.44. The spike seen at the crack tip is attributed to numerical inaccuracies within the program, as described earlier.

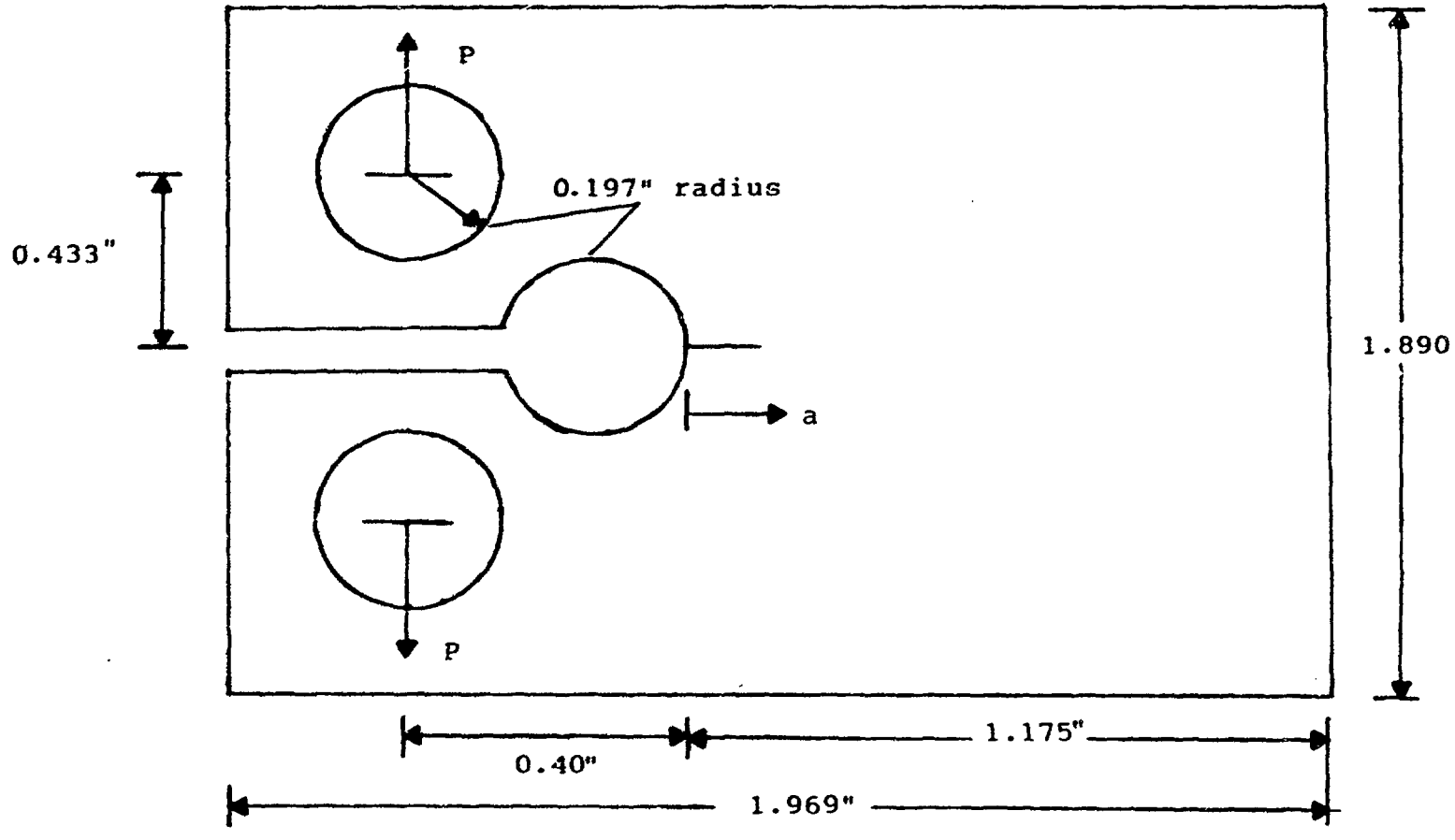

Figure 3.1: Round Notched Compact Tension Specimen

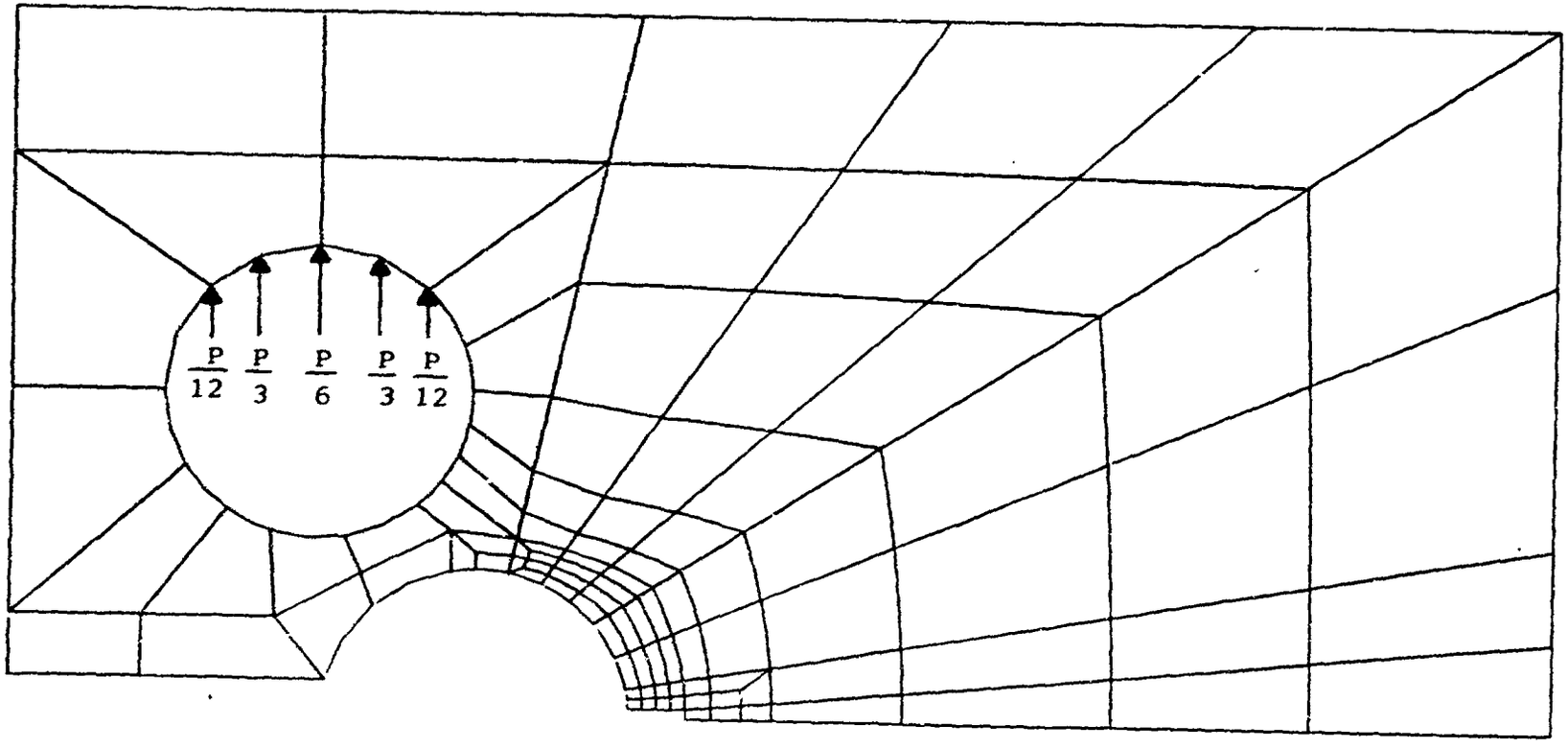

Figure 3.2: Cracked Notched Specimen Overall Model

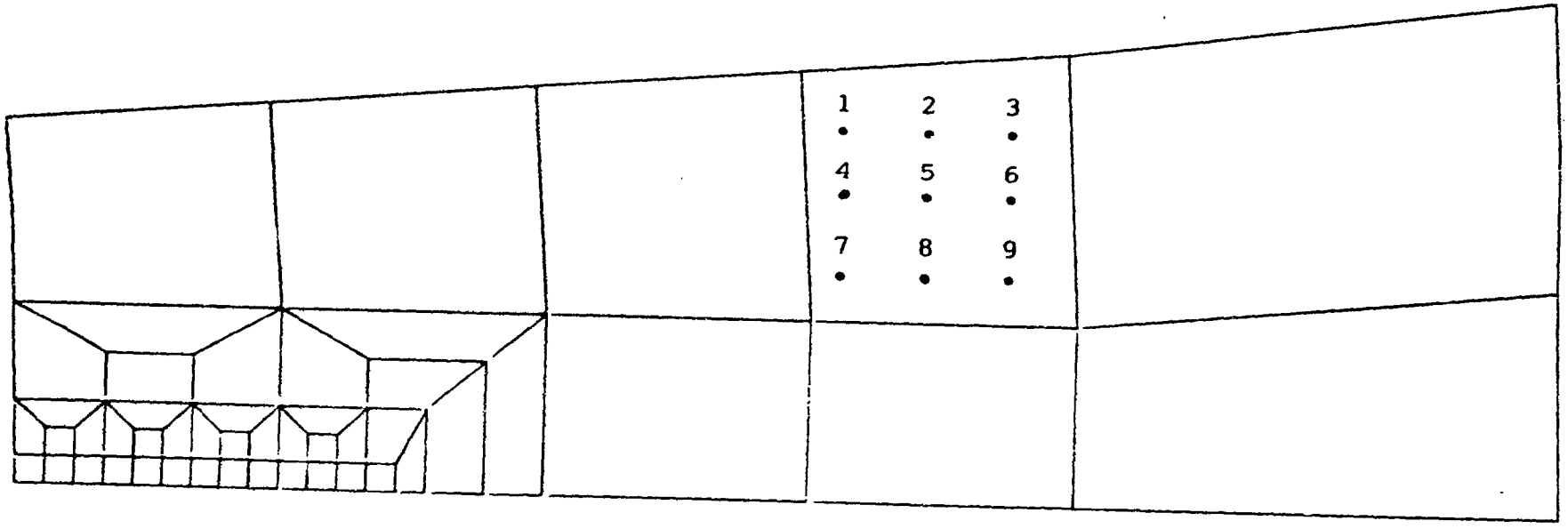

Figure 3.3: Crack Tip Refinement Elements and Typical Gauss Quadrature Points

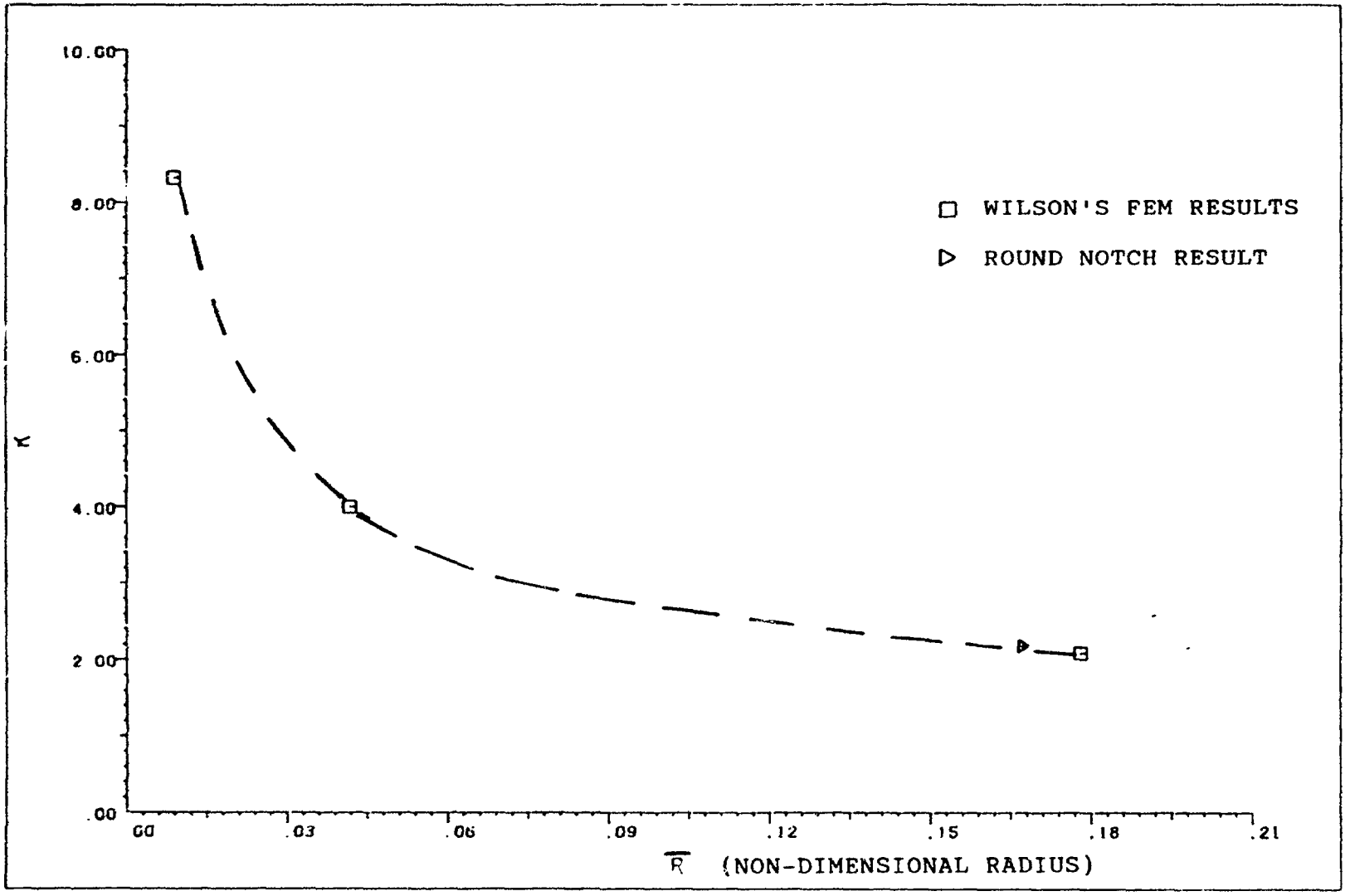

Figure 3.4: Elastic Stress Concentration, Round Notch Specimen.

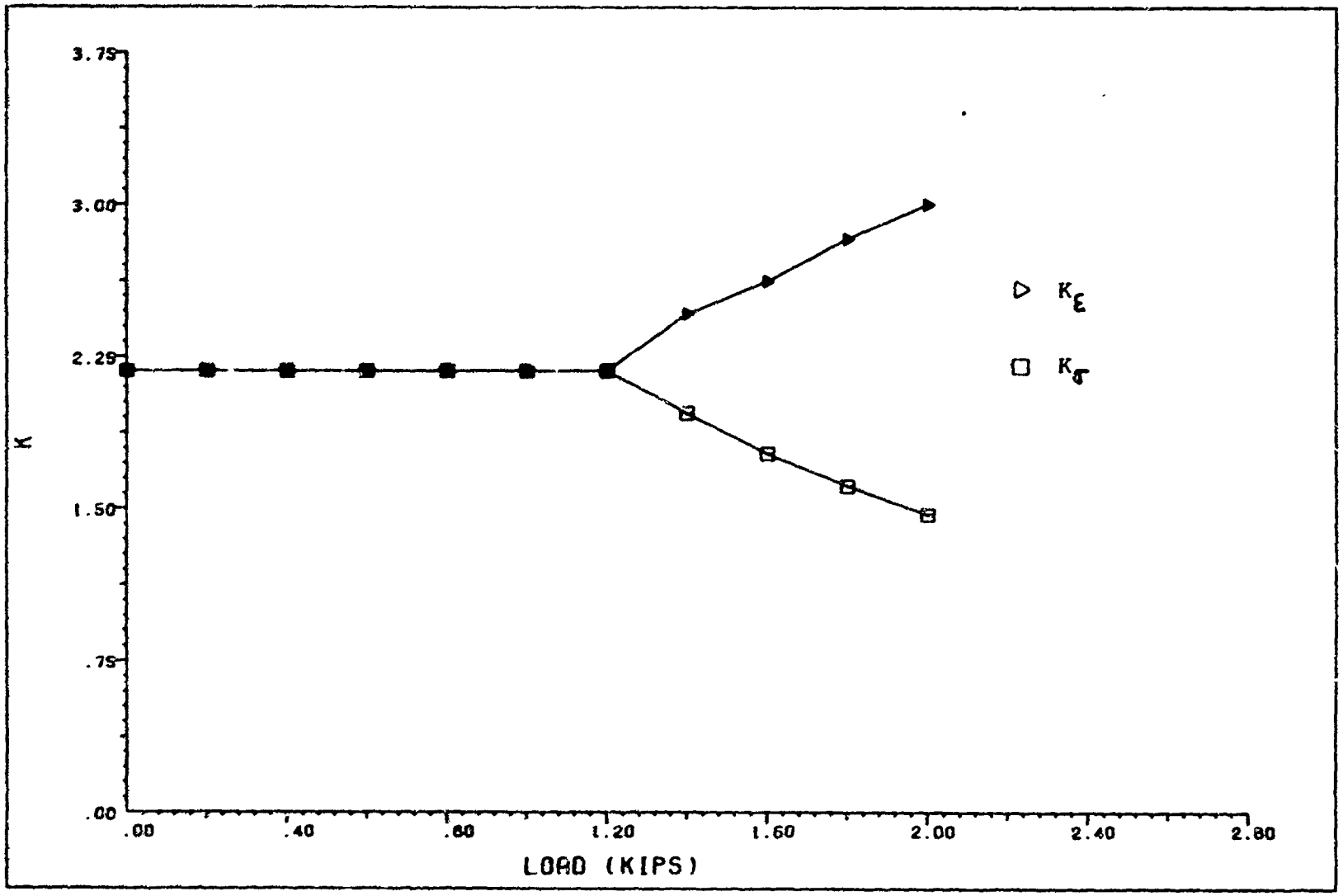

Figure 3.5: Stress and Strain Concentration using Viscoplastic Analysis

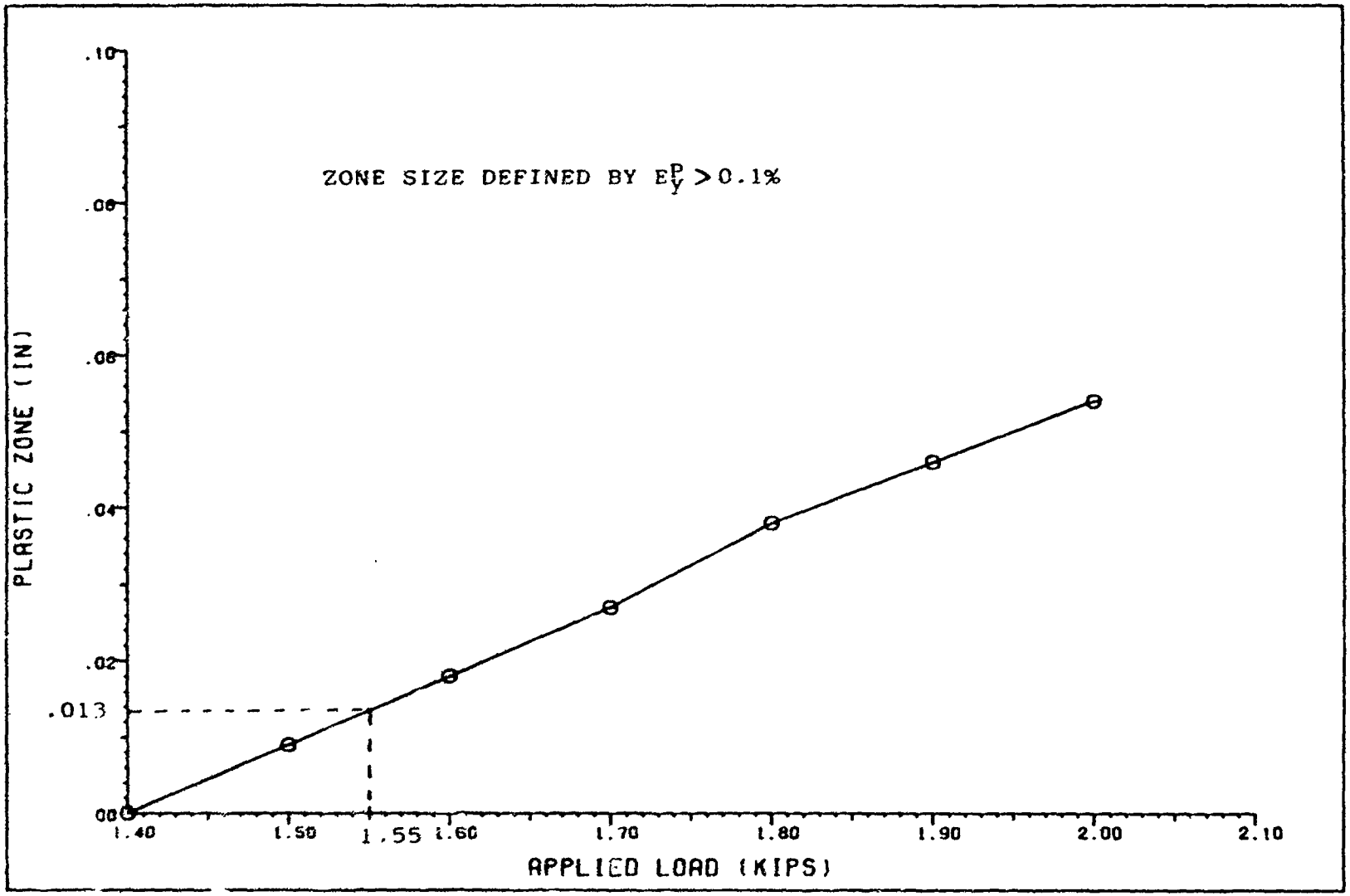

Figure 3.6: Plastic Zone Size versus Applied Load, Viscoplastic Analysis for Round Notch Specimen

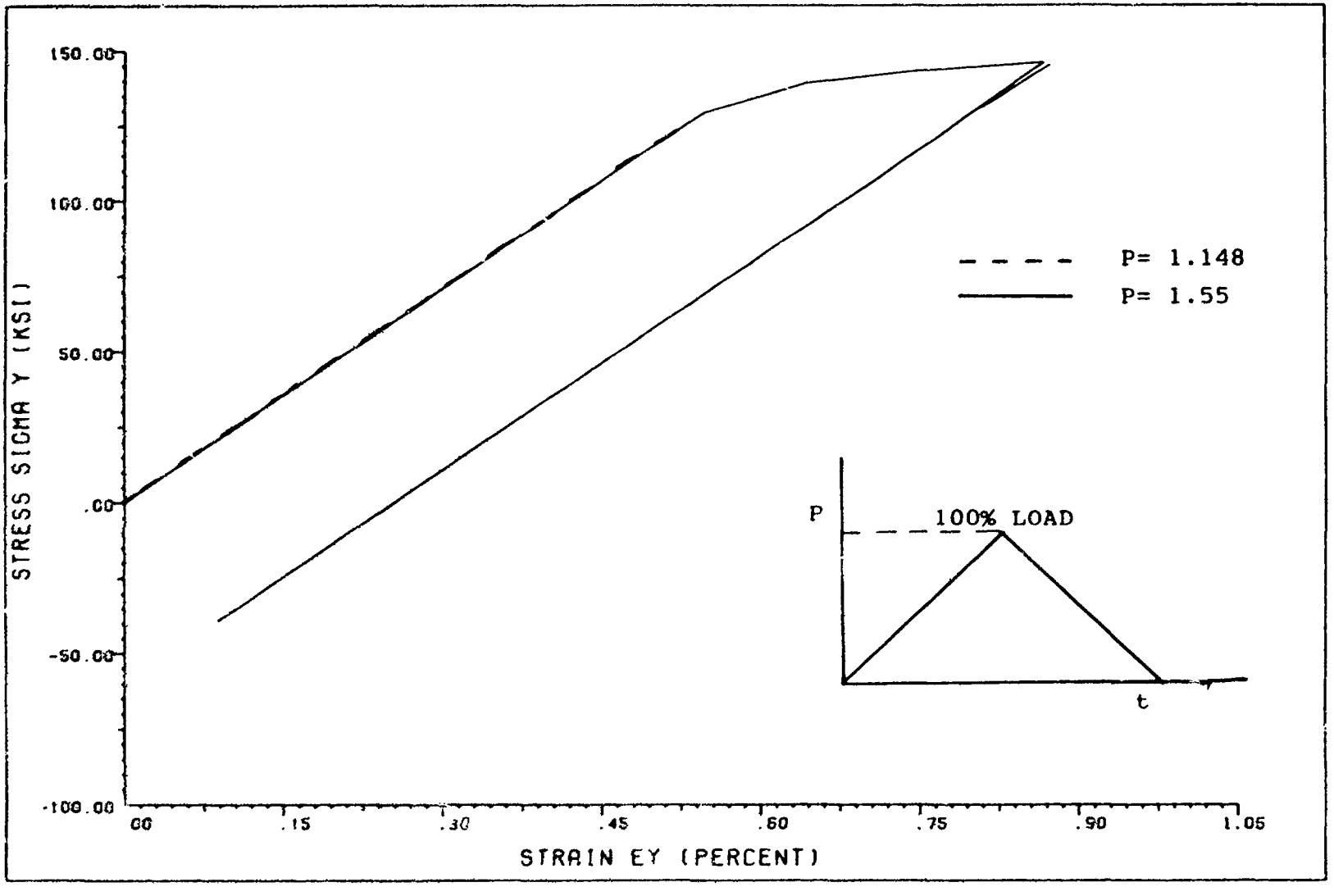

Figure 3.7: Uncracked Round Notch Stress-Strain Response During Cyclic Loading

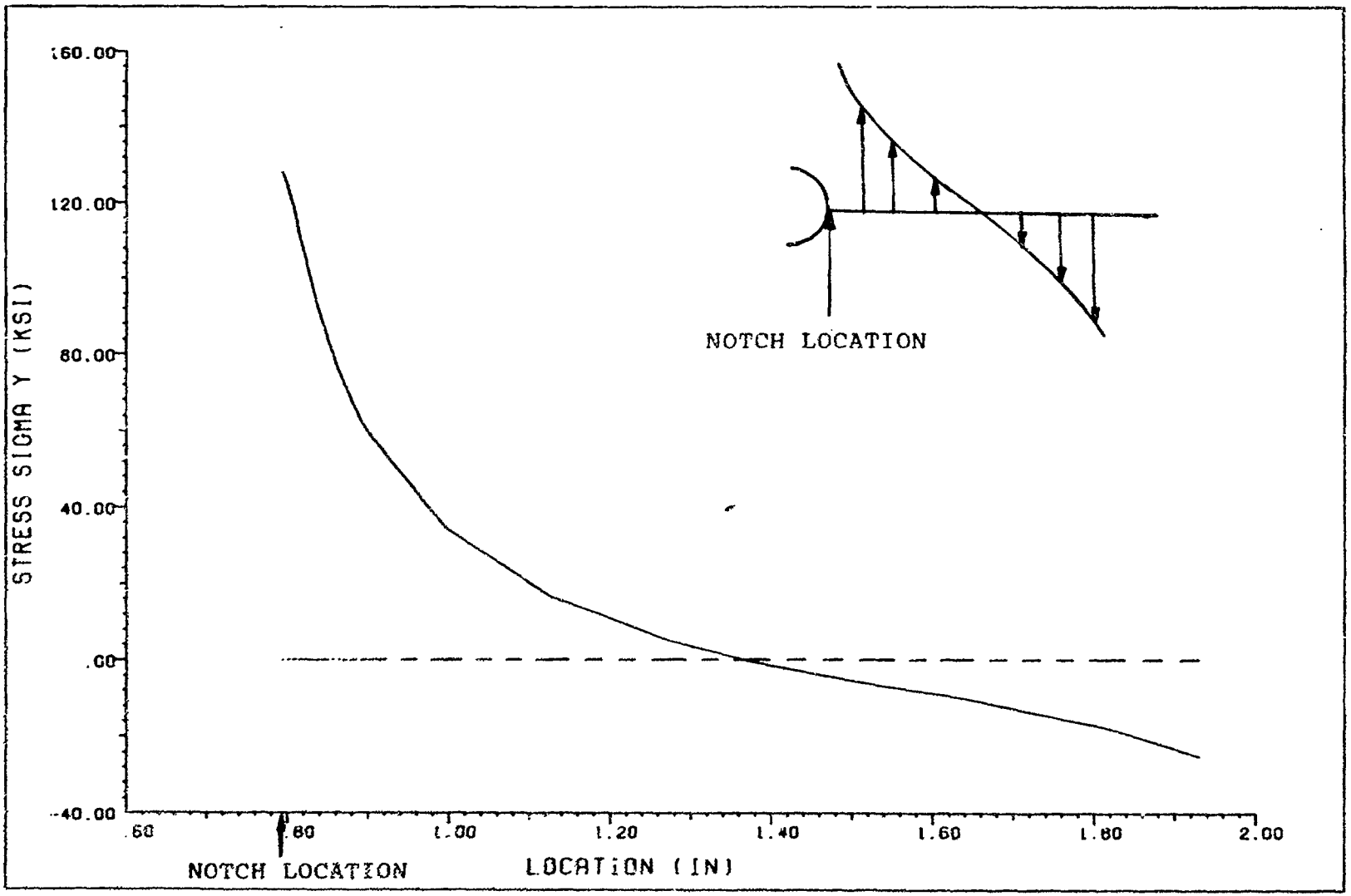

Figure 3.8: Uncracked Round Notch Stress Profile, Elastic Loading, P= 1.148 Kips

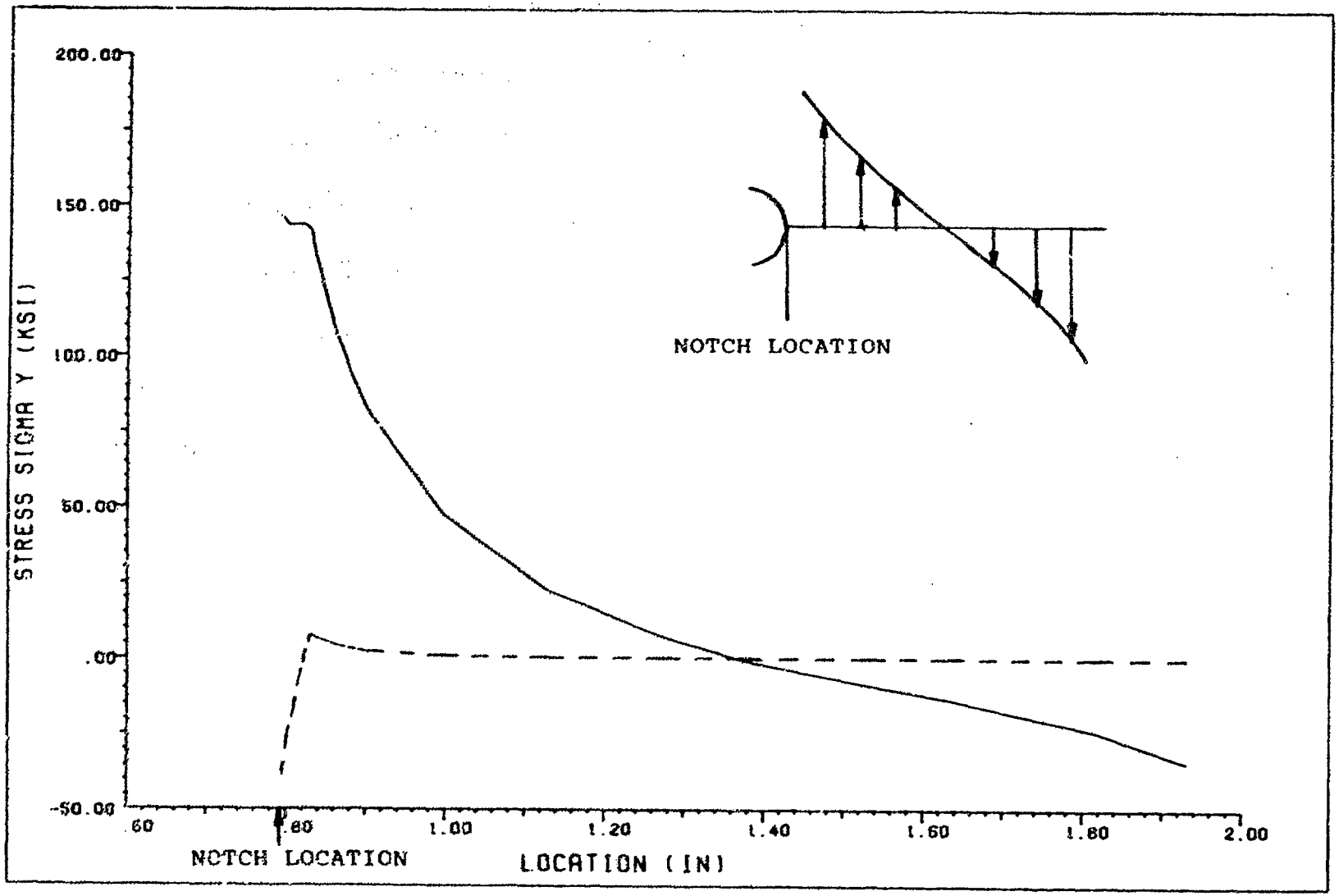

Figure 3.9: Uncracked Round Notch Stress Profile, Plastic Loading, P= 1.55 Kips

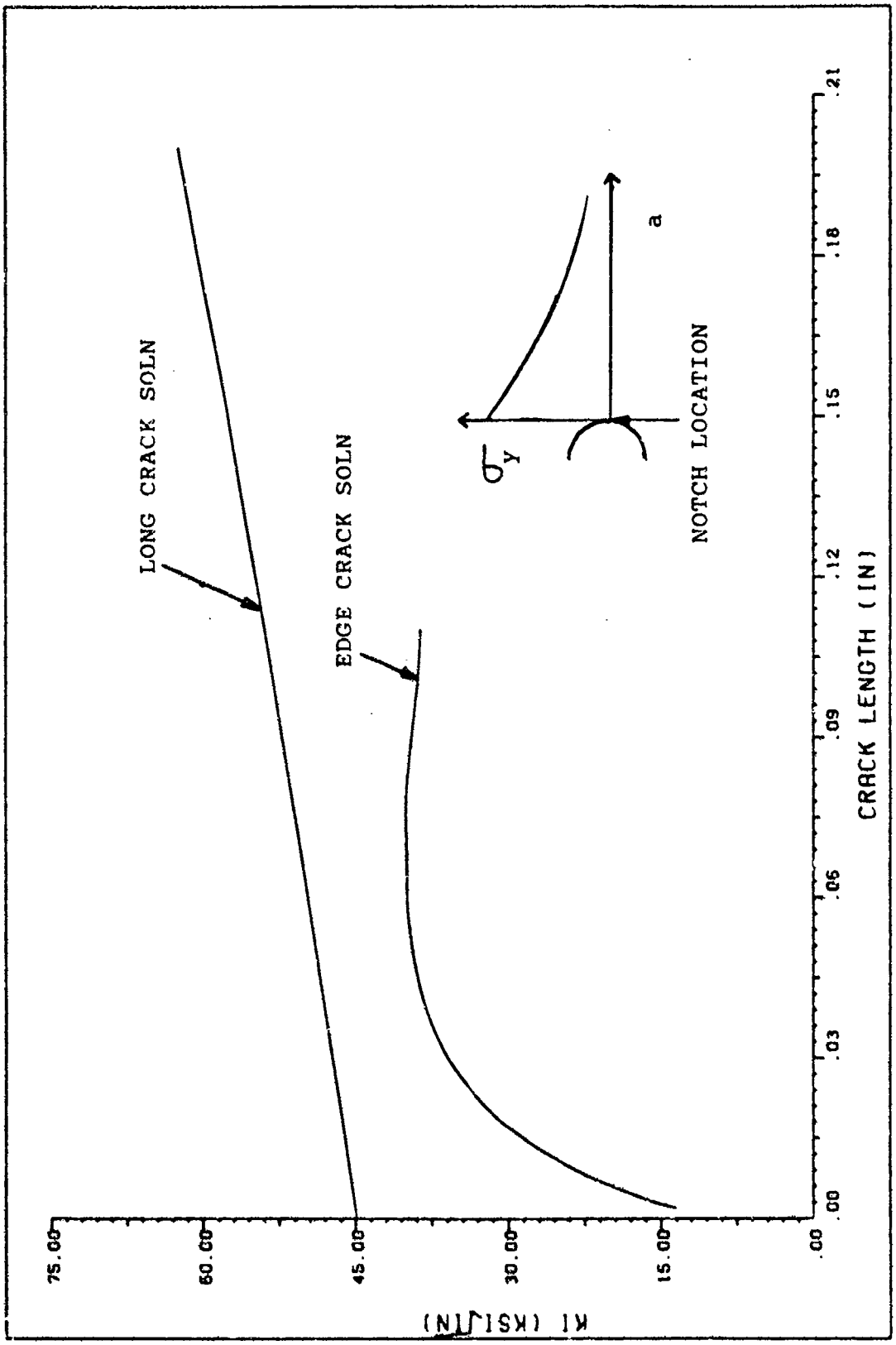

Figure 3.10: Round Notch Stress Intensity Solution Bounds

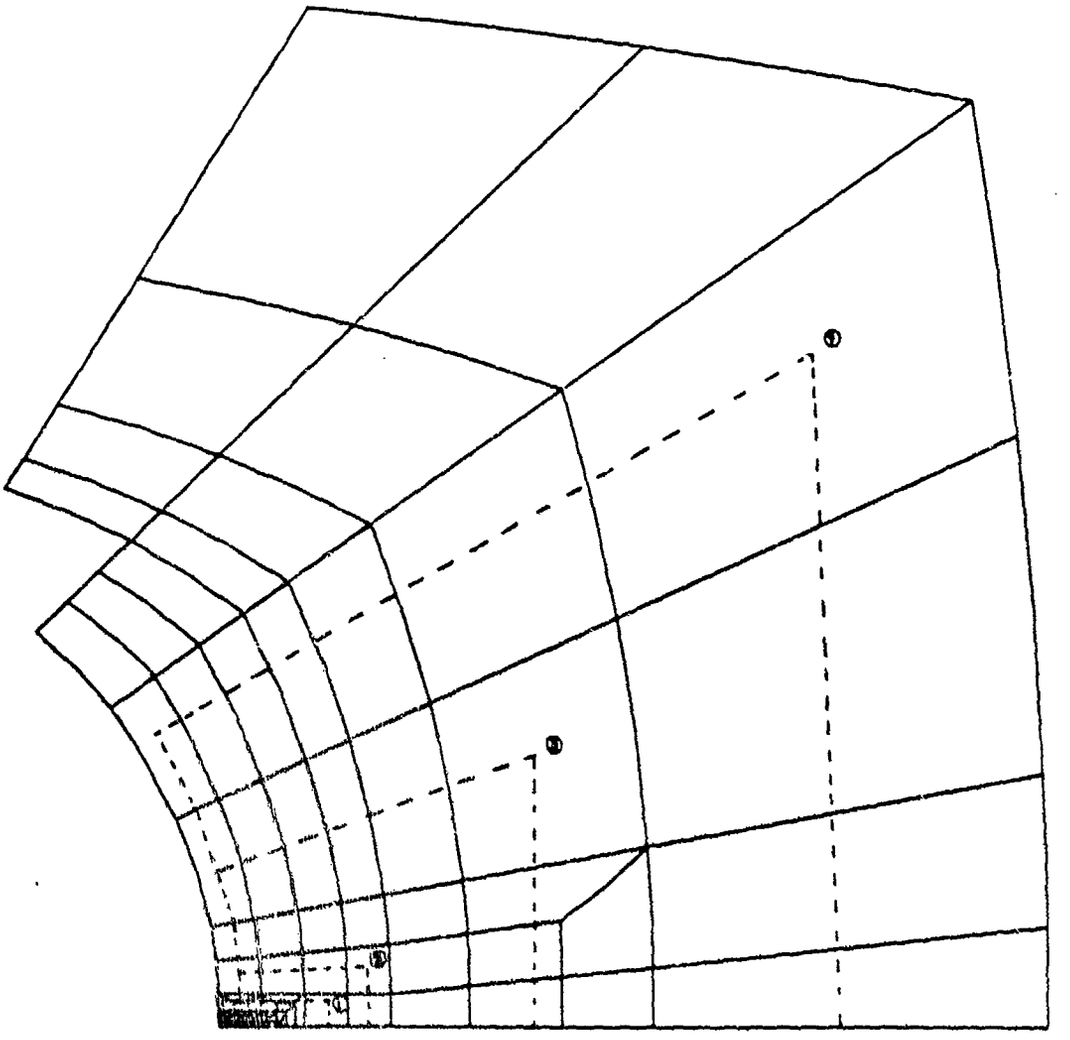

Figure 3.11: J-Integral Paths

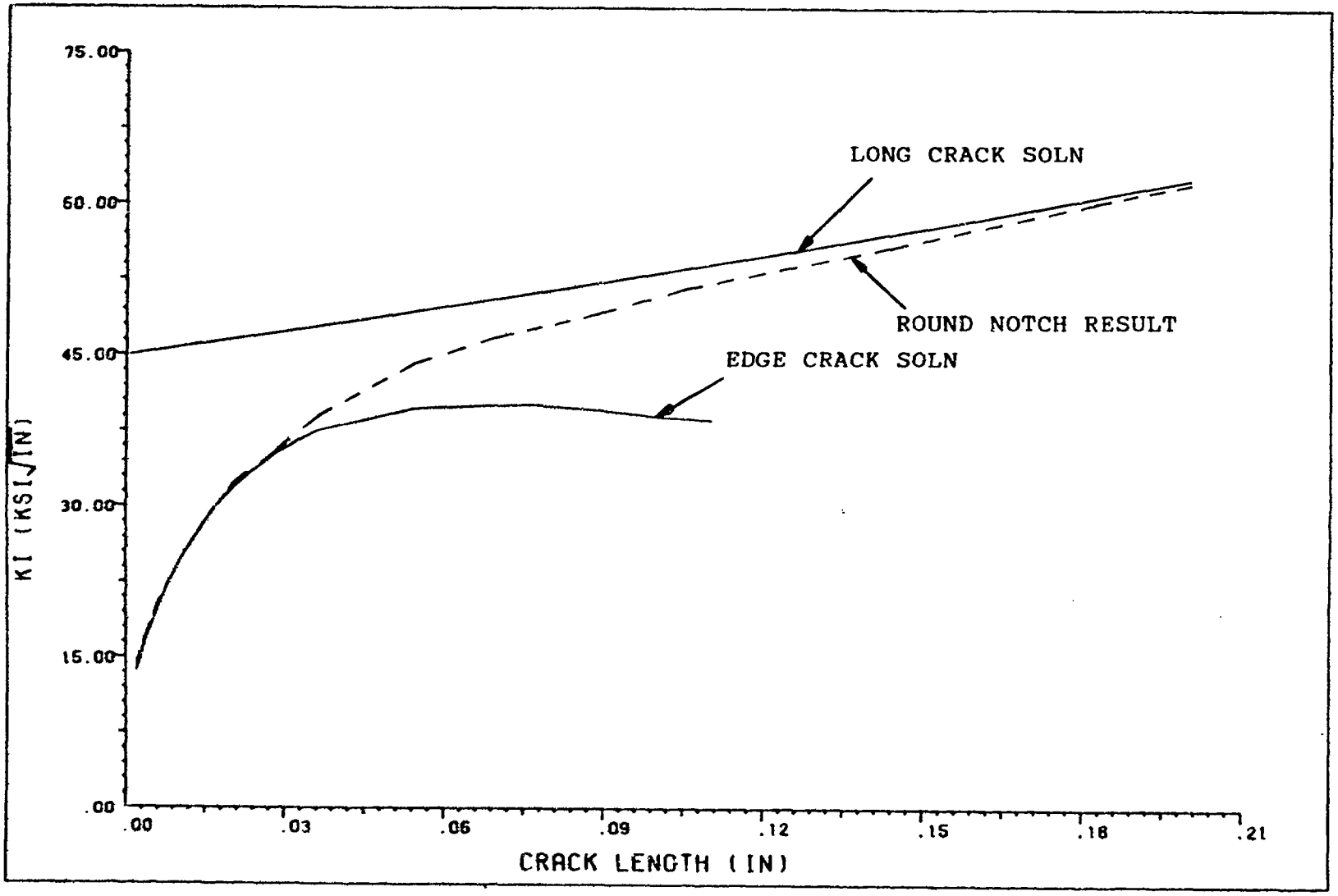

Figure 3.12: Stress Intensity Solution for Round Notch using J-Integral

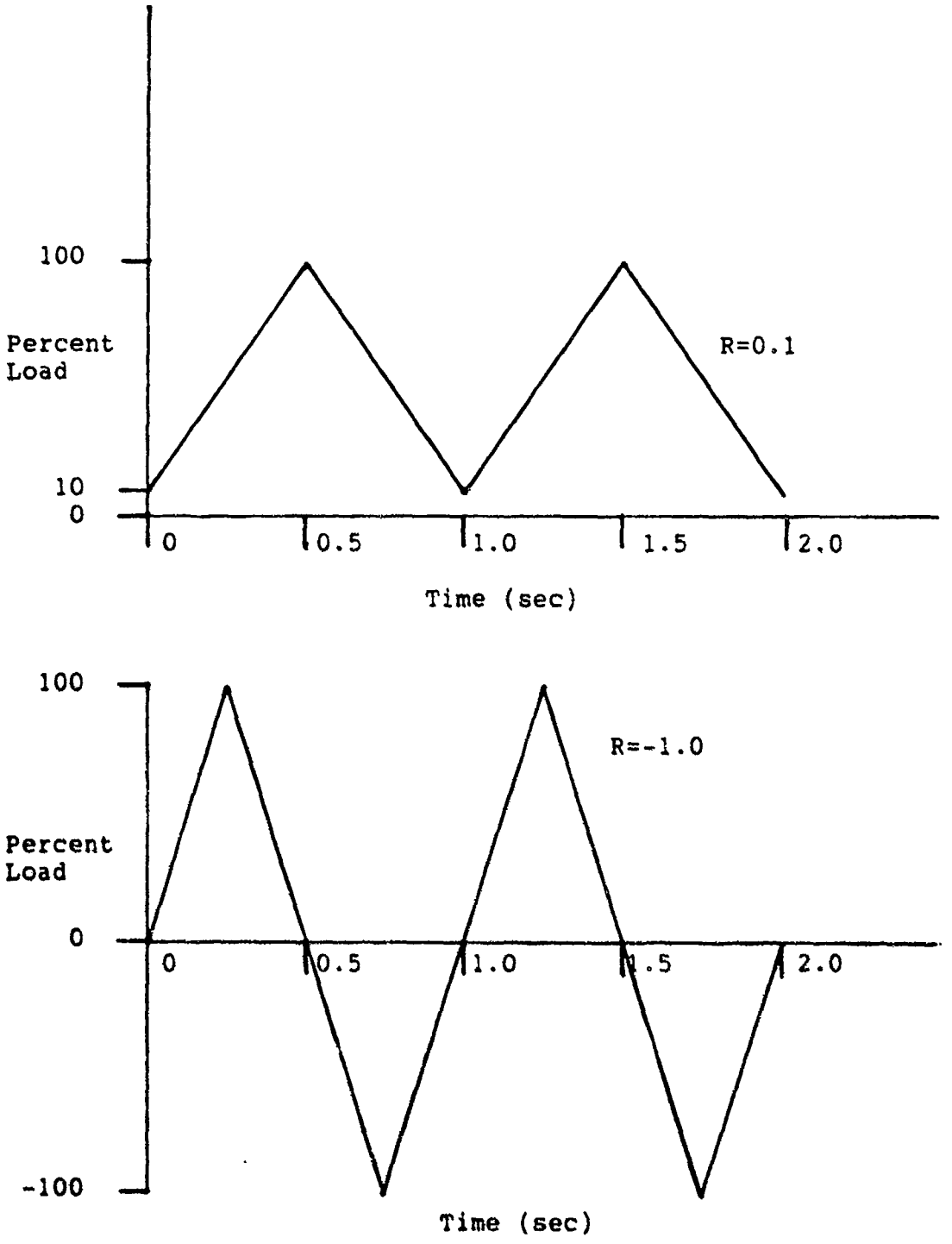

Figure 3.13: Load Ratio Cases Used in Round Notch Study

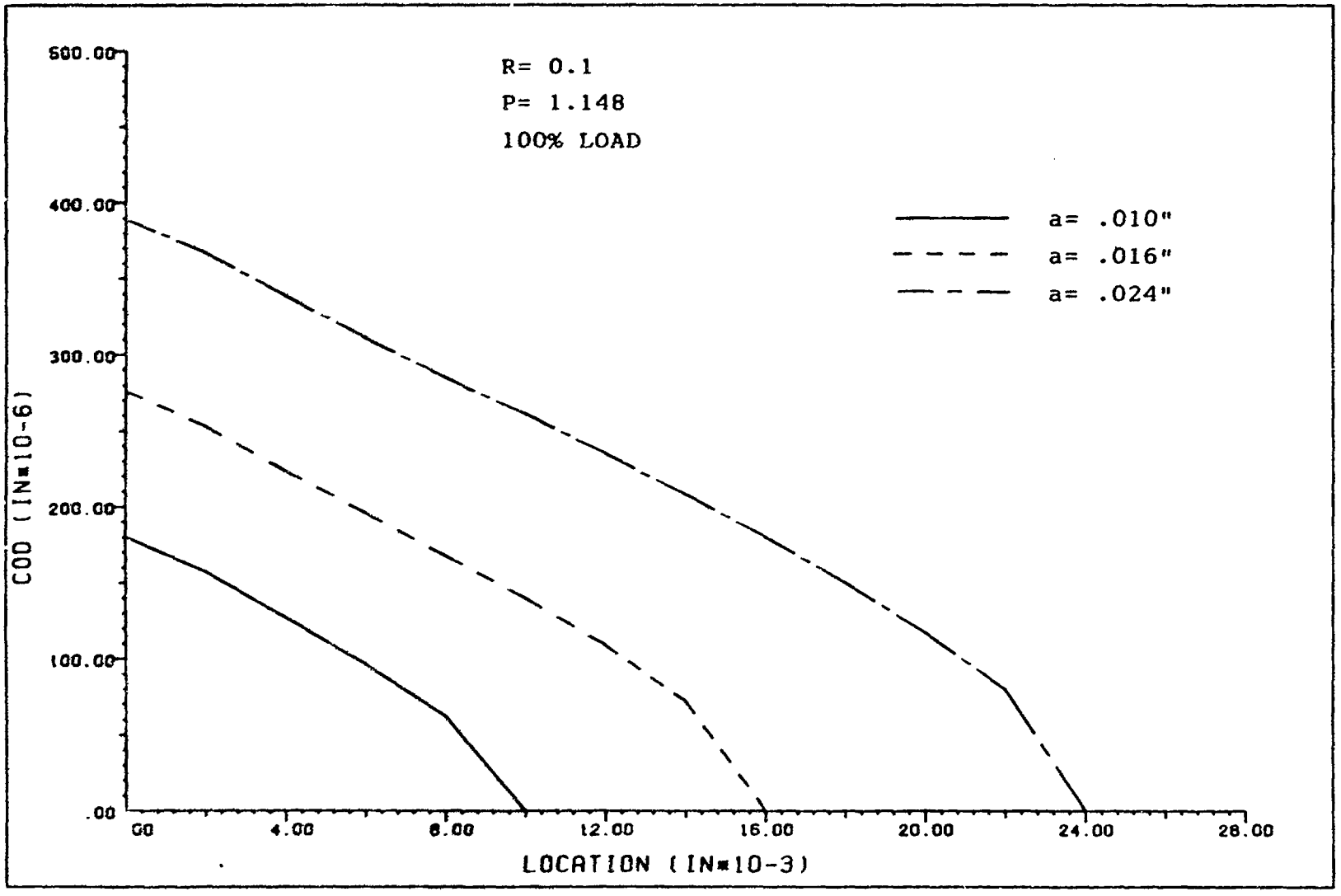

Figure 3.14: Crack Opening Profile, P= 1.148 Kips, R= 0.1, 100% Load

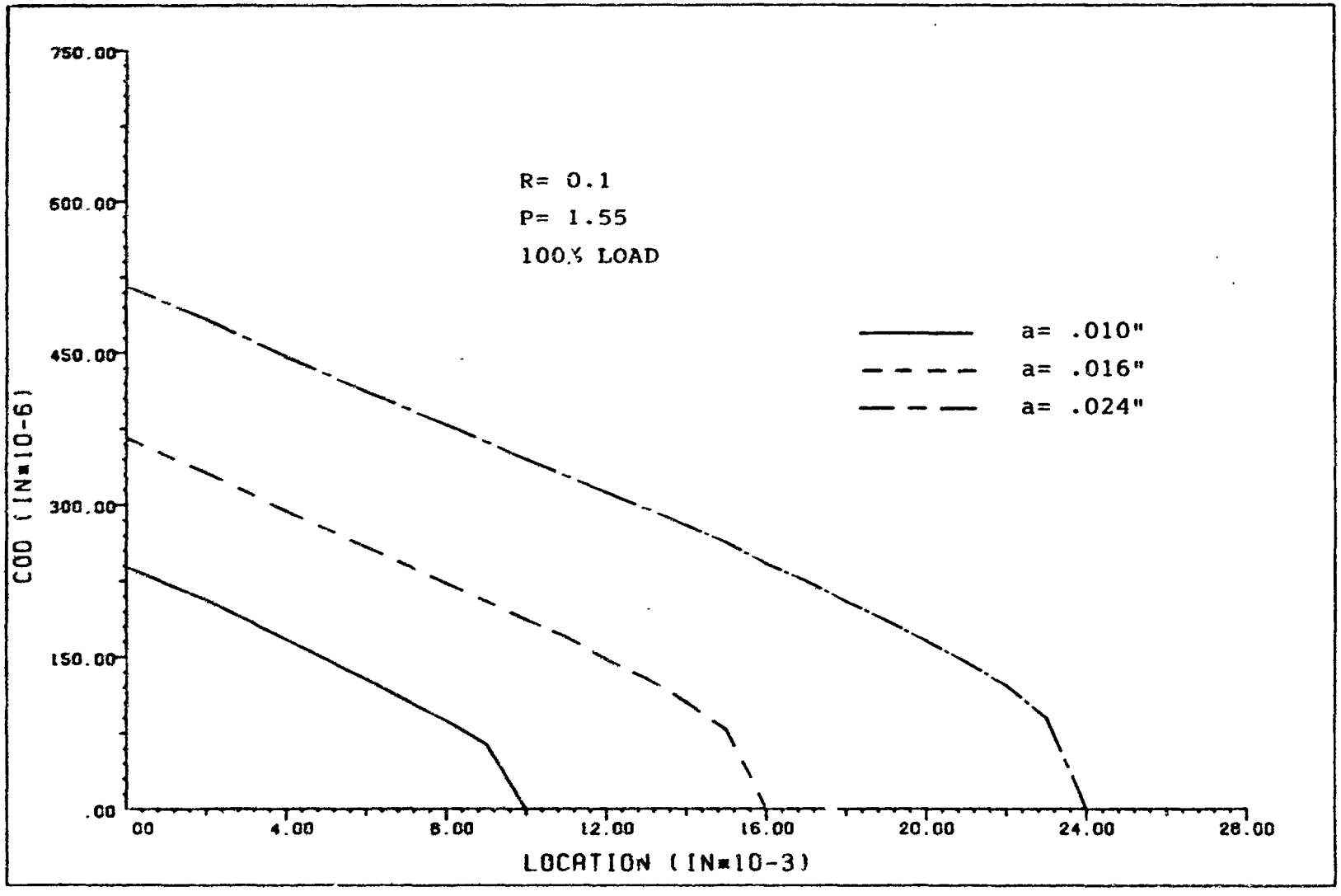

Figure 3.15: Crack Opening Profile, P= 1.55 Kips, R= 0.1, 100% Load

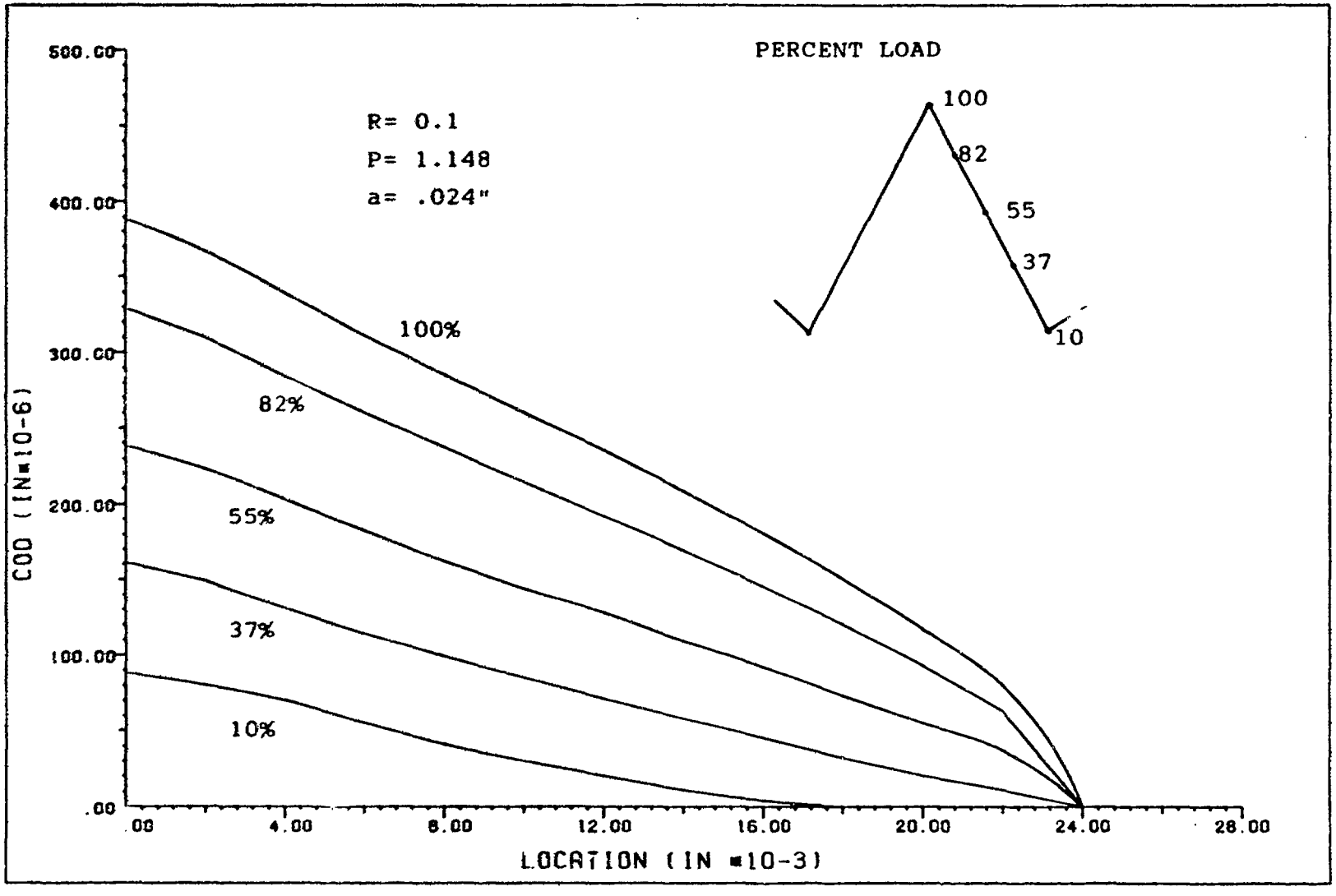

Figure 3.16: Crack Opening Profile at Partial Loading, a= .024", P= 1.148 Kips, R= 0.1

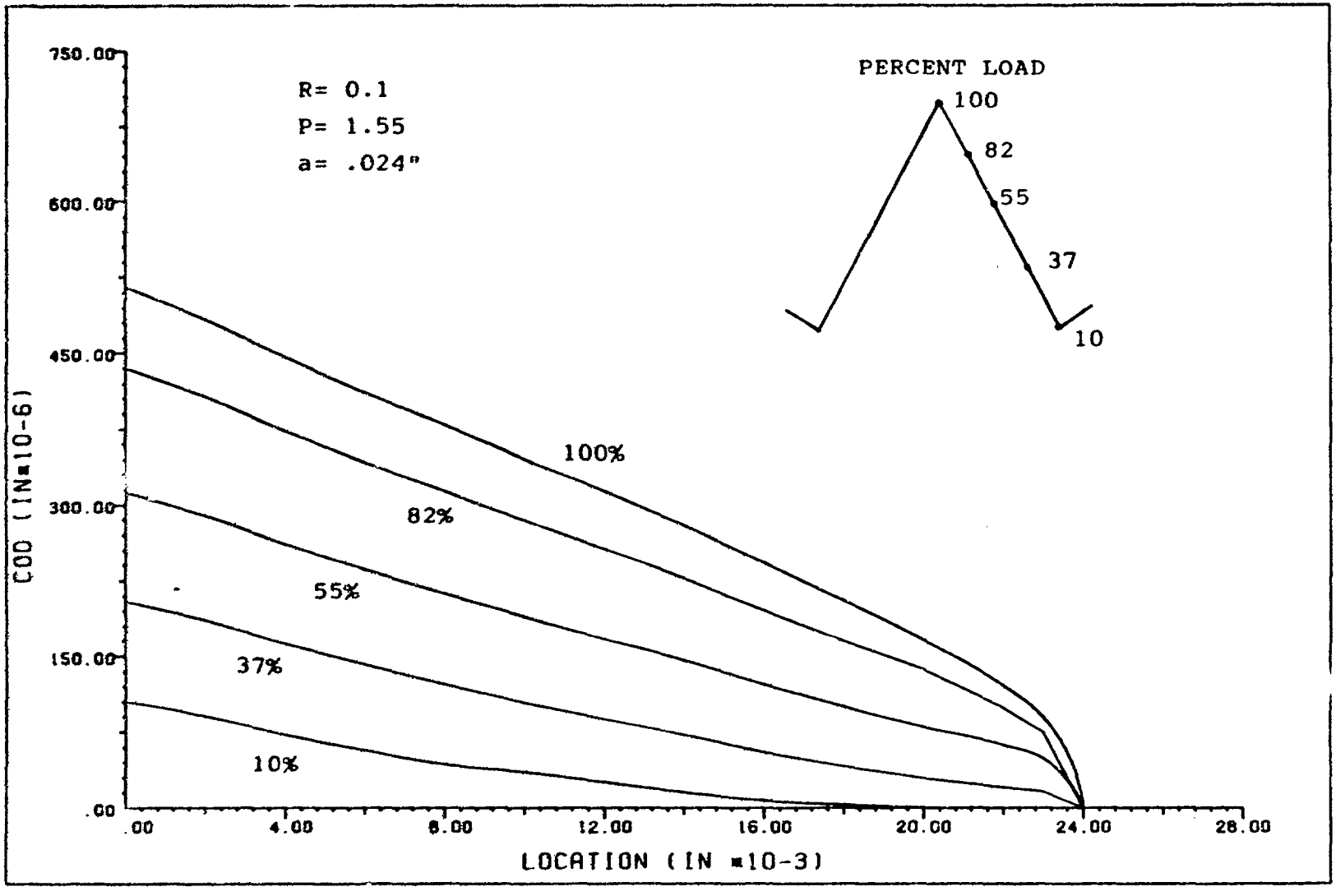

Figure 3.17: Crack Opening Profile at Partial Loading, a= .024", P= 1.55 Kips, R= 0.1

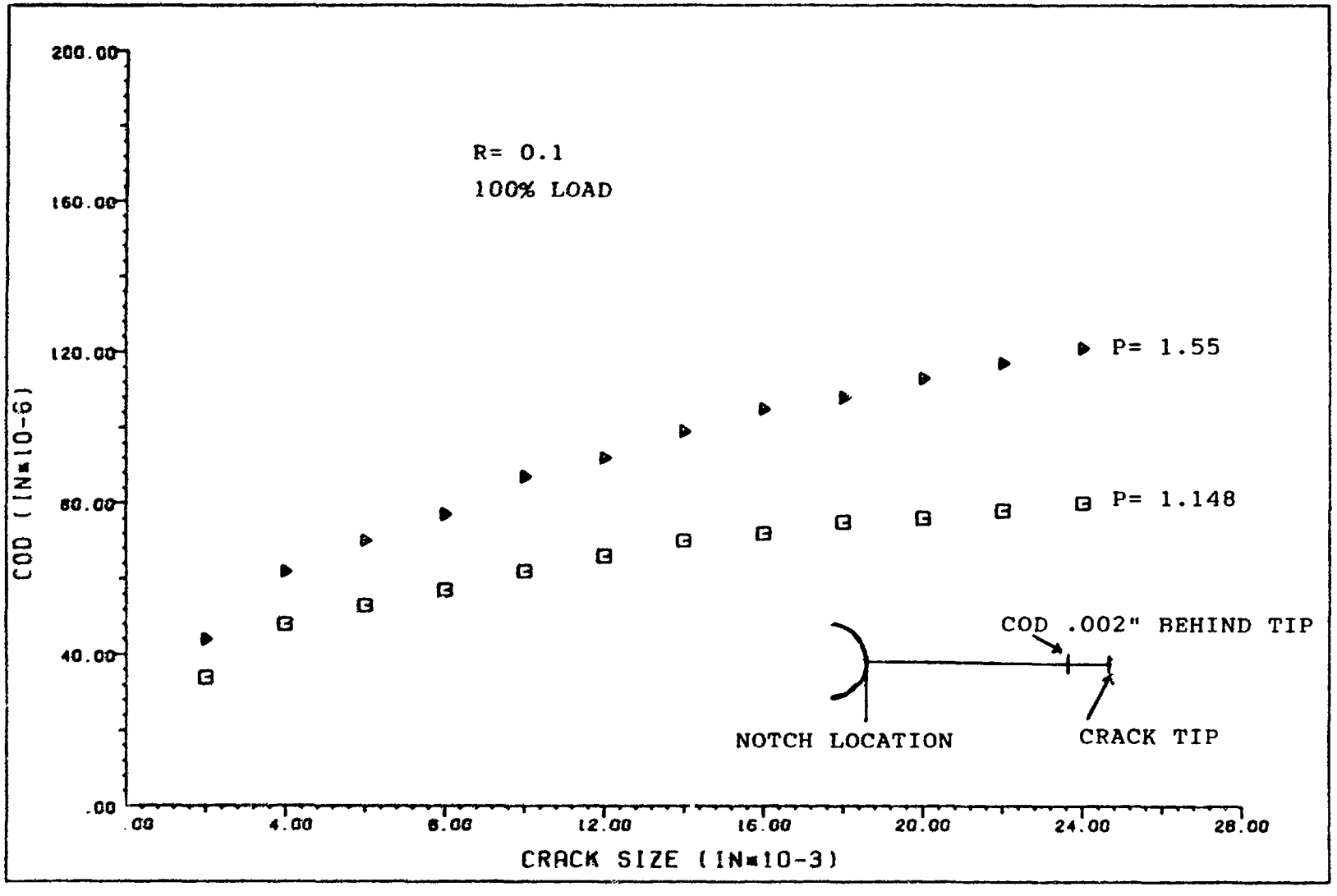

Figure 3.18: Crack Opening Displacement versus Crack Size for P= 1.148 and P= 1.55 Kips, R= 0.1, 100% Load

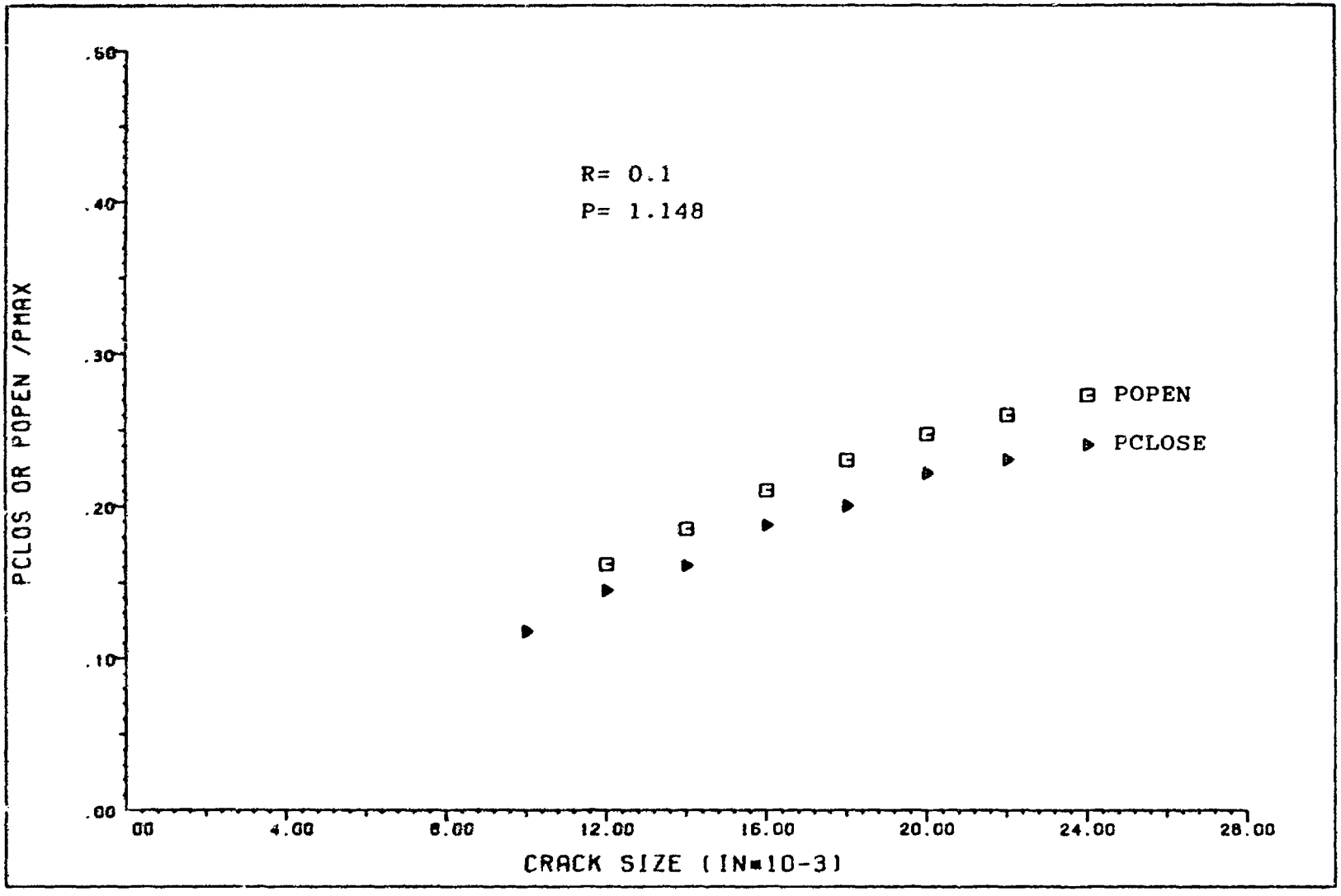

Figure 3.19: Closure Load, Closure .002" Behind Crack Tip, P= 1.148 Kips, R= 0.1

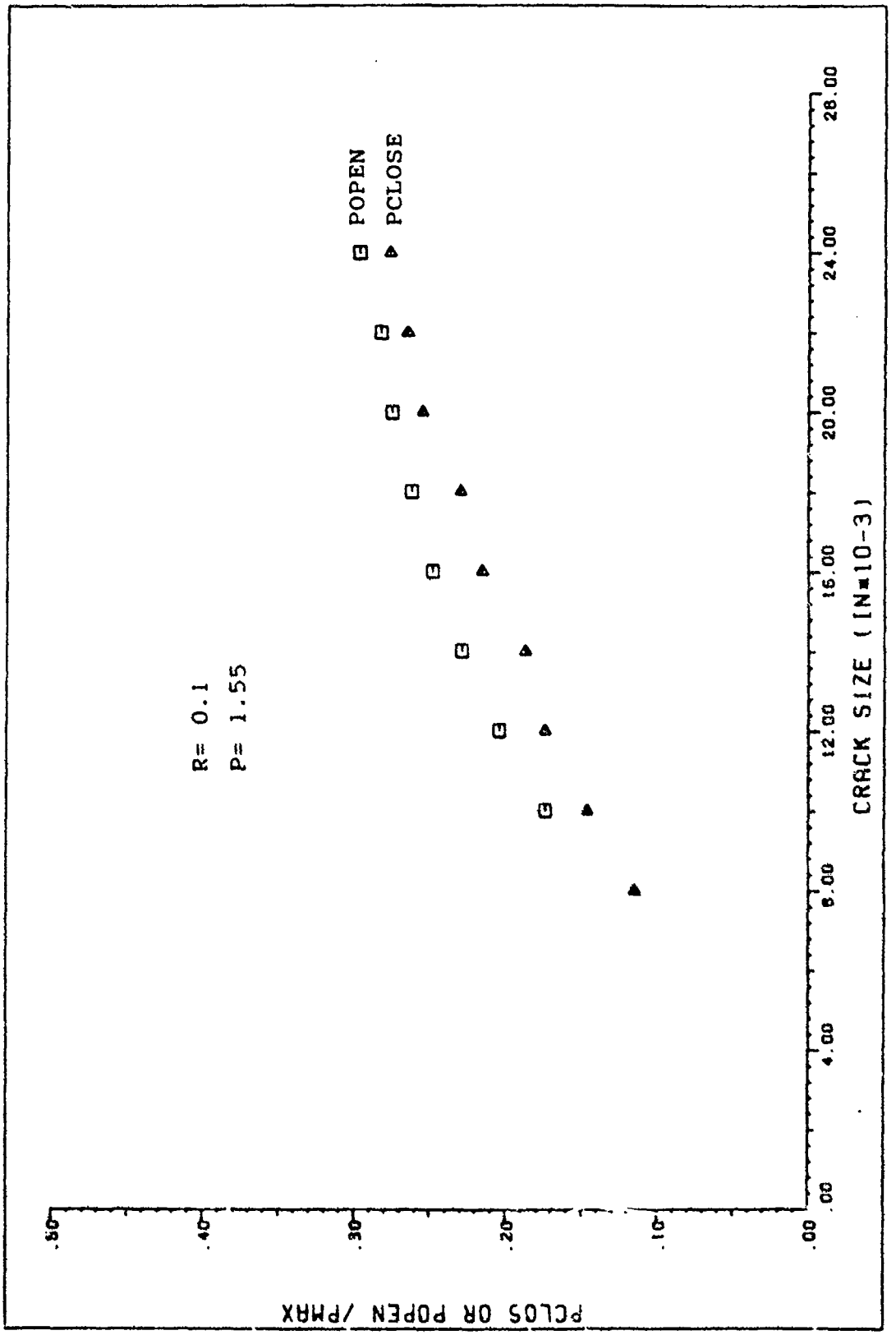

Figure 3.20: Closure Load, Closure .002" Behind Crack Tip, P= 1.55 Kips, R= 0.1

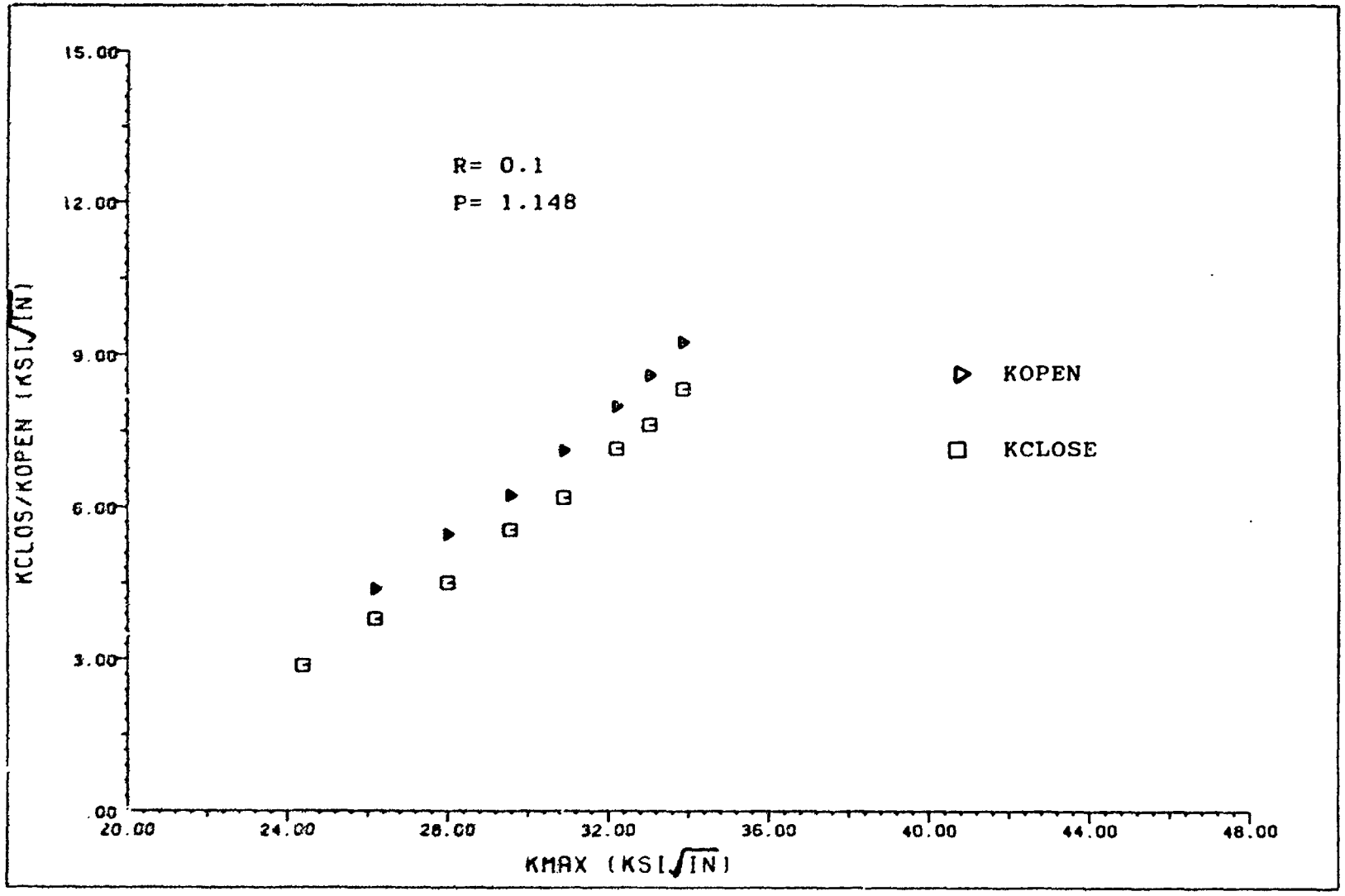

Figure 3.21: Closure .002" Behind Crack Tip versus Maximum Stress Intensity, P= 1.148 Kips, R= 0.1

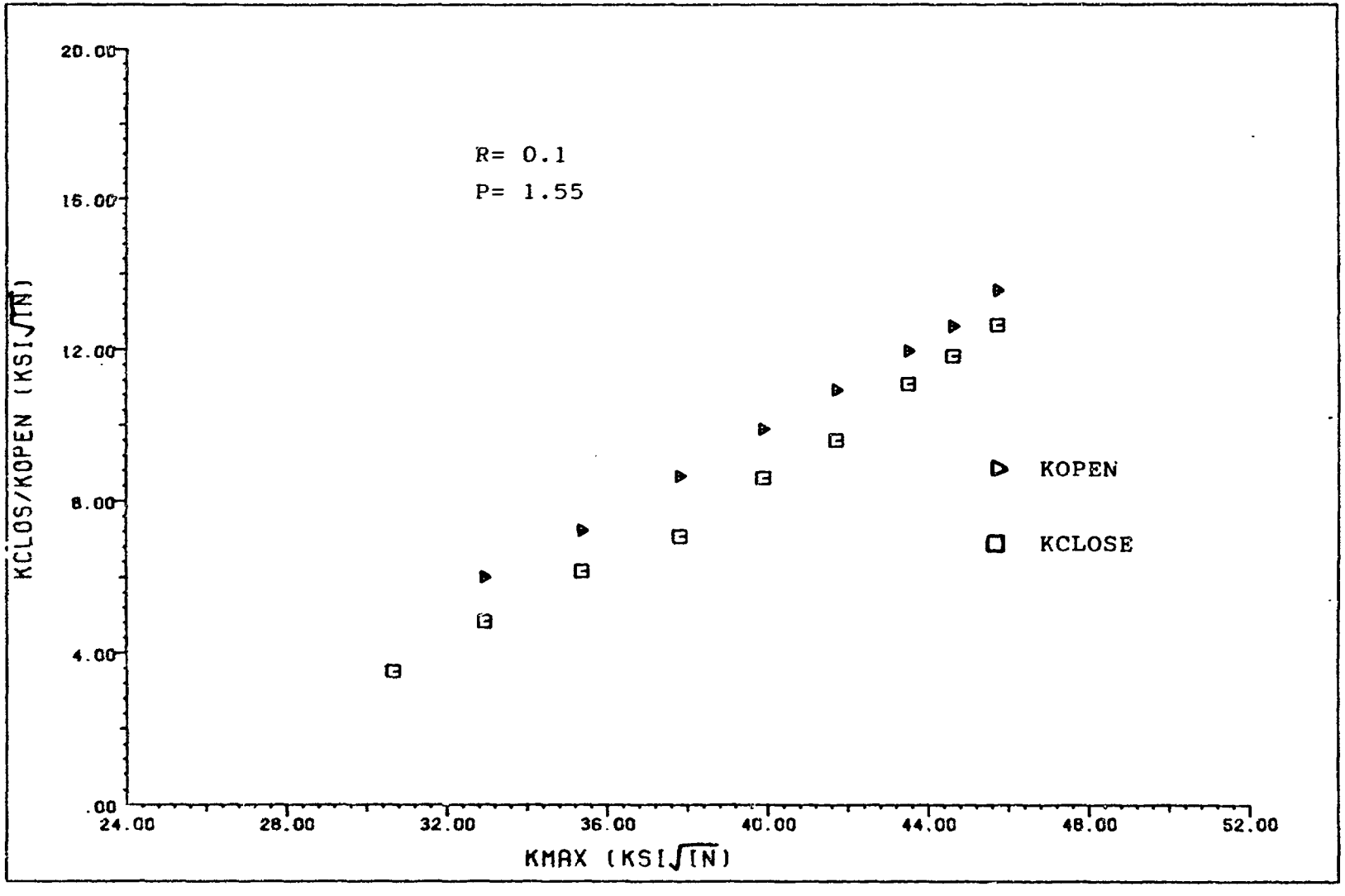

Figure 3.22: Closure .002" Behind Crack Tip versus Maximum Stress Intensity, P= 1.55 Kips, R= 0.1

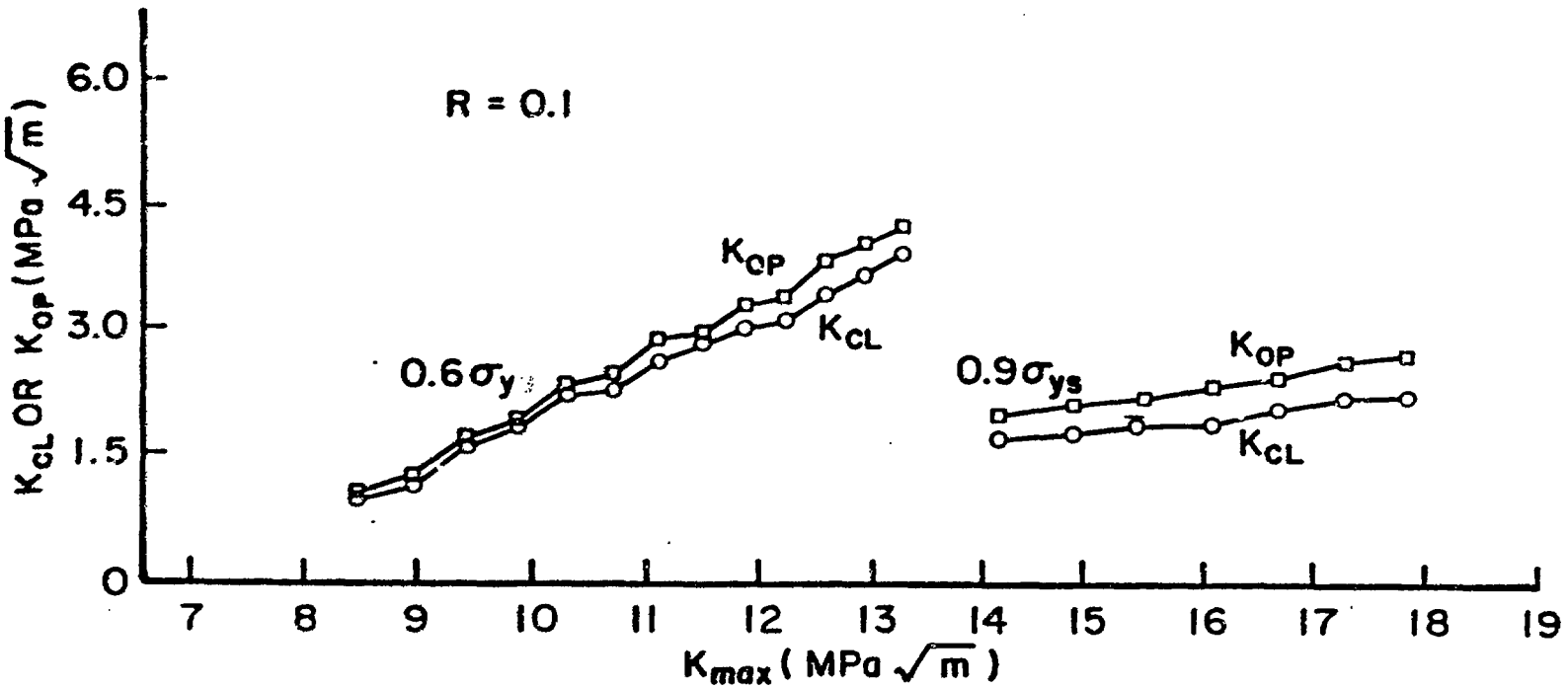

Figure 3.23: Crack Closure Stress Intensities for Single-Edge-Cracked Specimen (Ref. 5), R= 0.1

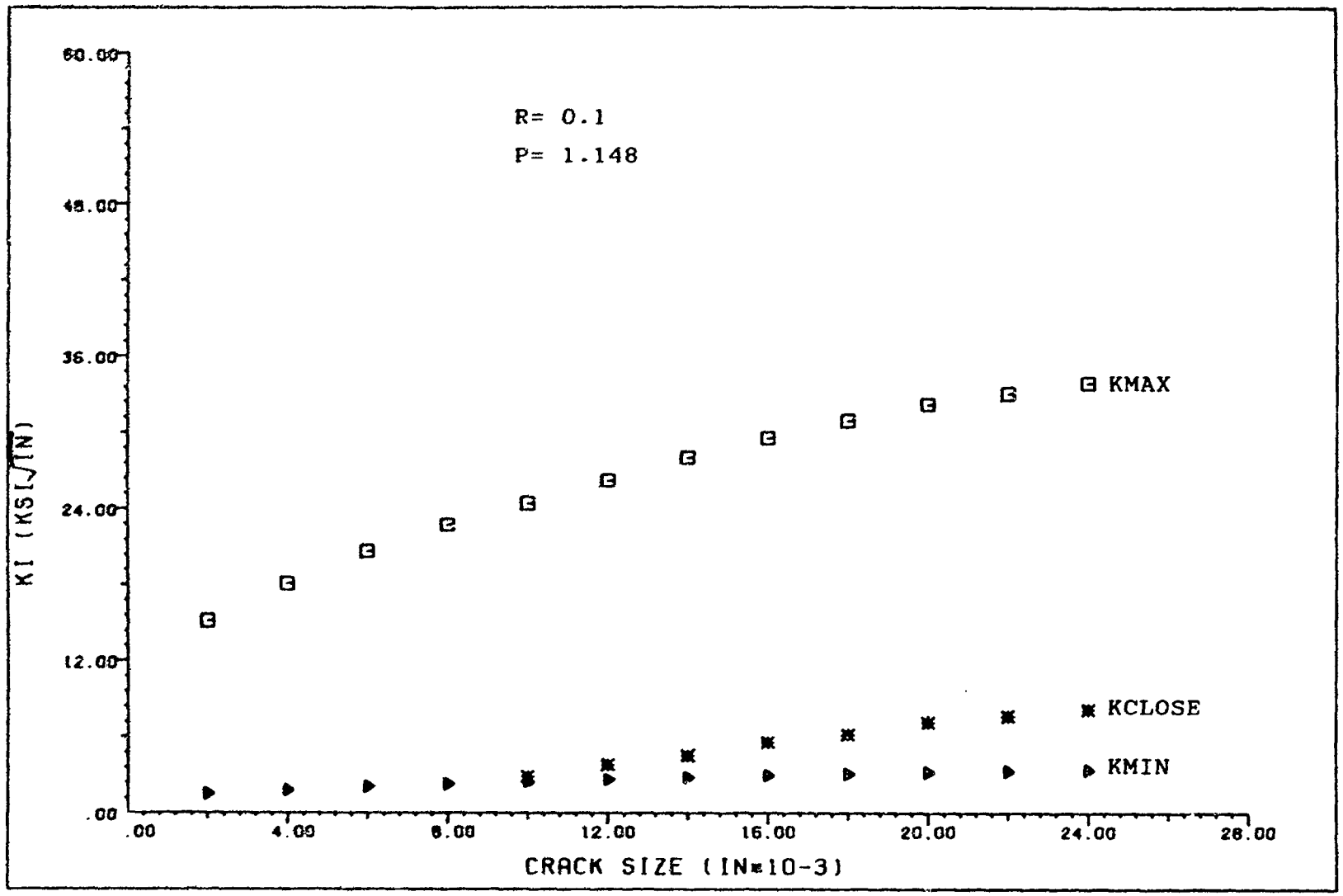

Figure 3.24: Stress Intensity versus Crack Size, P= 1.148 Kips, R= 0.1

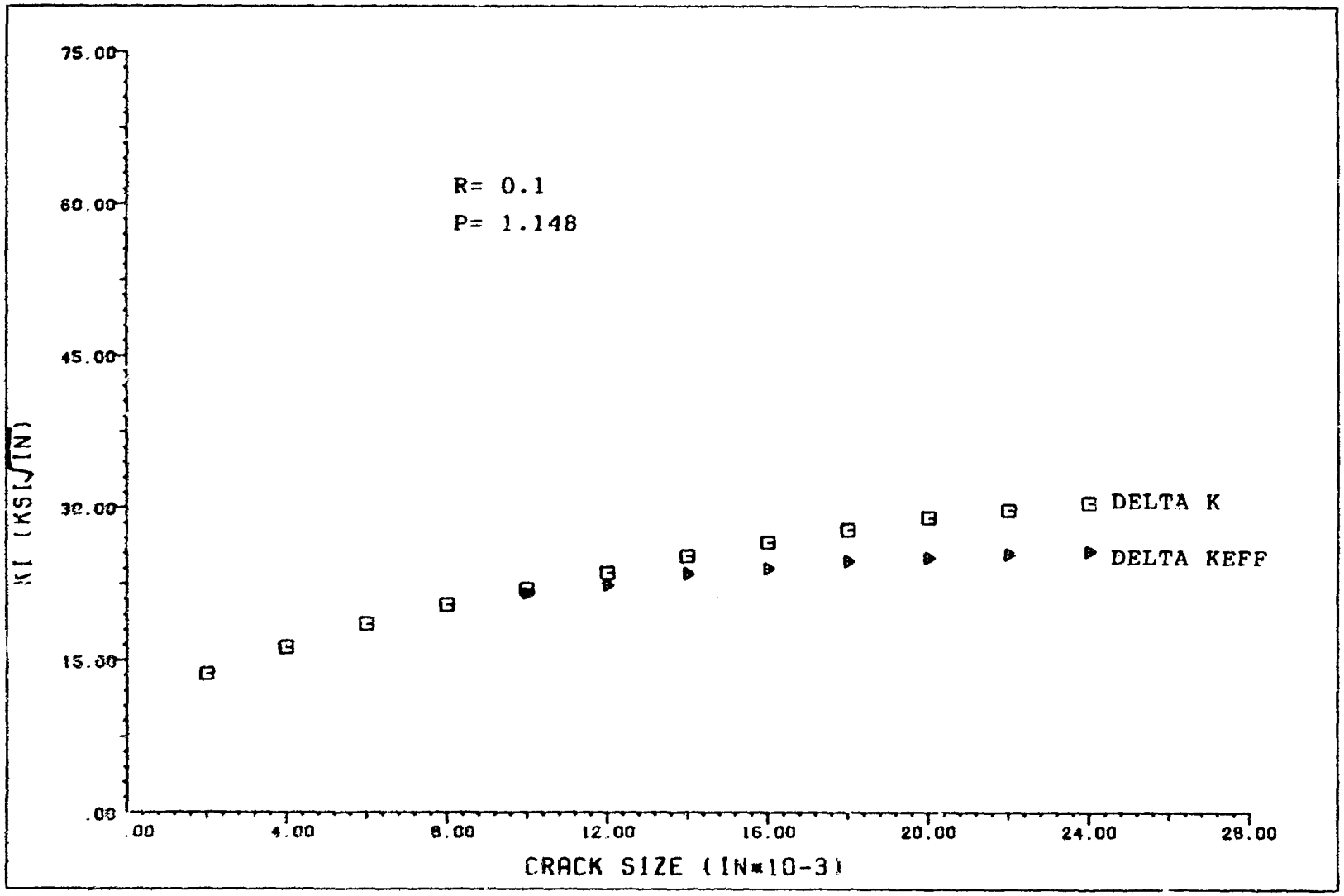

Figure 3.25: Stress Intensity Ranges versus Crack Size, P= 1.148 Kips, R= 0.1

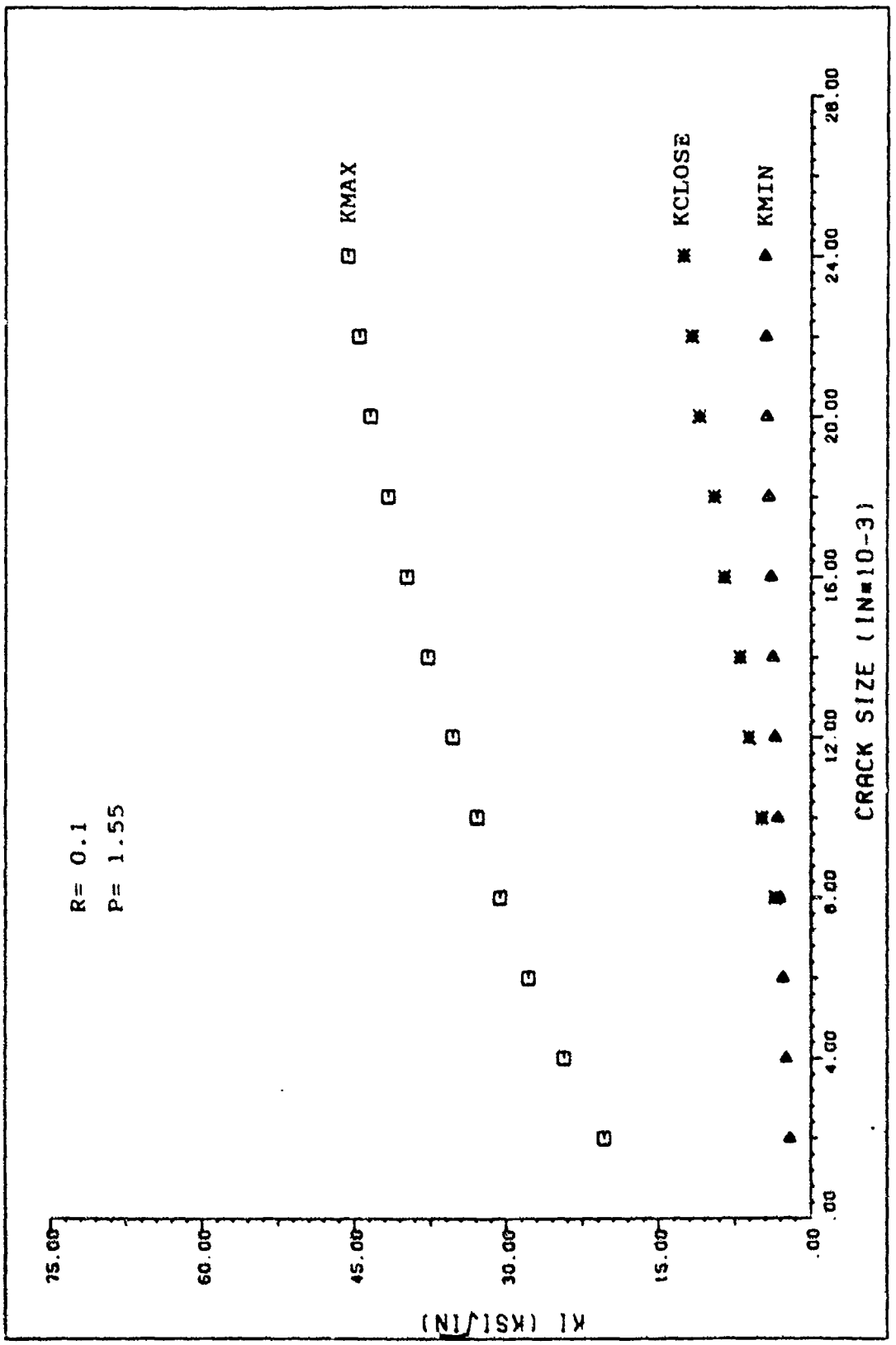

Figure 3.26: Stress Intensity versus Crack Size, P= 1.55 Kips, R= 0.1

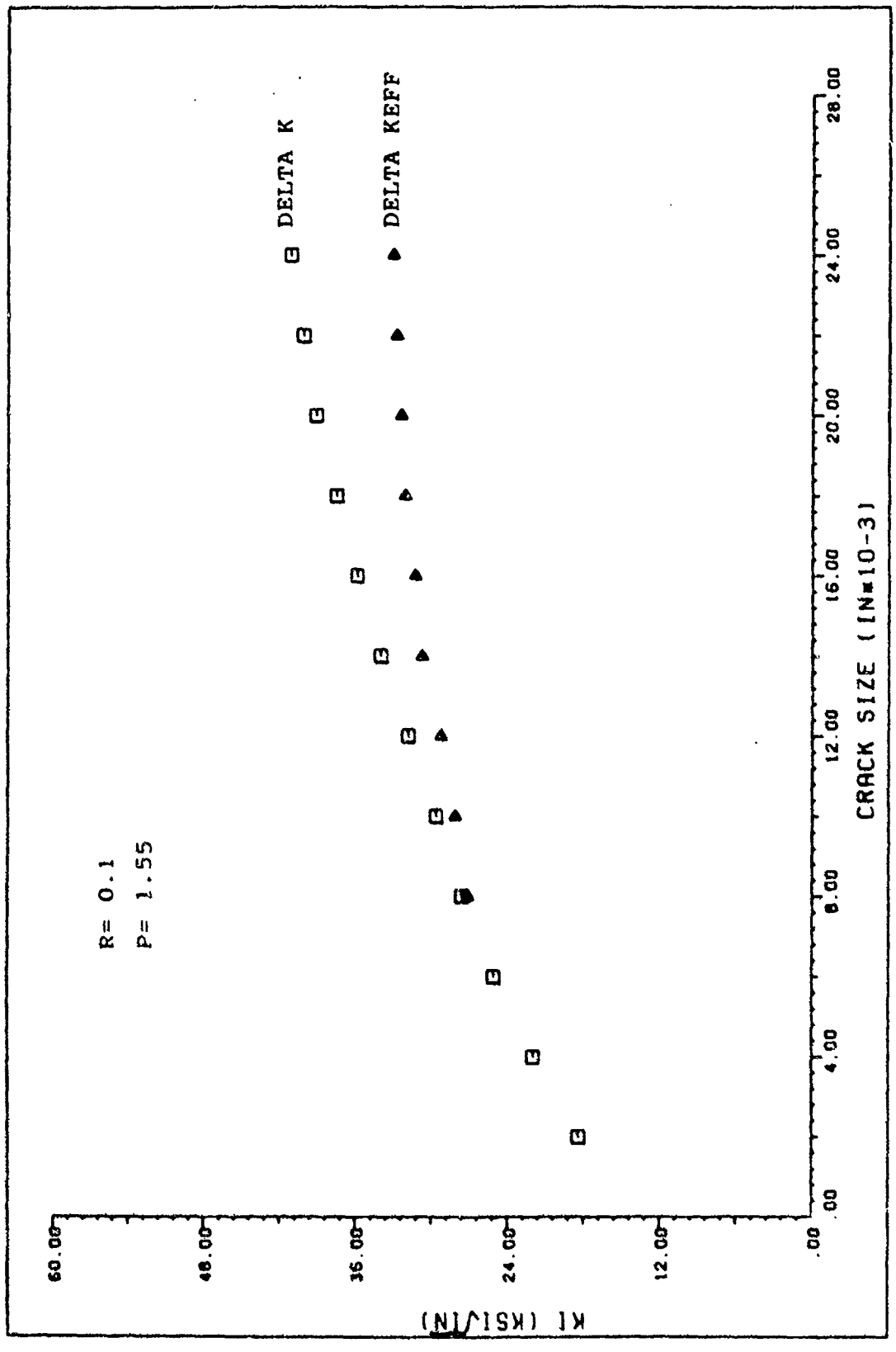

Figure 3.27: Stress Intensity Ranges versus Crack Size, P= 1.55 Kips, R= 0.1

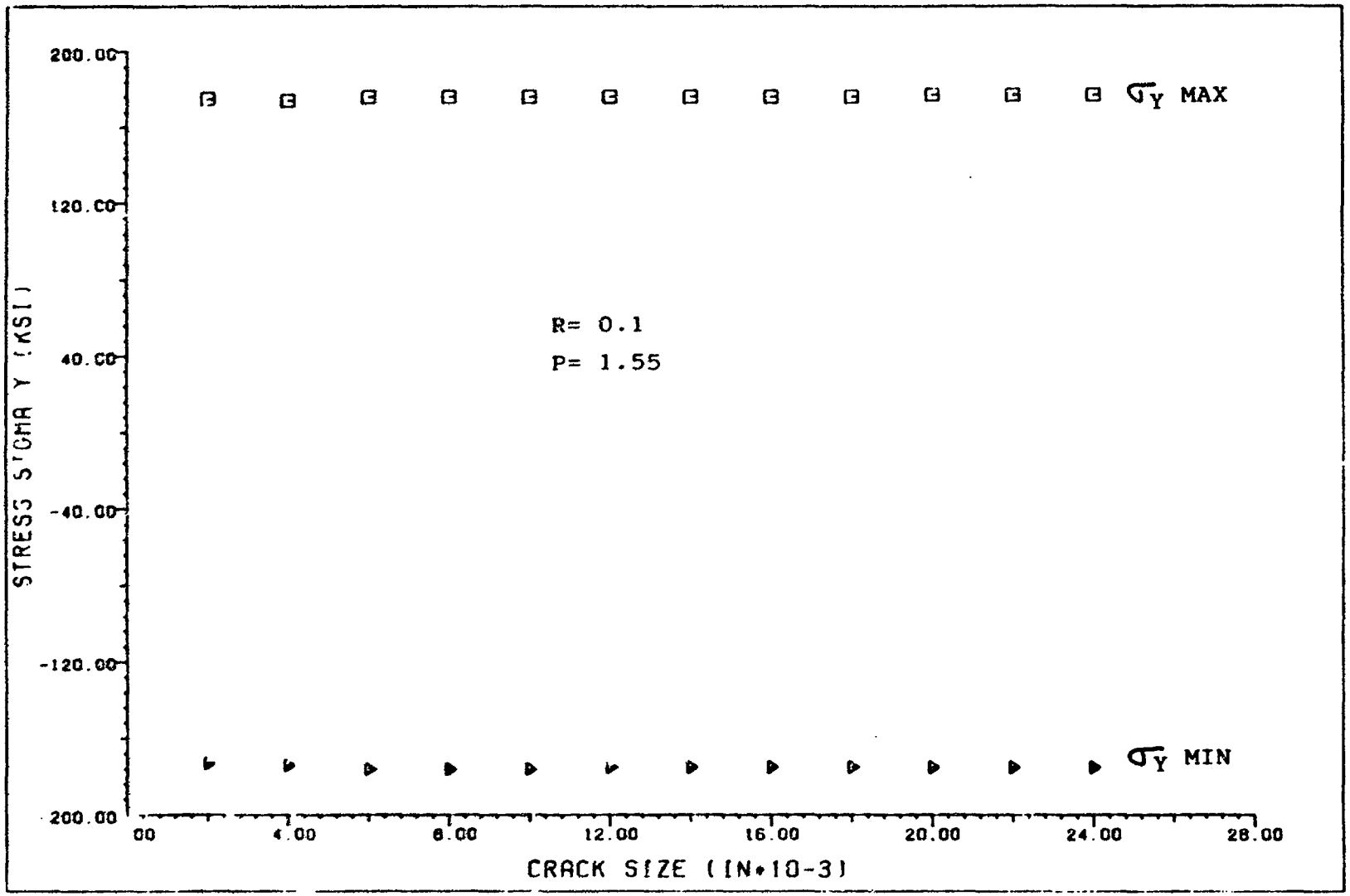

Figure 3.28: Crack Tip Stresses, P= 1.55 Kips, R= 0.1

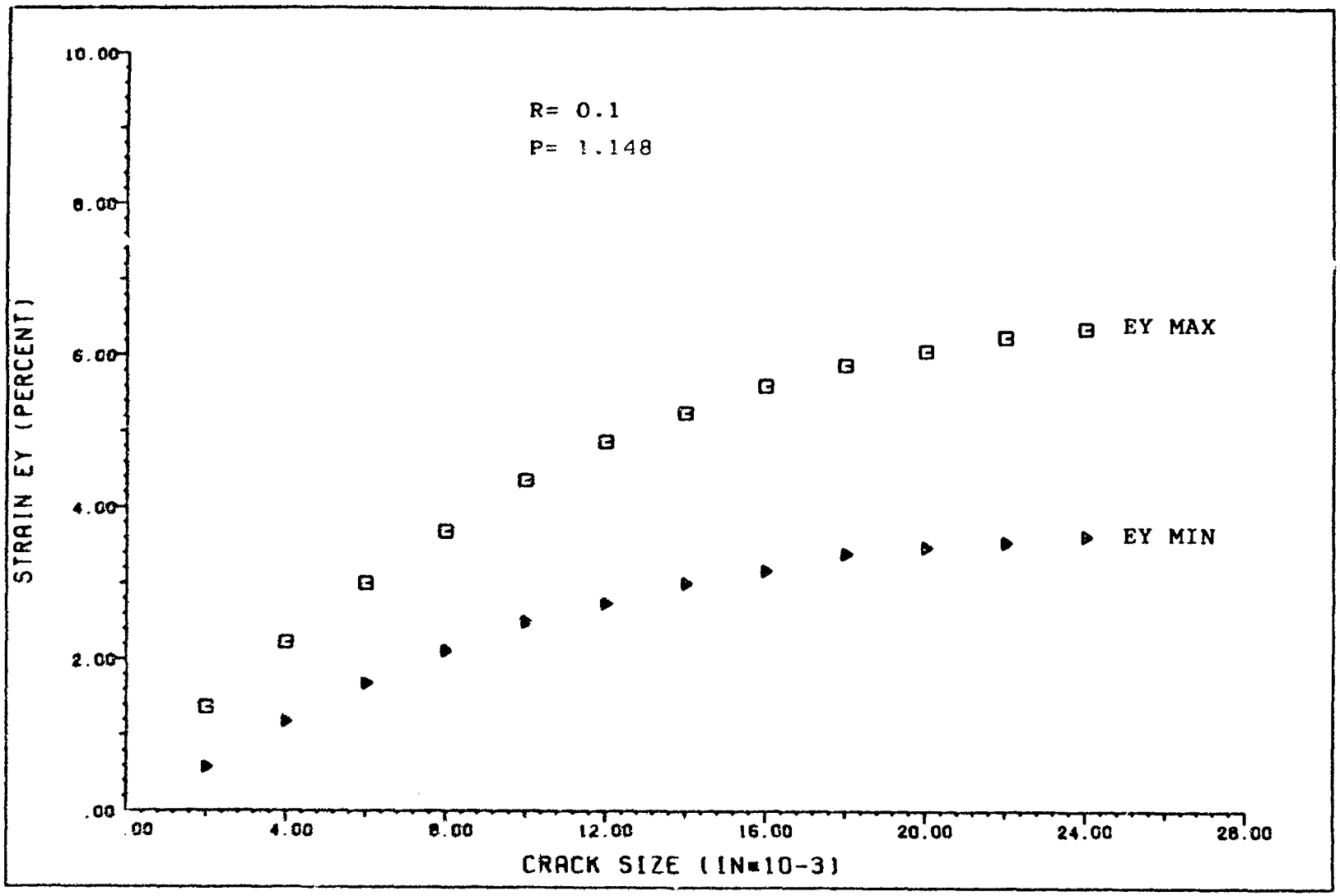

Figure 3.29: Crack Tip Strains, P= 1.148 Kips, R= 0.1

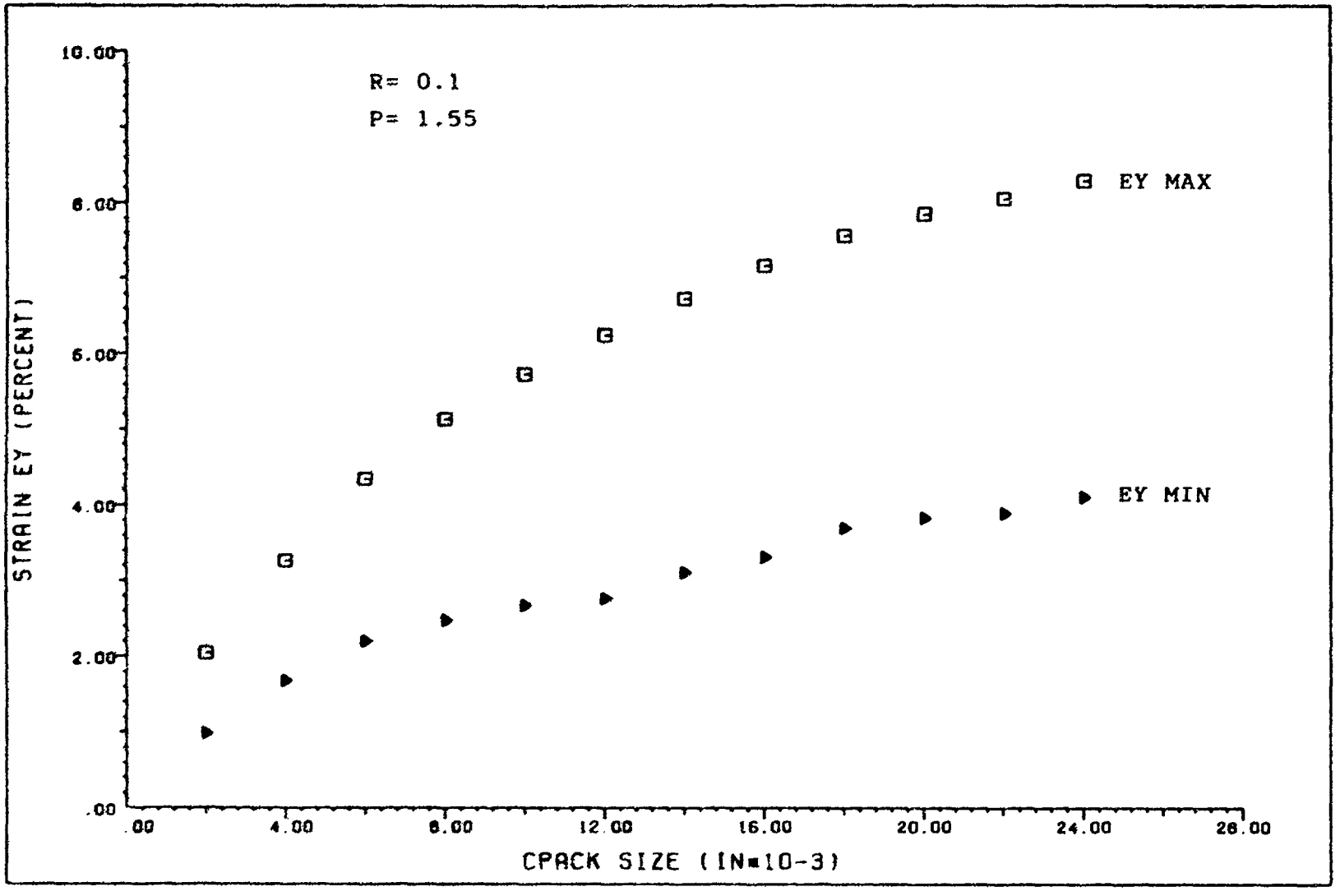

Figure 3.30: Crack Tip Strains, P= 1.55 Kips, R= 0.1

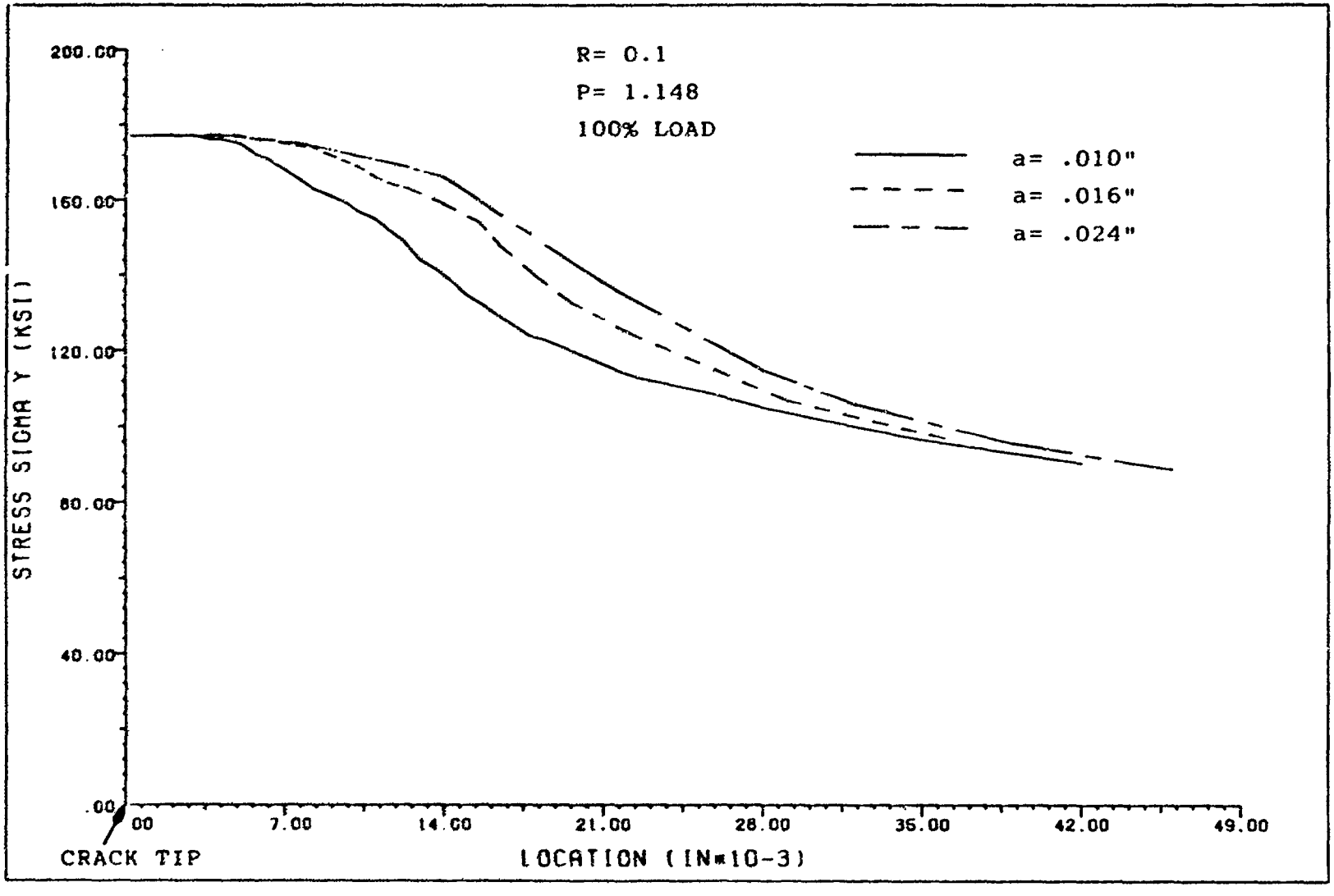

Figure 3.31: Stress Profile Ahead of Crack, P= 1.148 Kips, R= 0.1, 100% Load

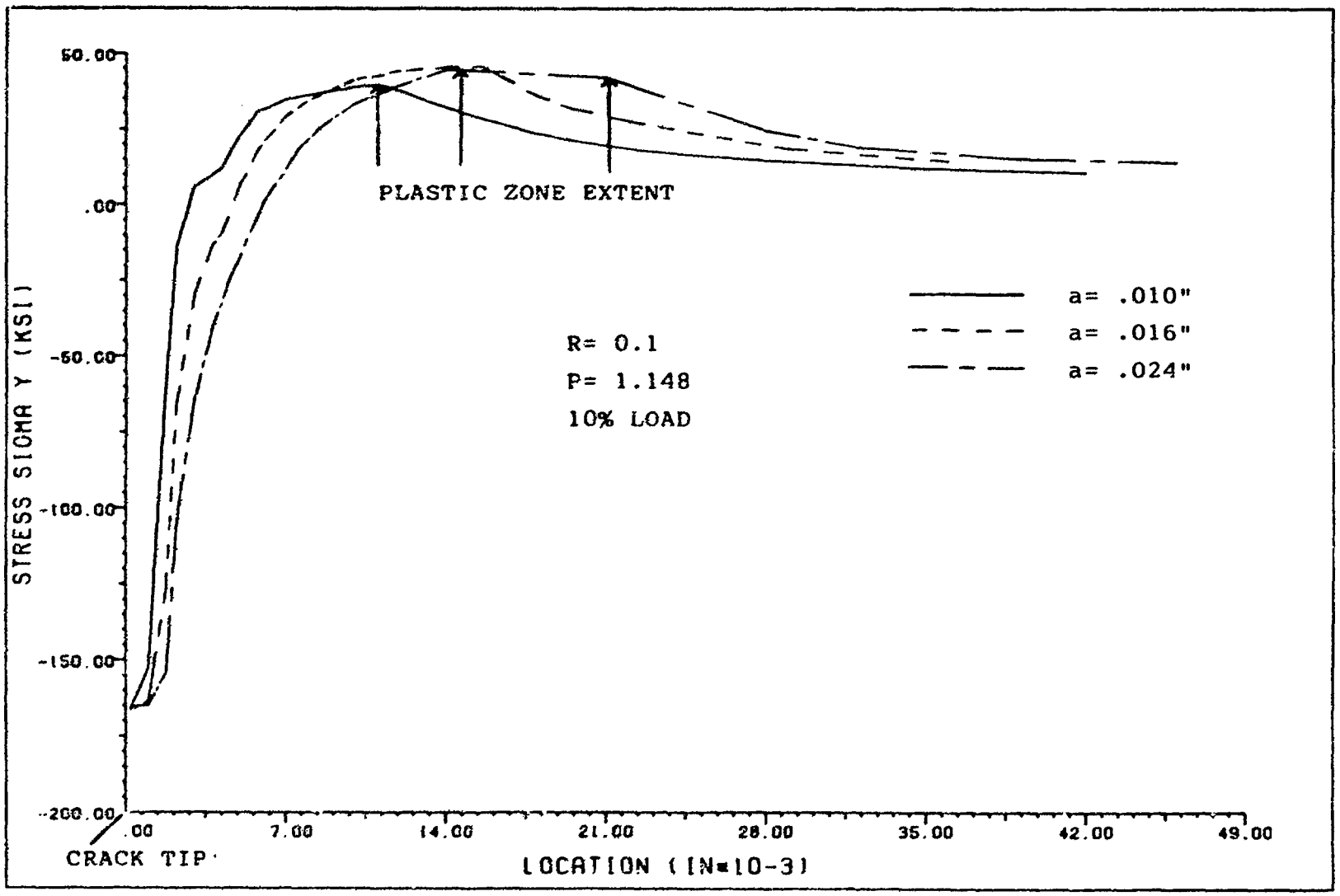

Figure 3.32: Stress Profile Ahead of Crack, P= 1.148 Kips, R= 0.1, 10% Load

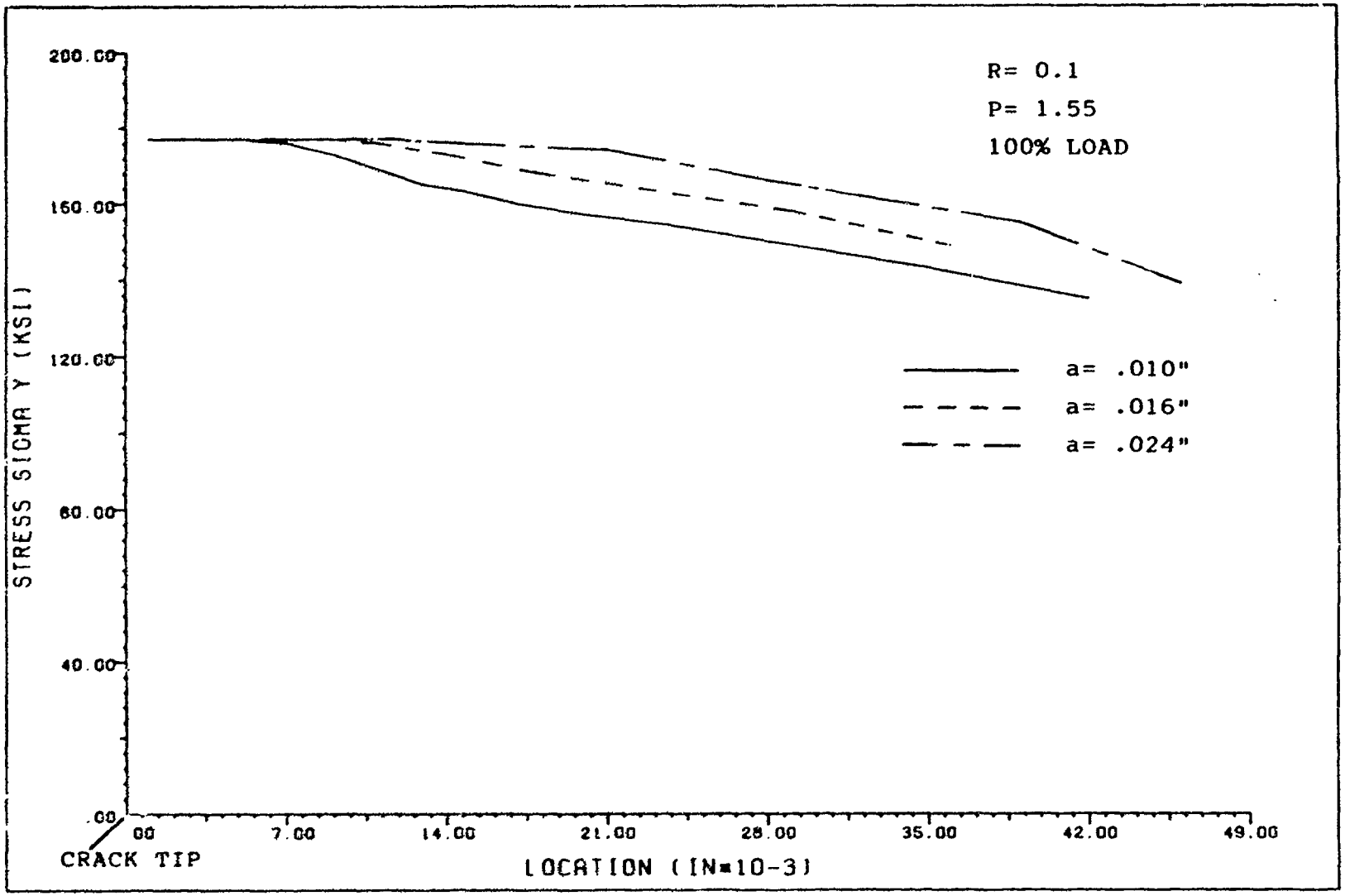

Figure 3.33: Stress Profile Ahead of Crack, P= 1.55 Kips, R= 0.1, 100% Load

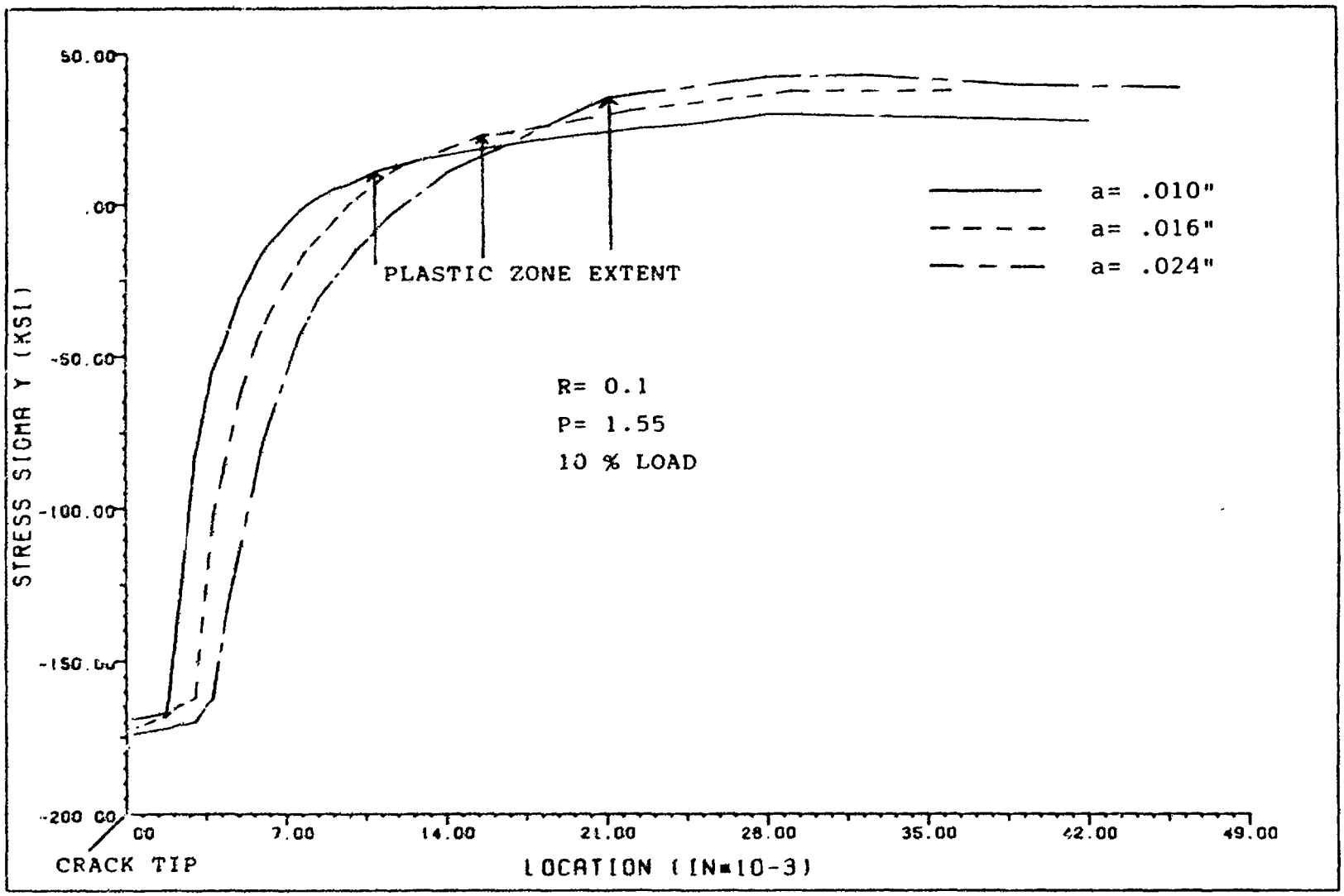

Figure 3.34: Stress Profile Ahead of Crack, P= 1.55 Kips, R= 0.1, 10% Load

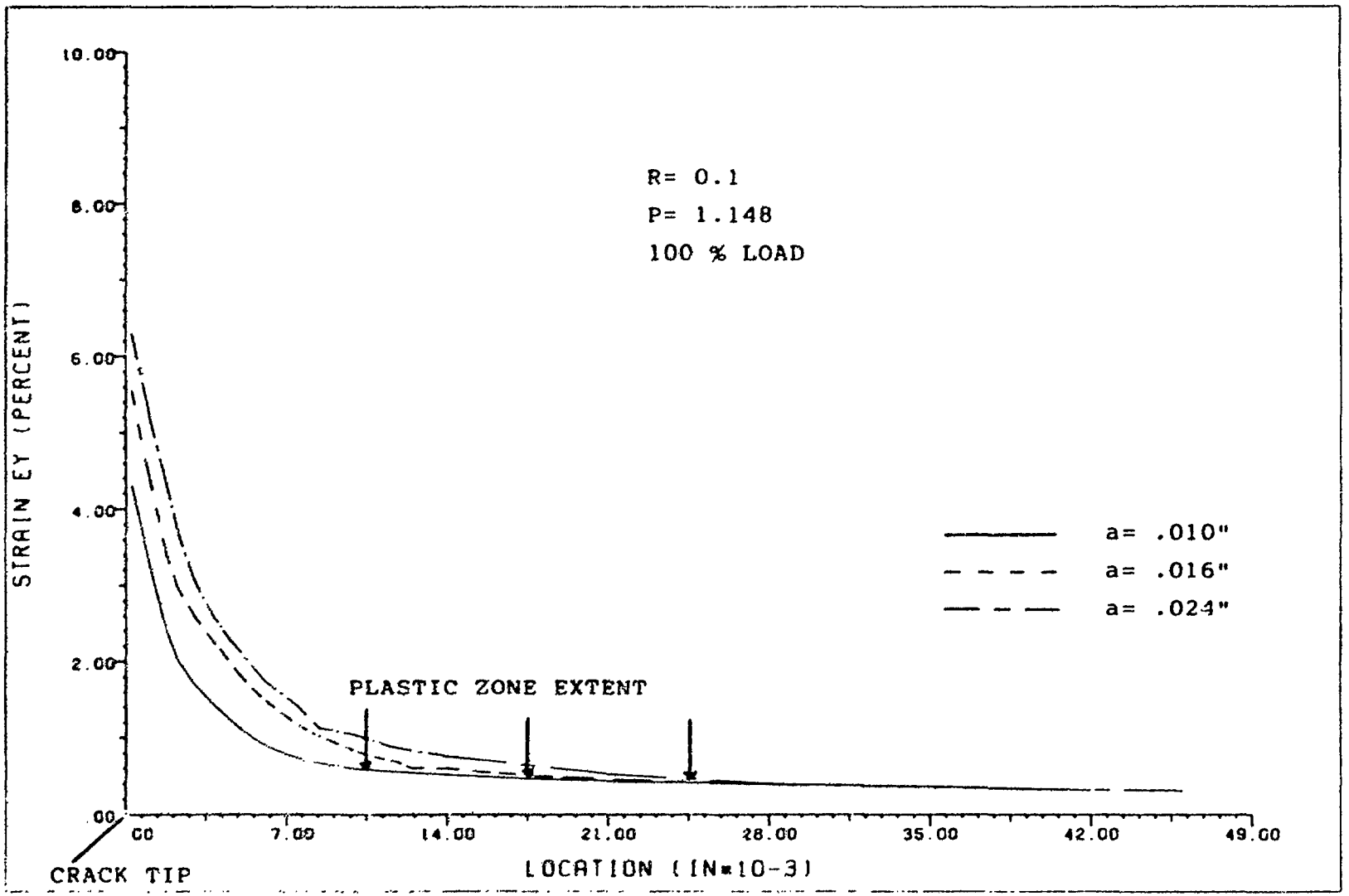

Figure 3.35: Strain Profile Ahead of Crack, P= 1.148 Kips, R= 0.1, 100% Load

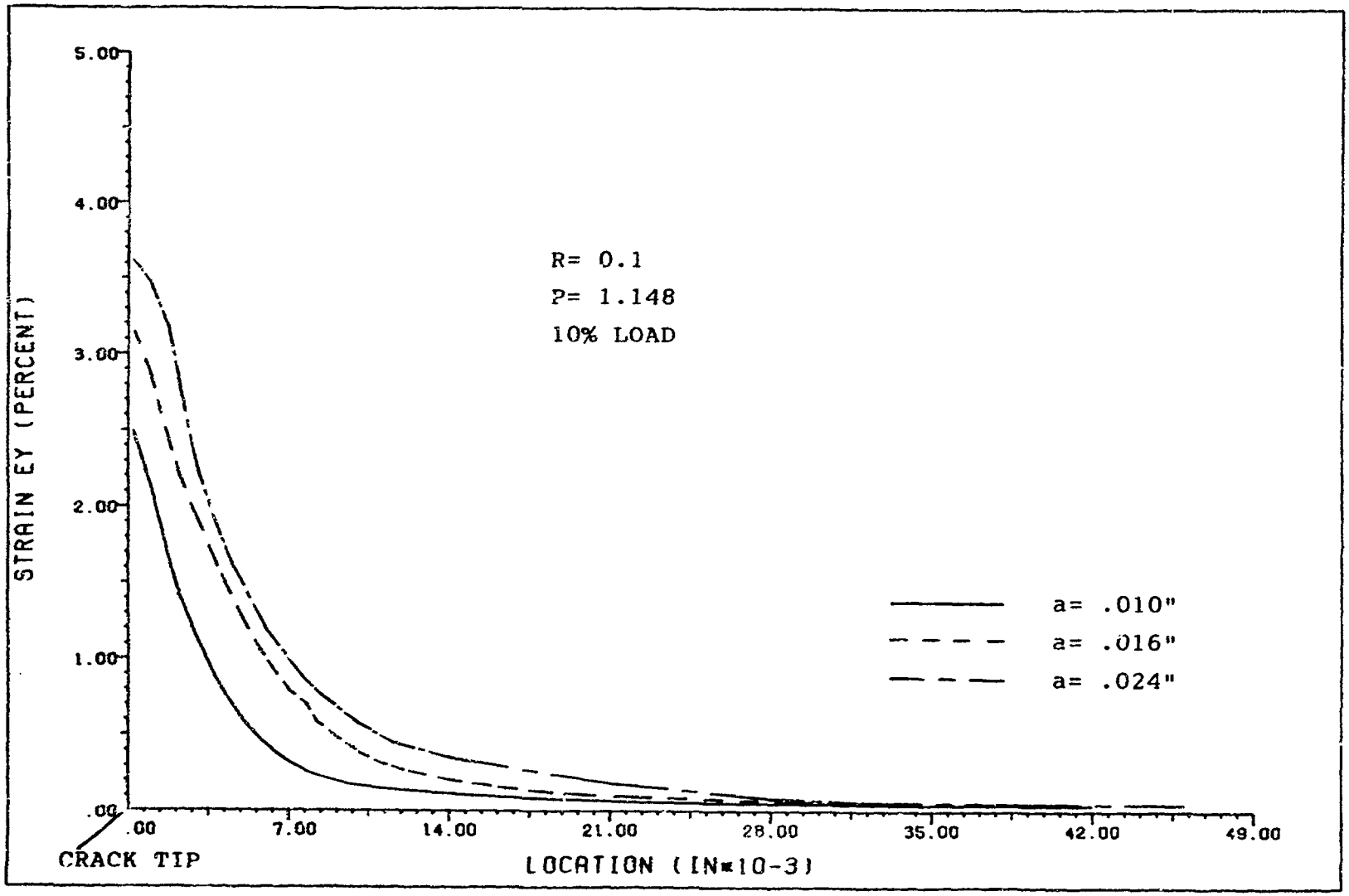

Figure 3.36: Strain Profile Ahead of Crack, P= 1.148 Kips, R= 0.1, 10% Load

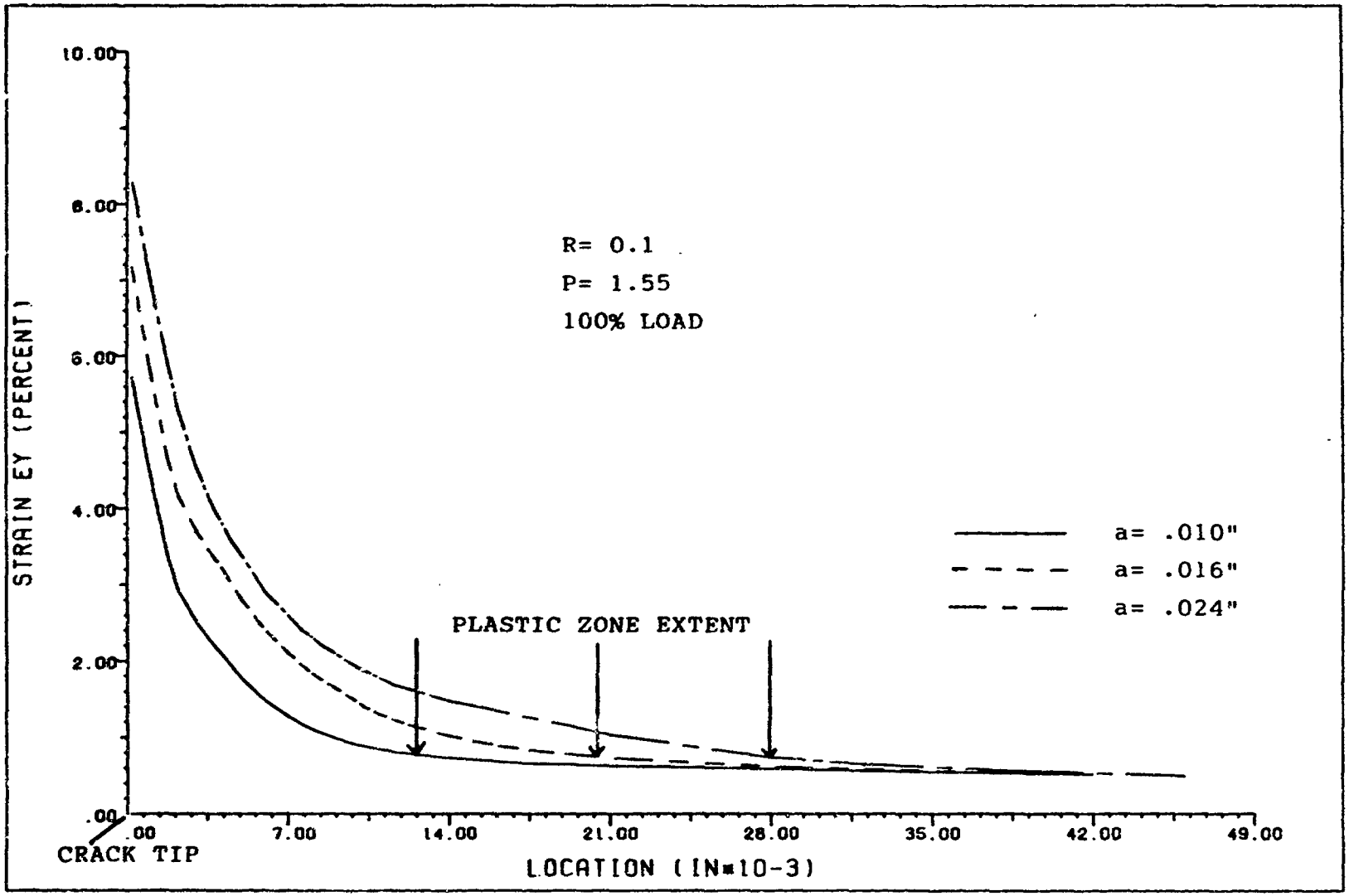

Figure 3.37: Strain Profile Ahead of Crack, P= 1.55 Kips, R= 0.1, 100% Load

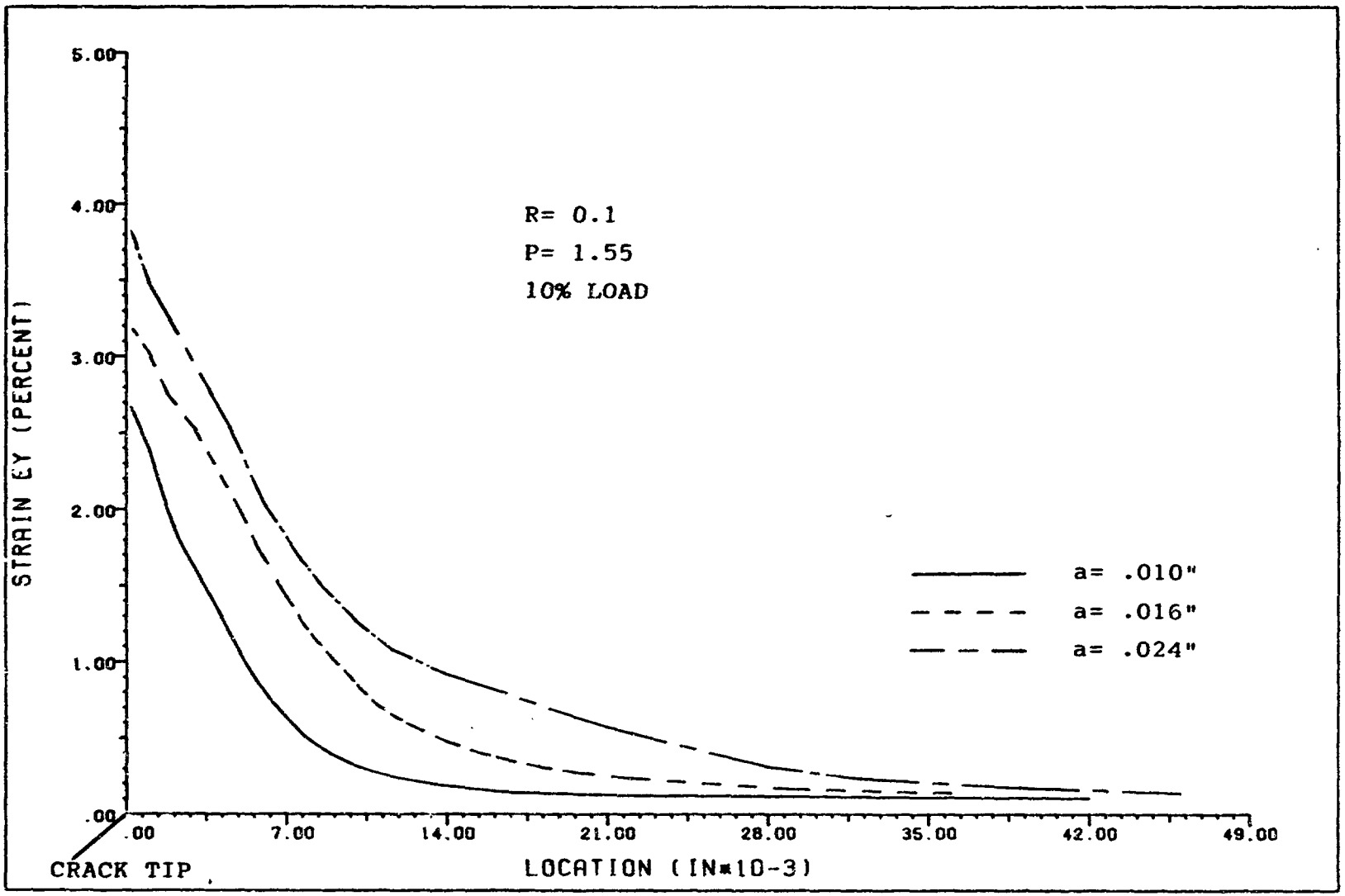

Figure 3.38: Strain Profile Ahead of Crack, P= 1.55 Kips, R= 0.1, 10% Load

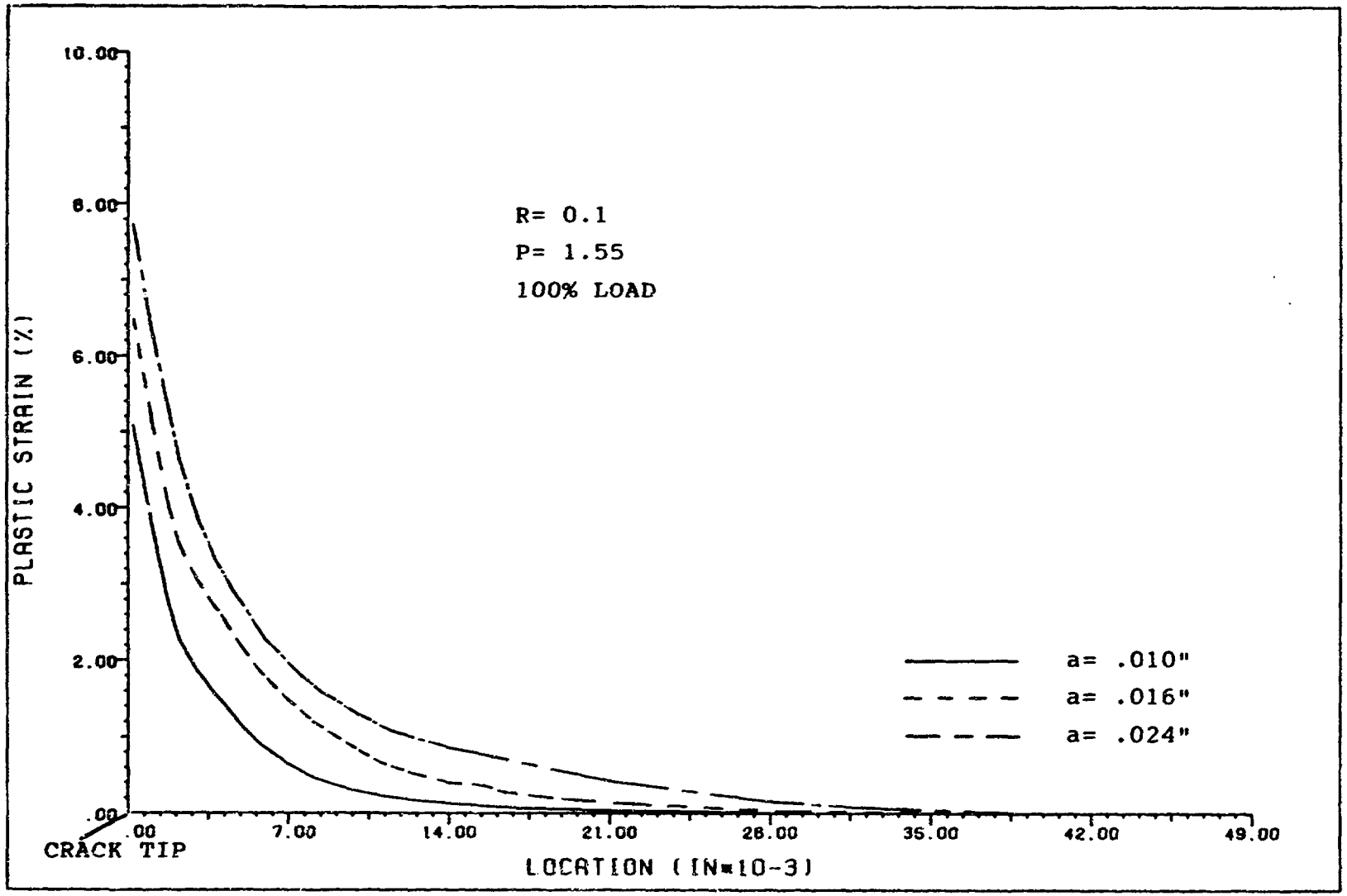

Figure 3.39: Plastic Strain Profile Ahead of Crack, P= 1.55 Kips, R= 0.1, 100% Load

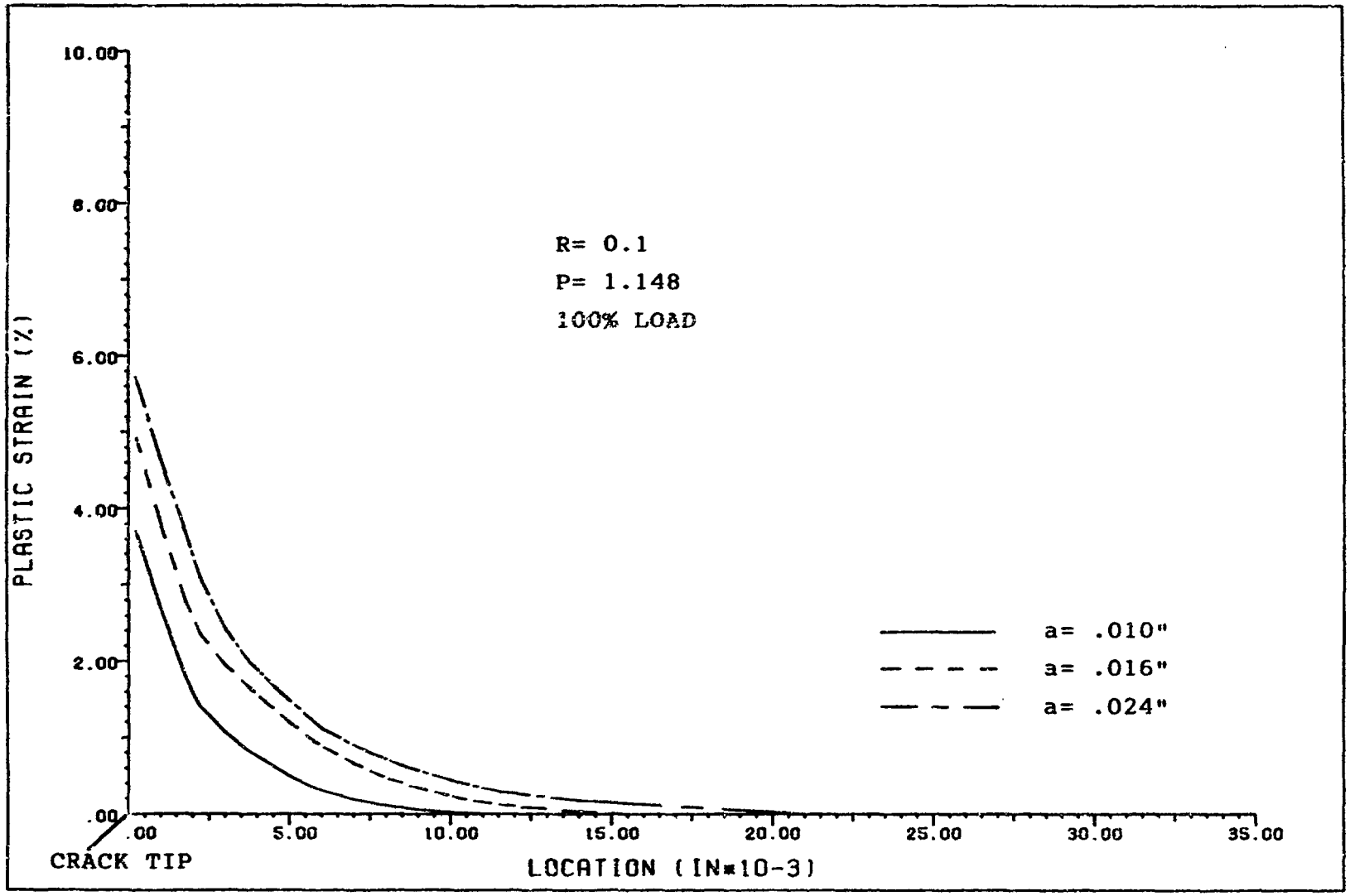

Figure 3.40: Plastic Strain Profile Ahead of Crack, P= 1.148 Kips, R= 0.1, 100% Load

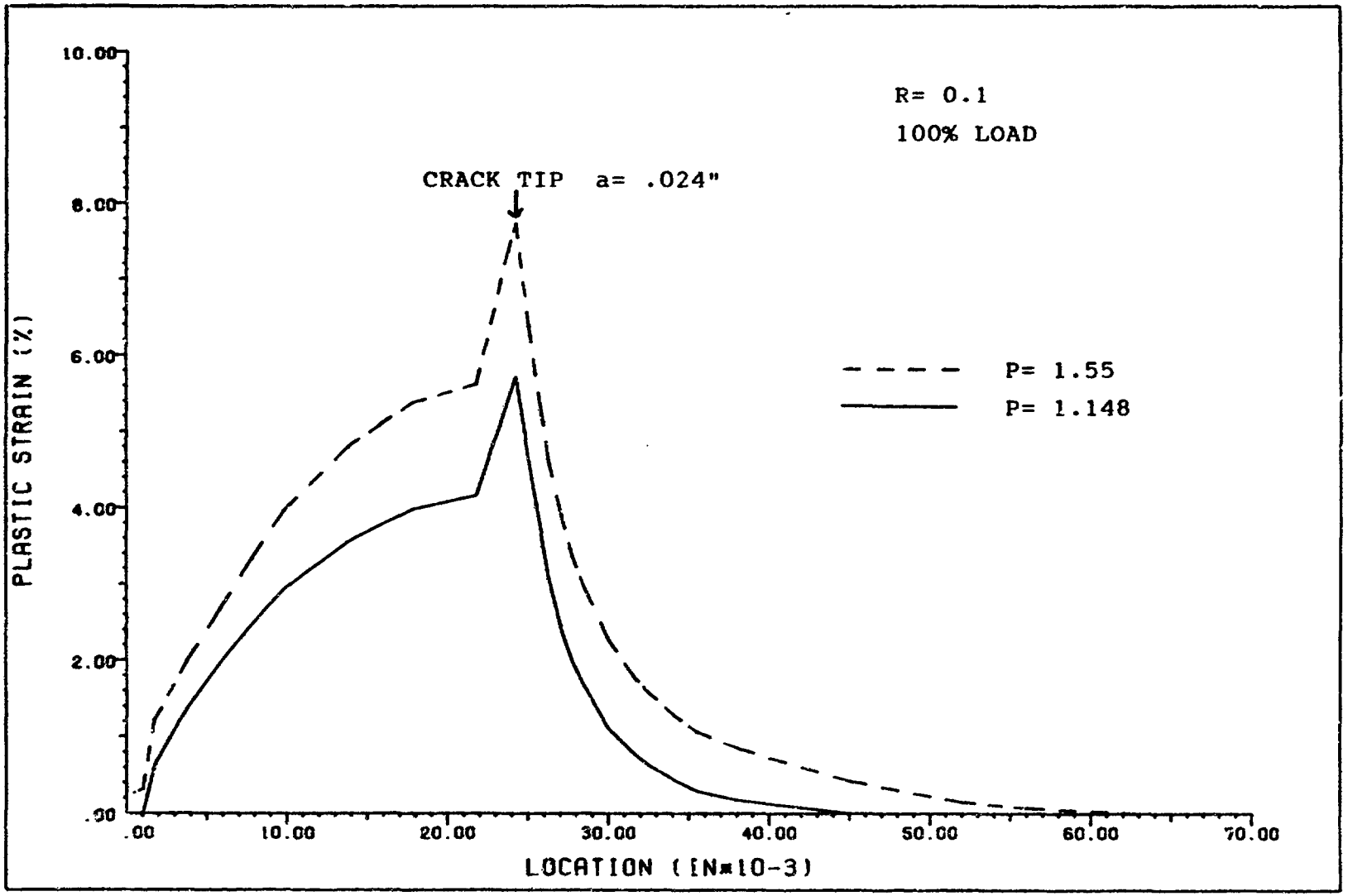

Figure 3.41: Accumulated Plastic Strain, a= .024", P= 1.148 and P= 1.55 Kips, R= 0.1

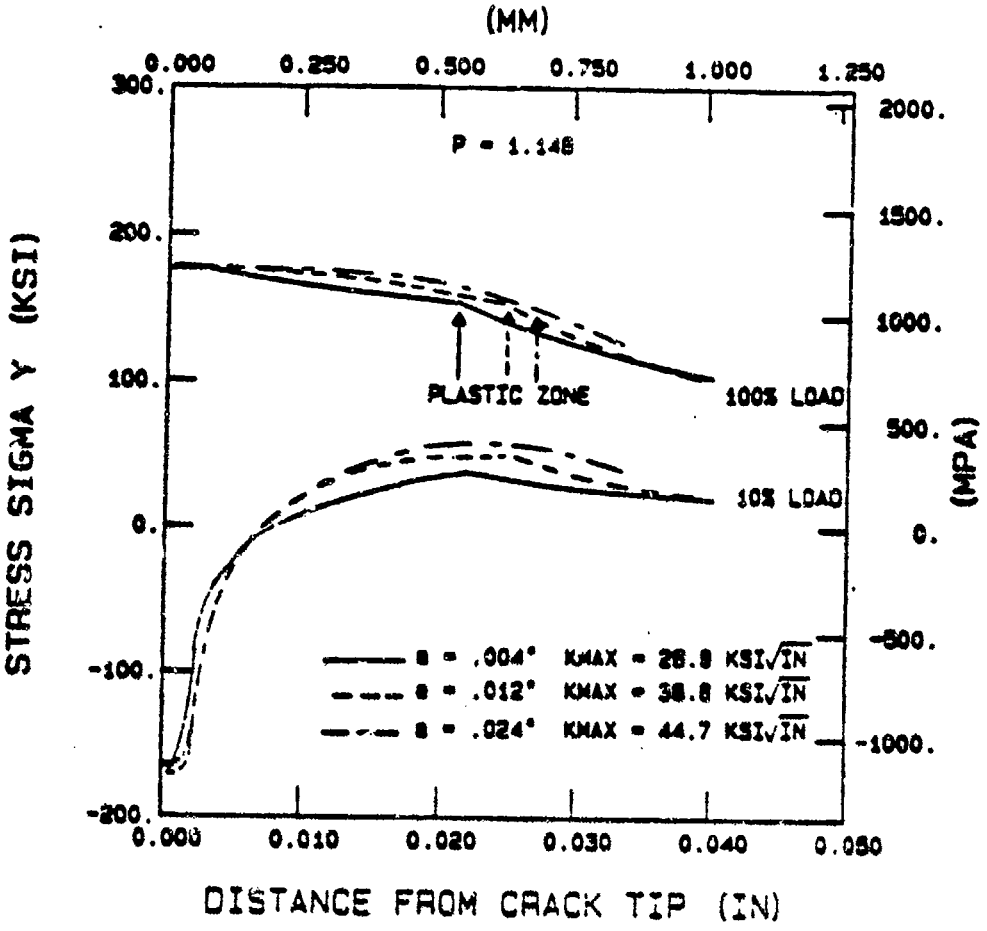

Figure 3.42: Stress Profile Ahead of Crack Tip for Blunt Notch Specimen (Ref. 4)

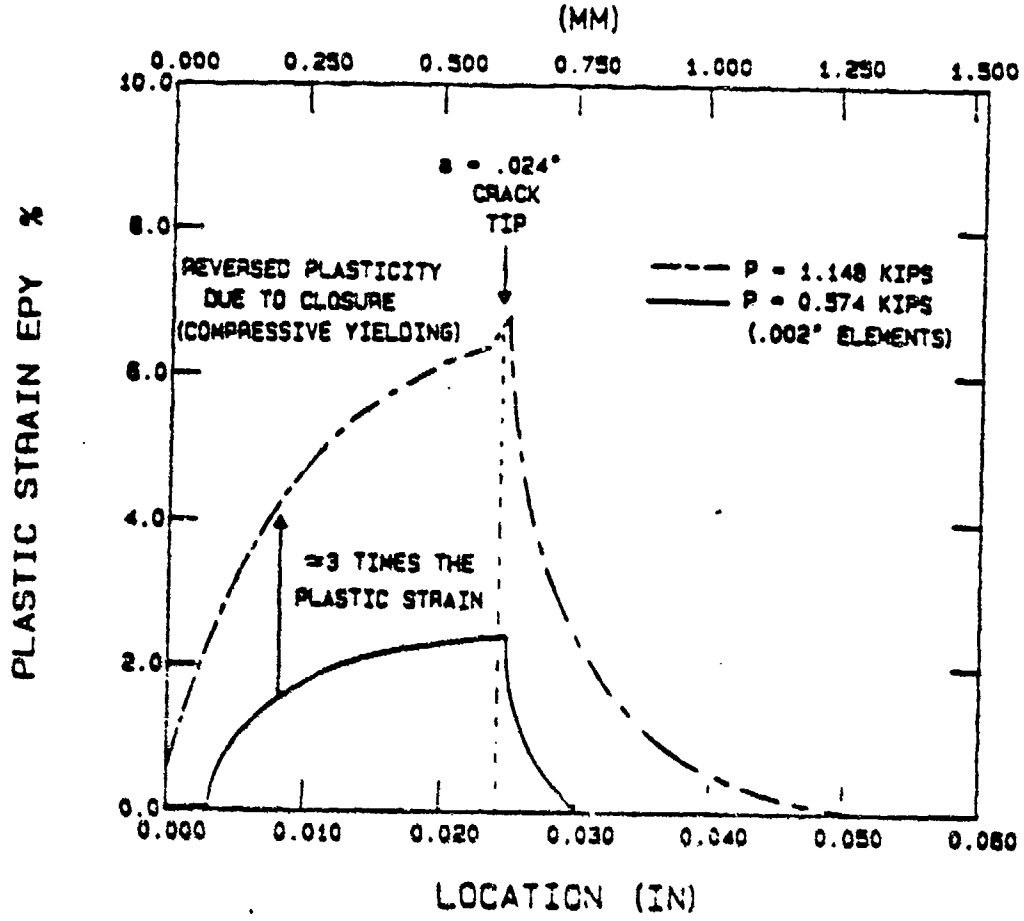

Figure 3.43: Accumulated Plastic Strain for Blunt Notch Specimen (Ref. 4)

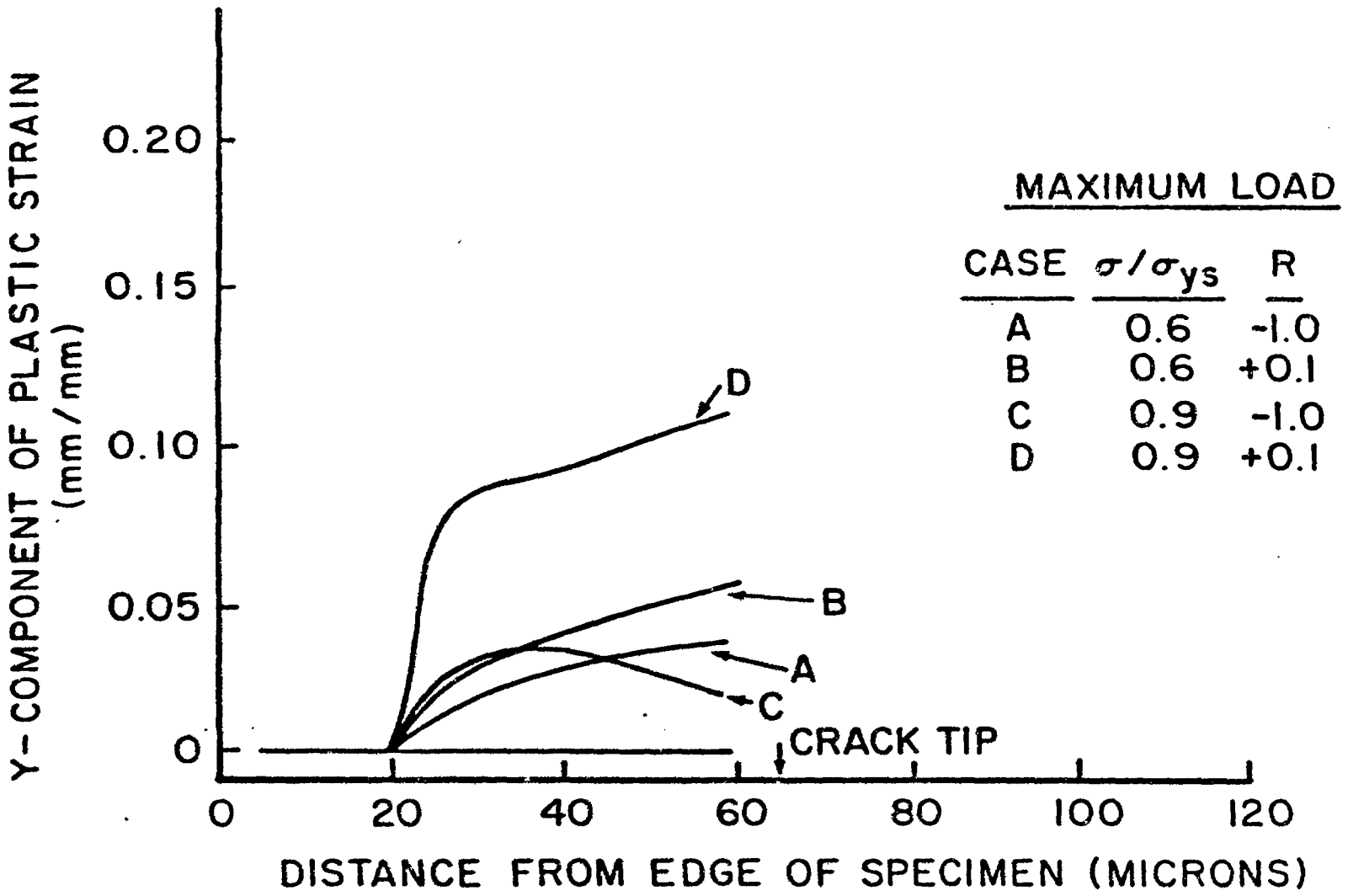

Figure 3.44: Plastic Strains Behind Crack Tip for Single-Edge-Cracked Specimen (Ref. 5)

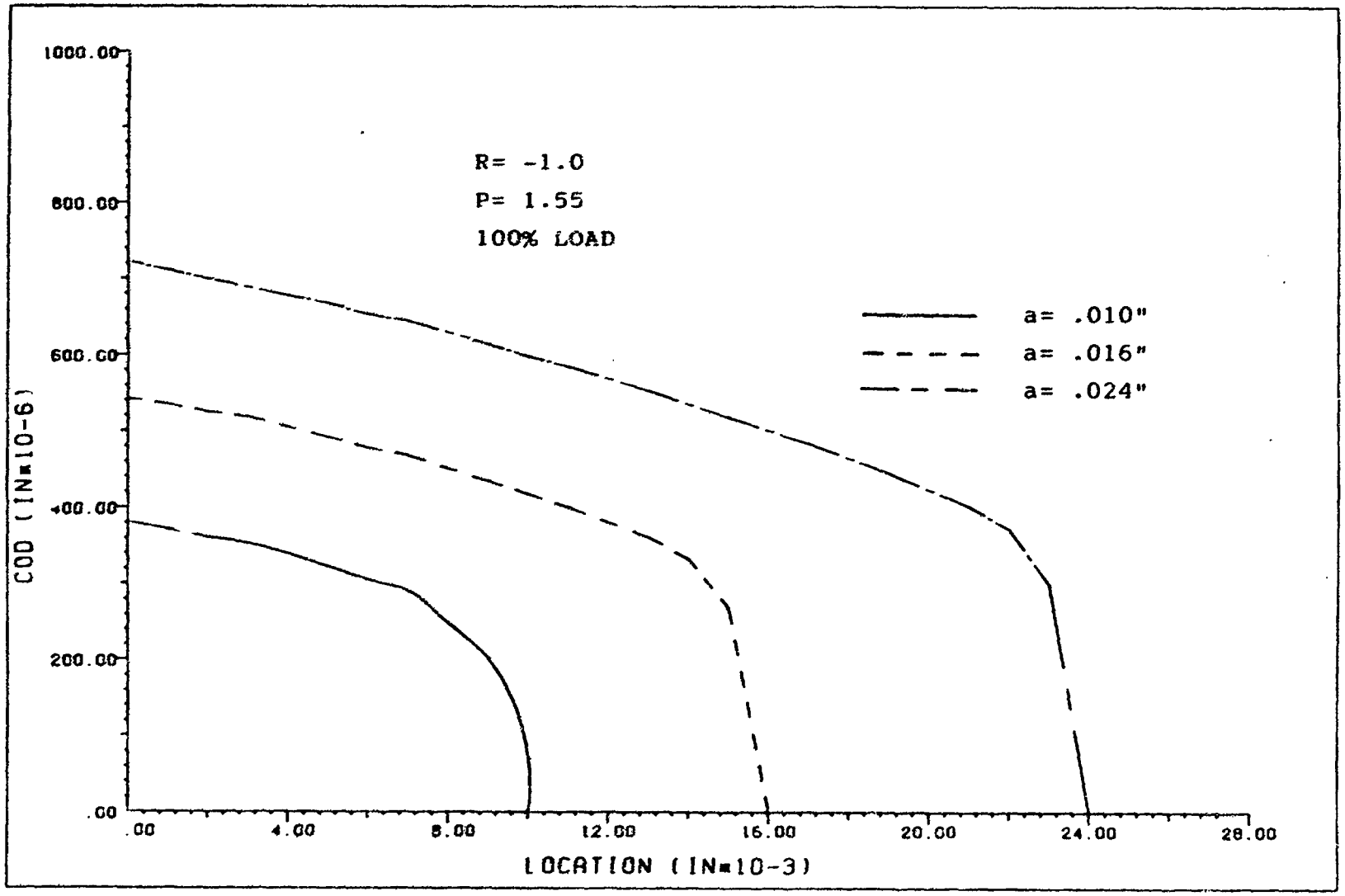

Figure 3.45: Crack Opening Profile, P= 1.55 Kips, R= -1.0, 100% Load

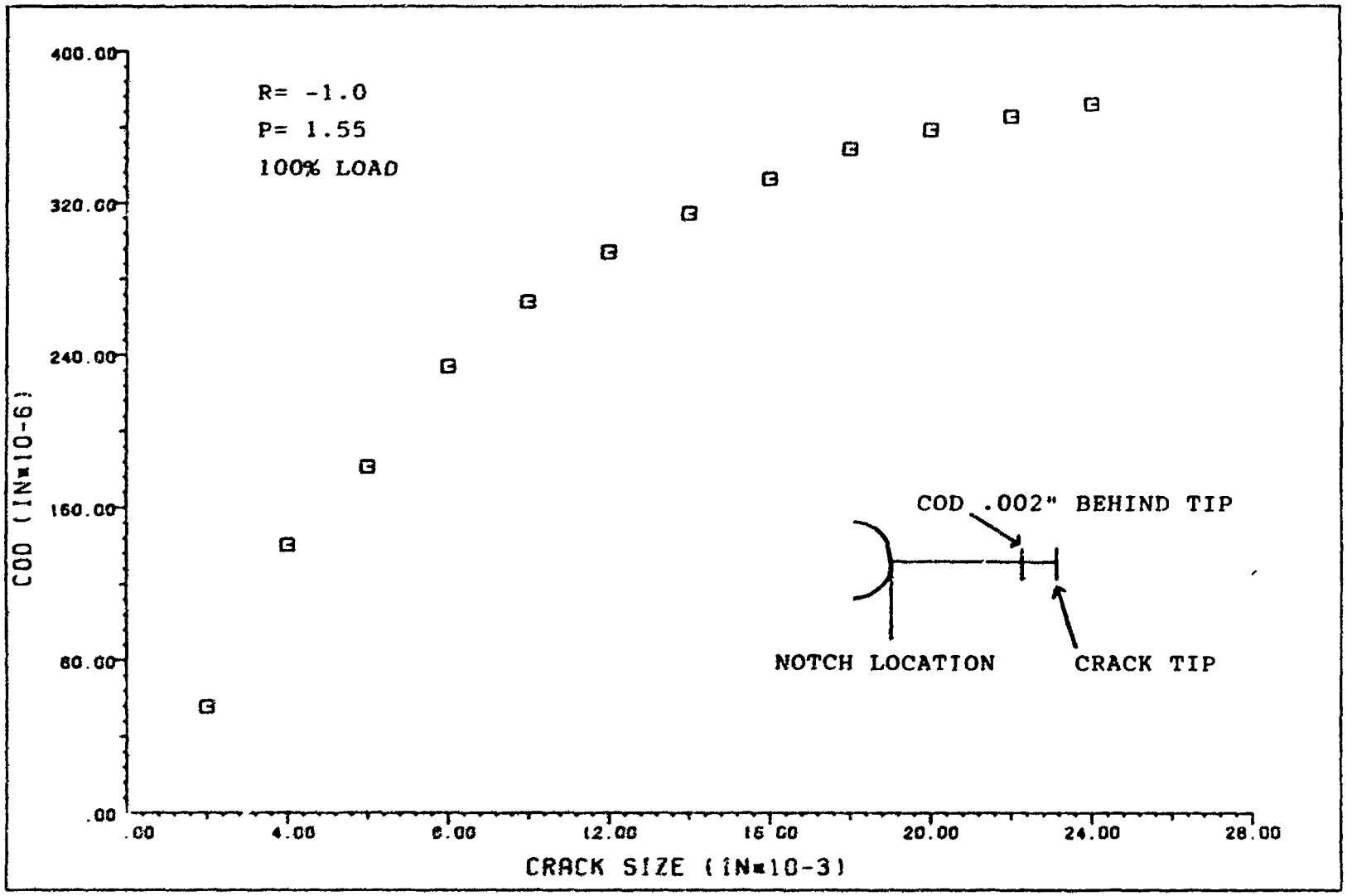

Figure 3.46: Crack Opening Displacement versus Crack Size, P= 1.55 Kips, R= -1.0, 100% Load

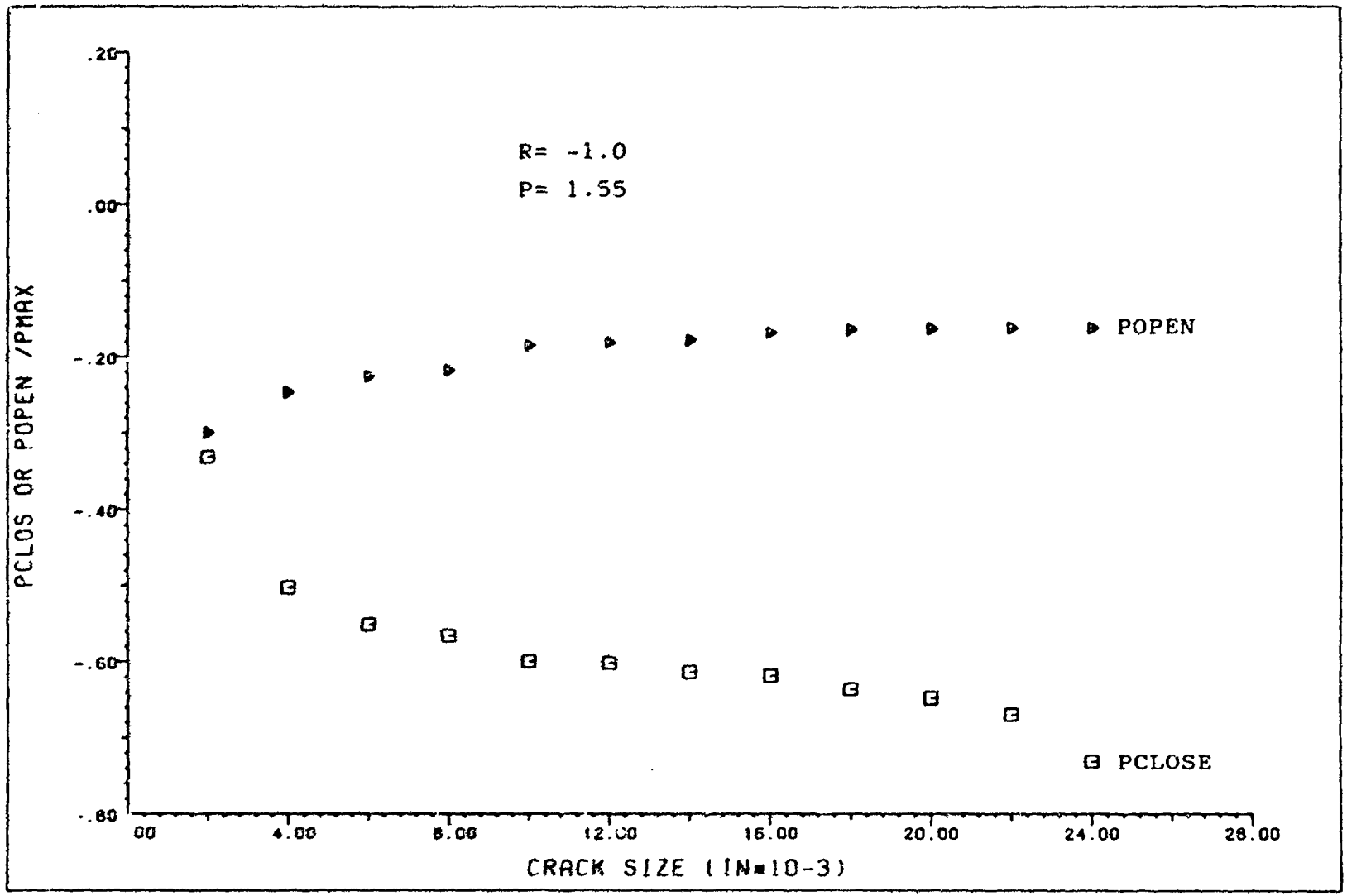

Figure 3.47: Closure and Opening Loads, P= 1.55 Kips, R= -1.0

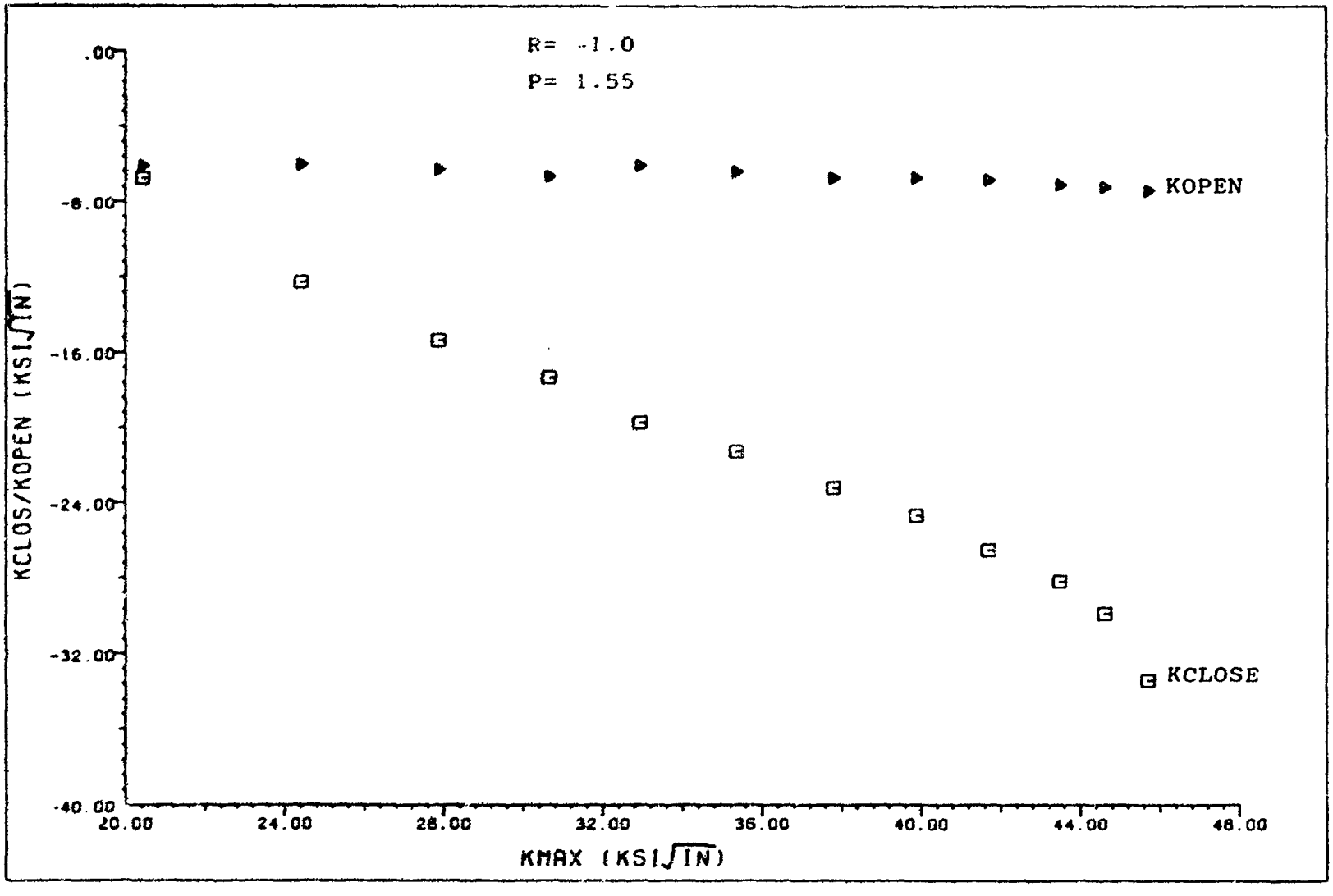

Figure 3.48: Closure and Opening Stress Intensities versus Maximum Stress Intensity for P= 1.55 Kips, R= -1.0

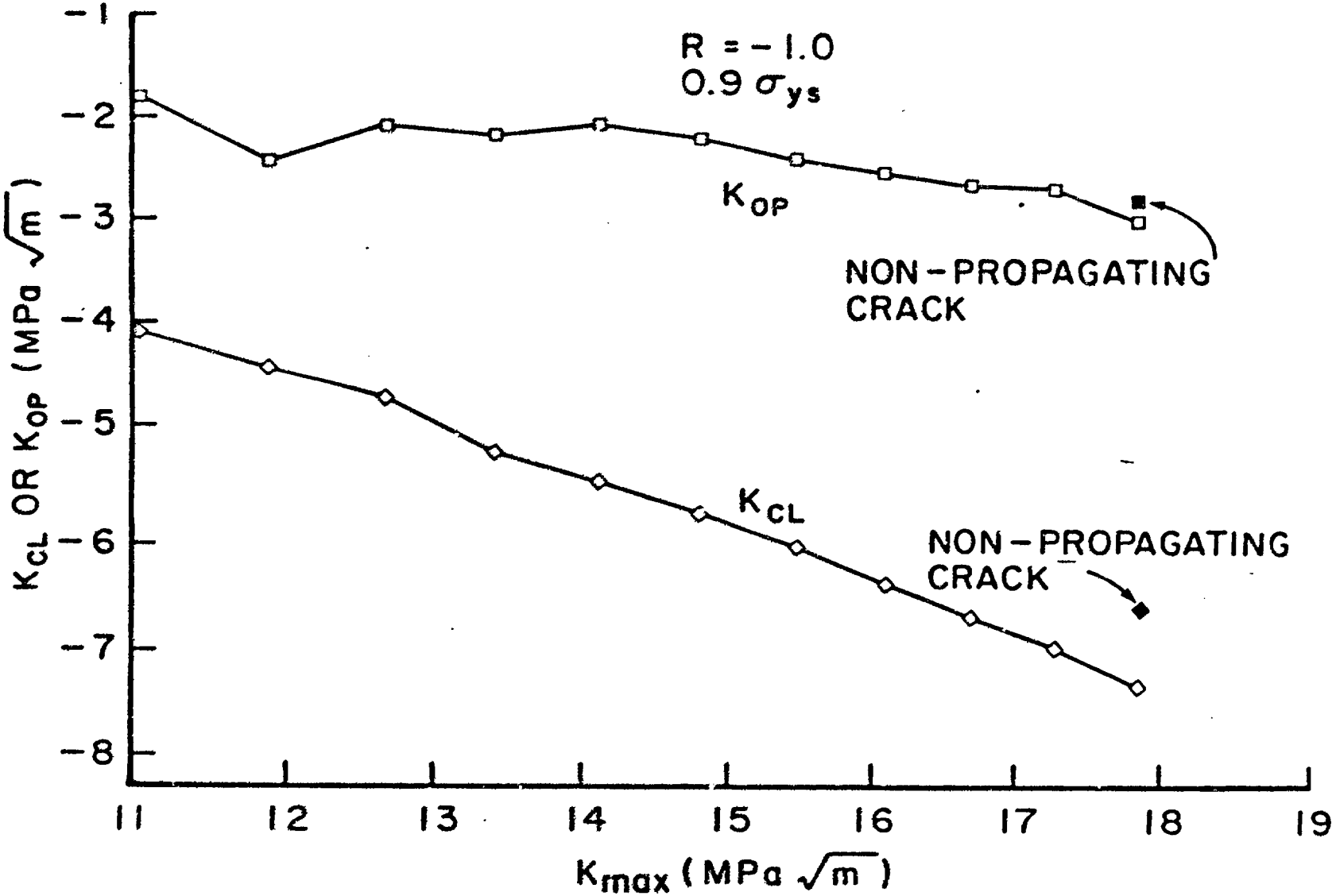

Figure 3.49: Crack Closure Stress Intensities for Single-Edge-Cracked Specimen (Ref. 5), R= -1.0

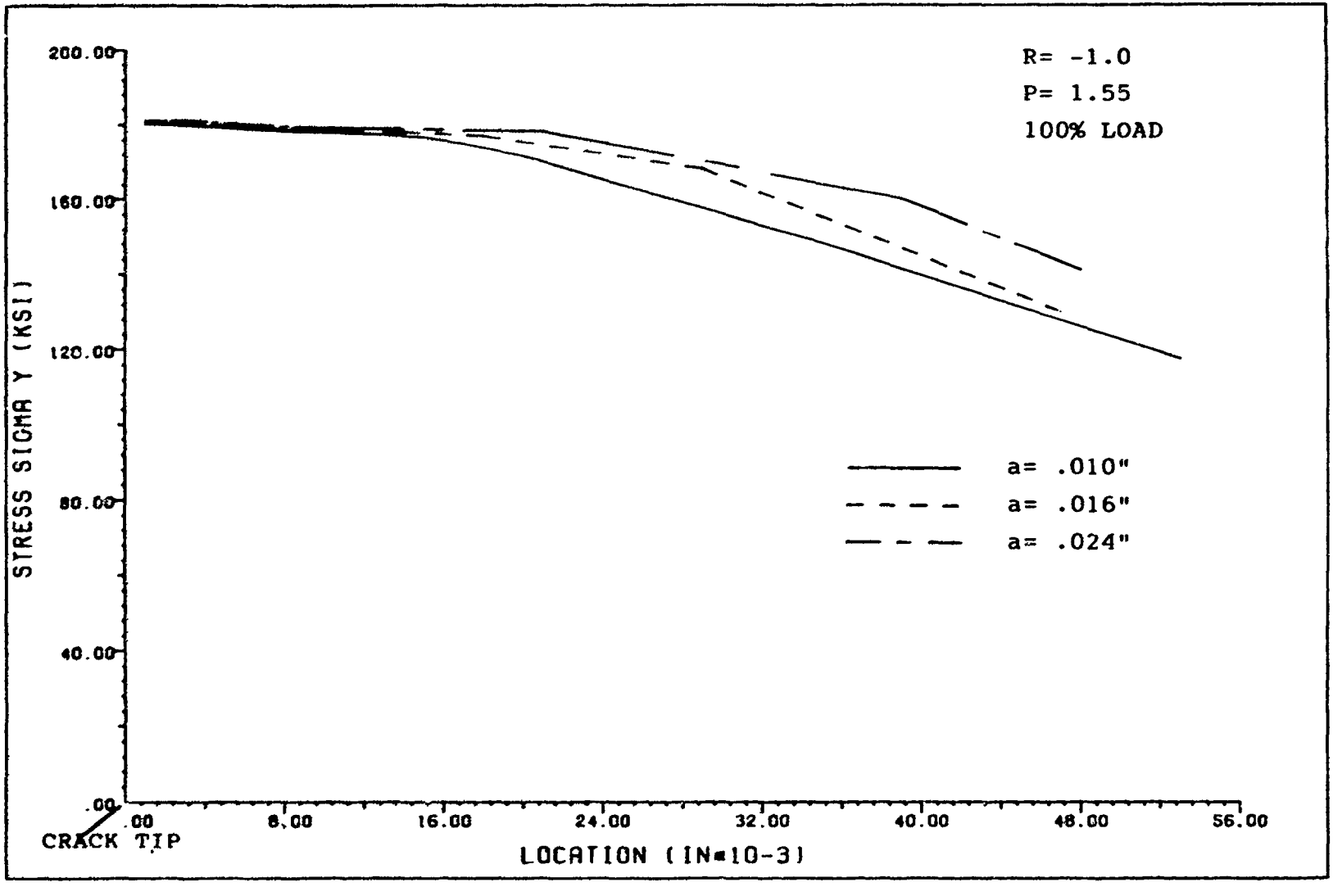

Figure 3.50: Stress Profile Ahead of Crack, P= 1.55 Kips, R= -1.0, 100% Load

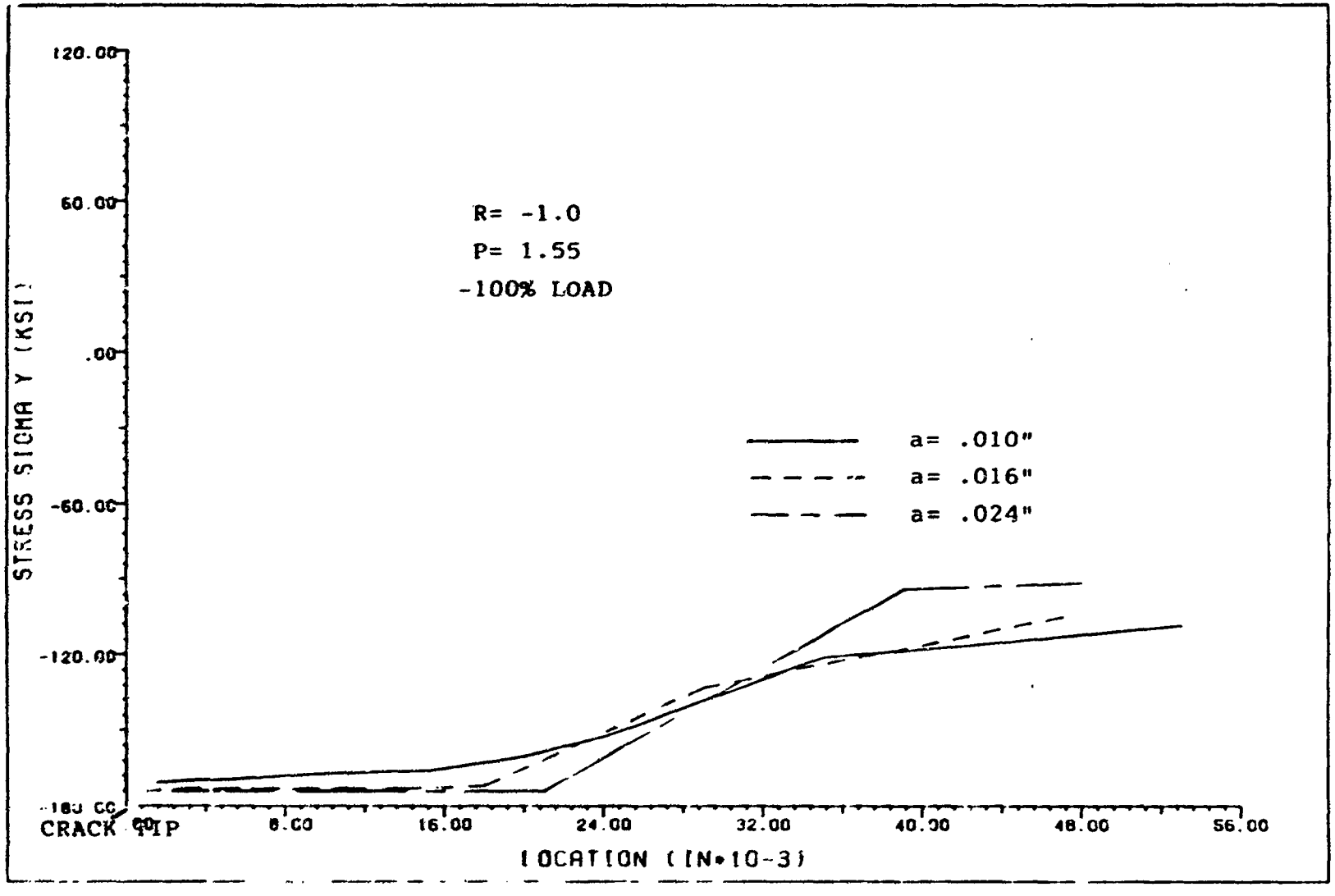

Figure 3.51: Stress Profile Ahead of Crack, P= 1.55 Kips, R= -1.0, -100% Load

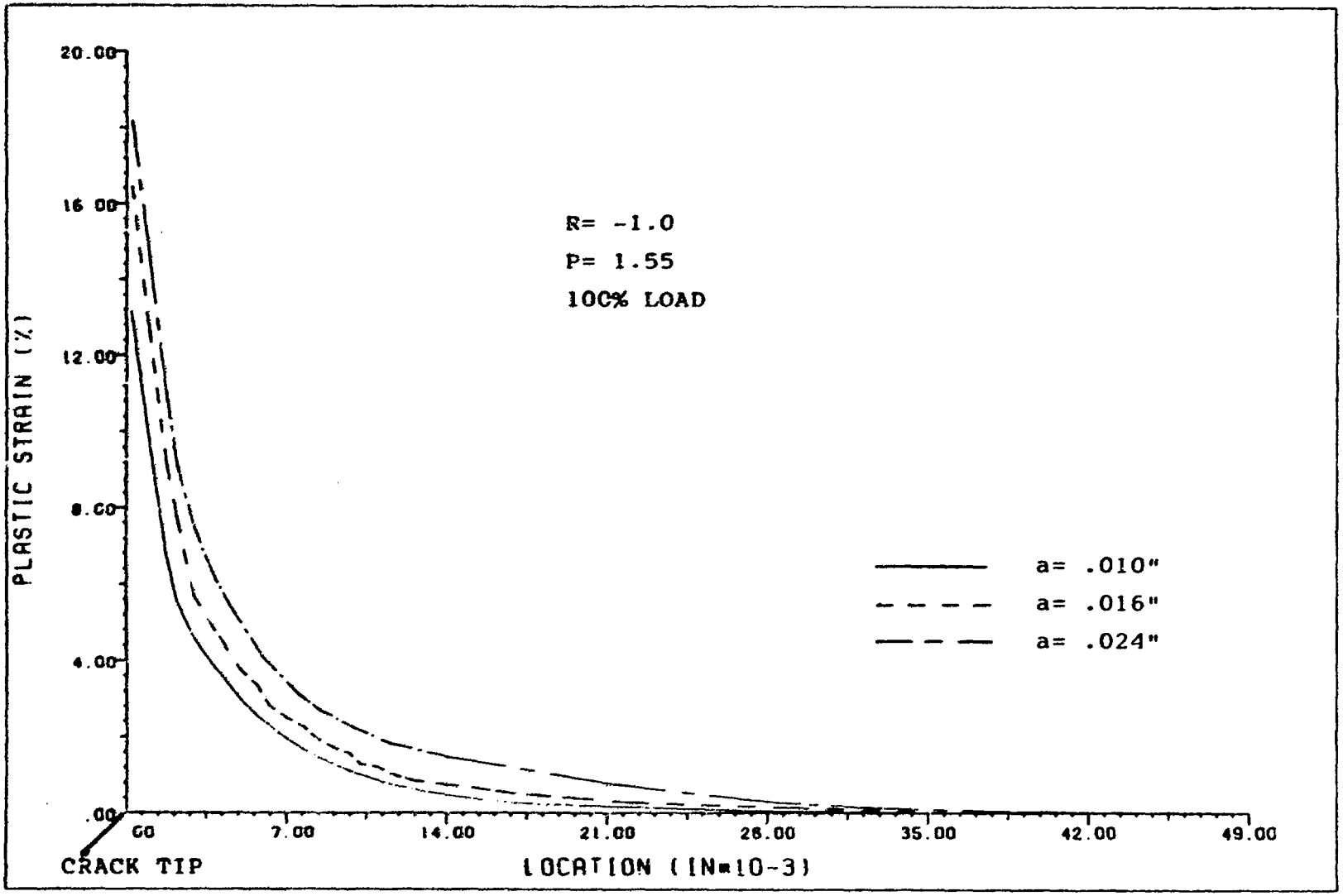

Figure 3.52: Plastic Strain Profile Ahead of Crack Tip, P= 1.55 Kips, R= -1.0, 100% Load

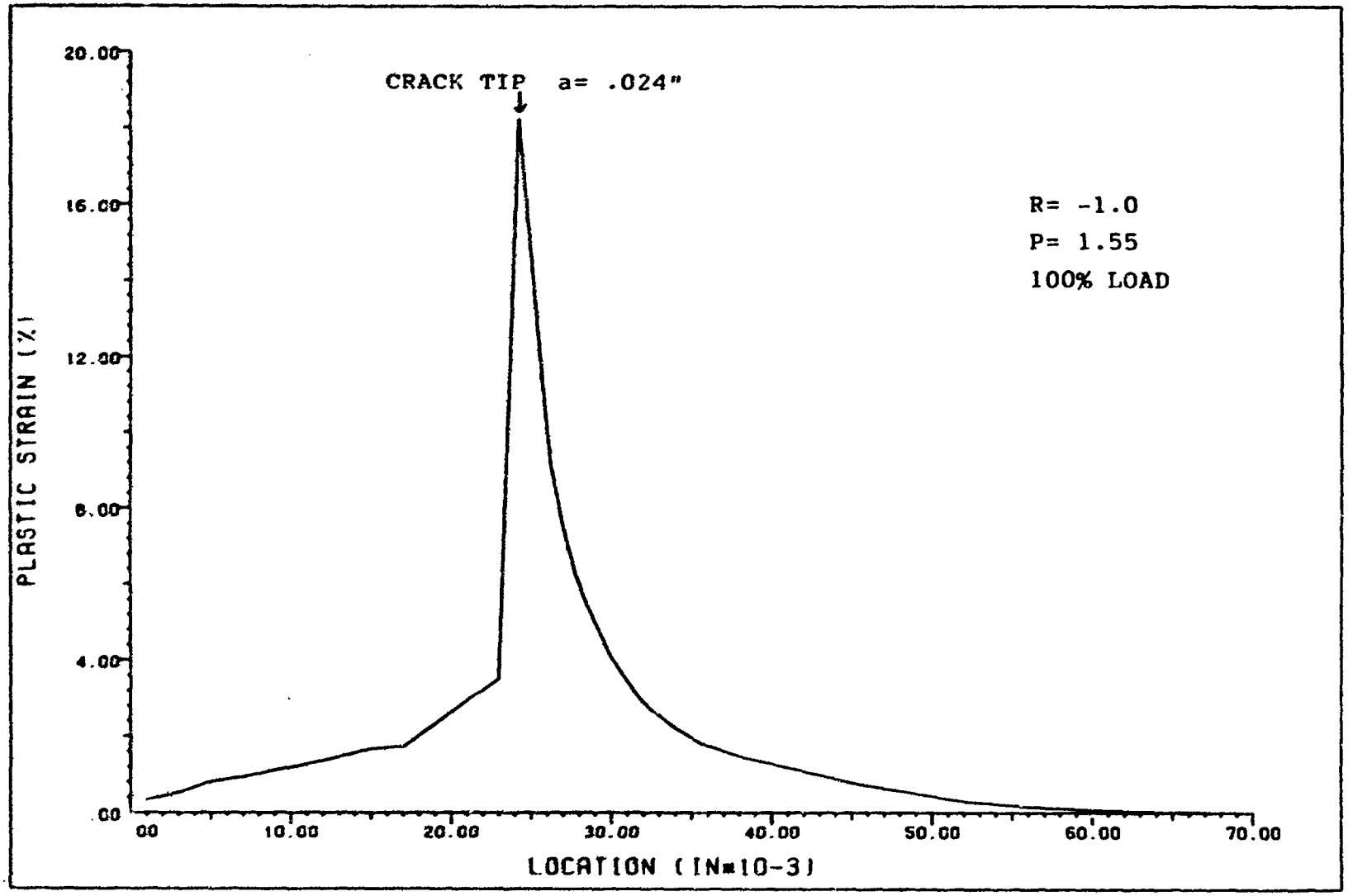

Figure 3.53: Accumulated Plastic Strain, a= .024", P= 1.55 Kips, R= -1.0

IV. Summary and Conclusions

A two-dimensional finite element code called SNAP was used to model crack growth from a round notch compact tension specimen of IN 718 at 1200°. The nonlinear material behavior was modeled using the Bodner-Partom viscoplastic flow law and an implicit scheme was used to integrate these plastic strain relations with respect to time.

The IN 718 specimen was modeled under cyclic conditions at two load levels with a load ratio of 0.1. The specimen was also analyzed under plastic loading with a load ratio of -1.0.

The following statements and conclusions are based on the fatigue analysis presented herein:

1. For cyclic loading frequencies of 1.0 Hz, it was found that the majority of plastic strain at the crack tip is accumulated in the first load cycle.

2. For the round notch specimen, an elastic stress concentration factor of 2.18 was obtained numerically. This result compared favorably to that found by Wilson (24) and was approximately one-half the value found by Mercer (4) for a blunt notch specimen. Thus, the round notch geometry was seen to have lower notch stress values than that of a blunt notch geometry.

3. An elastic stress intensity solution for a crack growing from the round notch was determined using the SNAP finite element model. The round notch stress intensity was

seen to approximate the edge crack solution for short cracks and approach the compact tension specimen solution for long cracks. The notch influence region on the elastic stress intensity was observed to be on the order of one notch radius (approximately 0.2 inches). This phenomenon was also seen by Mercer in his blunt notch work.

4. In general, the crack growth trends (i.e., stress-strain values, crack opening displacements, and opening and closure information) for a crack growing from a round notch agree with those seen in the blunt notch and single-edge-cracked specimens. Thus, we can optimistically state that these trends observed are those typically encountered in short crack studies. This short crack behavior is easily seen from the stress and strain values ahead of the crack tip, where the crack tip plastic zone is approximately the same size as the crack length.

5. For the load ratio case of 0.1, the crack had to grow a significant amount before closure was observed. This "delayed" crack closure is attributed to the round notch geometry condition. For the load ratio case of -1.0, crack closure was immediately encountered. Thus, closure develops quicker for a negative load ratio condition than for a positive load ratio case. This observation was also seen in the single-edge-cracked specimen (5).

It is believed that the round notch fatigue crack results presented herein will add to the body of knowledge

concerning high temperature cyclic crack growth and may provide some insight into the problems associated with fatigue growth of short cracks.

Bibliography

1. Military Standard: Engine Structural Integrity Program (ENSIP), MIL-STD-1783 (USAF), 30 November, 1984.

2. Brockman, Robert A., SNAP: A Simple Nonlinear Analysis Program for Education and Research, University of Dayton Research Institute Report: UDR-TM-82-06, February, 1982.

3. Bodner, S.R., and Partom, Y., "Constitutive Equations for Elastic-Viscoplastic Strain-Hardening Materials," Journal of Applied Mechanics, Vol. 42: 385-389, 1975.

4. Mercer, J.G., "Viscoplastic Analysis of Fatigue Cracks at Notches by the Finite Element Method," PhD Dissertation, AFIT/DS/AA/86-2, Air Force Institute of Technology, Department of Aeronautics and Astronautics, September, 1986.

5. Nicholas, T., Palazotto, A., and Bednarz, E., "An Analytical Investigation of Plasticity Induced Closure Involving Short Cracks," presented at the National Symposium on Fracture Mechanics, Charleston, S.C., June 1986.

6. Leis, B.N., and Forte, T.P., "Fatigue Growth of Initially Physically Short Cracks in Notched Aluminum and Steel Plates," ASTM STP 743, American Society for Testing and Materials, 100-124, 1981.

7. Smith, R.A., and Miller, K.J., "Fatigue Cracks at Notches," International Journal of Mechanical Science, Vol. 19, 11-22, 1977.

8. El Haddad, M.H., Smith, K.N., and Topper, T.H., "Fatigue Crack Propagation of Short Cracks," Journal of Engineering Materials and Technology, Vol. 101, No. 1, 42-46, 1979.

9. El Haddad, M.H., Topper, T.H., and Topper, T.N., "Fatigue Life Predictions of Smooth and Notched Specimens Based on Fracture Mechanics," Journal of Engineering Materials and Technology, Vol. 103, 91-96, 1981.

10. Elber, W., "Fatigue Crack Closure Under Cyclic Tension," Engineering Fracture Mechanics, Vol. 2, 37-45, 1970.

11. Newman, J.C., "A Finite Element Analysis of Fatigue Crack Closure," American Society for Testing and Materials, ASTM STP 590, 281-301, 1976.

12. Hinnerichs, T.D., "Viscoplastic and Creep Crack Growth Analysis by the Finite Element Method," PhD Dissertation, AFIT/DS/AA/80-2, Air Force Institute of Technology, Department of Aeronautics and Astronautics, September, 1980.

13. Broek, D., Elementary Fracture Mechanics, (Third Edition), The Hague: Martinus Nijhoff Publishers, 1983.

14. Fedderson, C.E., "Evaluation and Prediction of the Residual Strength of Center Cracked Tension Panels," ASTM STP 486, 50-78, 1971.

15. "Standard Test Method for Constant-Load-Amplitude Fatigue Crack Growth Rates Above 10^{-8} m/cycle," ASTM Standard E647-83, 1985 Annual Book of ASTM Standards, Volume 3.01, Metals--Mechanical Testing; Elevated and Low-Temperature Tests, American Society for Testing Materials; 739-759, 1985.

16. Smail, J.W., "The Viscoplastic Crack Growth Behavior of a Compact Tension Specimen Using the Bodner-Partom Flow Law," Master's Thesis, AFIT/GAE/AA/81D-28, Air Force Institute of Technology, Department of Aeronautics and Astronautics, December, 1982.

17. Beaman, R., "The Determination of the Bodner Material Coefficients for IN 718 and Their Effects on Cyclic Loading," Master's Thesis, AFIT/GAE/AA/84M-1, Air Force Institute of Technology, March, 1984.

18. Owen, D.R., and Hinton, E., Finite Elements in Plasticity, Pineridge Press, Swansea, U.K., 1980.

19. Newman, J.C., "Finite Element Analysis of Fatigue Crack Propagation--Including the Effects of Crack Closure," PhD Dissertation, Virginia Polytechnic Institute and State University, May, 1974.

20. Rice, J.R., "A Path Independent Integral and the Approximate Analysis of Strain Concentration by Notches and Cracks," Journal of Applied Mechanics, Volume 35: 379-386, 1968.

21. Yamada, Y., et al, "Plastic Stress-Strain Matrix and Its Application for the Solution of Elastic-Plastic Problems by the Finite Element Method," International Journal for Mechanical Structures, Volume 10: 343-354, 1968.

22. Henkel, C.L., "Crack Closure Characteristics Considering Center Cracked and Compact Tension Specimens," Master's Thesis, AFIT/GAE/AA/84D-9, Air Force Institute of Technology, Department of Aeronautics and Astronautics, December, 1984.

23. Wilson, R.E., "The High Temperature Viscoplastic Fatigue Behavior of IN 100 Using the Bodner-Partom Flow Law," Master's Thesis, AFIT/GAE/AA/83S-6, Air Force Institute of Technology, Department of Aeronautics and Astronautics, September, 1983.

24. Wilson, W.K., "Elastic-Plastic Analysis of Blunt Notched CT Specimens and Applications," Journal of Pressure Vessel Technology, Transactions of the ASME: 293-298, November, 1974.

VITA

Gary L. Chestnut was born on 19 August 1958 in Wilmington, North Carolina. He graduated from New Hanover High School in 1976. He attended the University of North Carolina at Charlotte, where he received his B.S. in Engineering Science, Mechanics, and Materials in 1982 and was commissioned as a second lieutenant in the United States Air Force. He then served as a mechanical engineer at the Harry G. Armstrong Aerospace Medical Research Laboratory (AAMRL) at Wright-Patte son Air Force Base. While at AAMRL, he completed a majority of his M.S. requirements by part-time study. He then entered the School of Engineering, Air Force Institute of Technology, in June 1987.

UNCLASSIFIED

SECURITY CLASSIFICATION OF THIS PAGE

AD-A189 577

REPORT DOCUMENTATION PAGE

Form Approved OMB No. 0704-0188

1a. REPORT SECURITY CLASSIFICATION: UNCLASSIFIED	1b. RESTRICTIVE MARKINGS: None
2a. SECURITY CLASSIFICATION AUTHORITY	3. DISTRIBUTION/AVAILABILITY OF REPORT: Approved for public release; Distribution unlimited
2b. DECLASSIFICATION/DOWNGRADING SCHEDULE	
4. PERFORMING ORGANIZATION REPORT NUMBER(S): AFIT/GAE/AA/87D-3	5. MONITORING ORGANIZATION REPORT NUMBER(S)
6a. NAME OF PERFORMING ORGANIZATION: School of Engineering; 6b. OFFICE SYMBOL (If applicable): AFIT/ENY	7a. NAME OF MONITORING ORGANIZATION
6c. ADDRESS (City, State, and ZIP Code): Air Force Institute of Technology, Wright-Patterson AFB OH 45433-6583	7b. ADDRESS (City, State, and ZIP Code)
8a. NAME OF FUNDING/SPONSORING ORGANIZATION: Air Force Wright Aero Lab; 8b. OFFICE SYMBOL (If applicable): MLLN	9. PROCUREMENT INSTRUMENT IDENTIFICATION NUMBER
8c. ADDRESS (City, State, and ZIP Code): AFWAL/MLLN, Wright-Patterson AFB OH 45433-6583	10. SOURCE OF FUNDING NUMBERS: PROGRAM ELEMENT NO. / PROJECT NO. / TASK NO / WORK UNIT ACCESSION NO.

11. TITLE (Include Security Classification): See box 19

12. PERSONAL AUTHOR(S): Gary L. Chestnut, Capt, USAF

13a. TYPE OF REPORT	13b. TIME COVERED	14. DATE OF REPORT (Year, Month, Day)	15. PAGE COUNT
MS Thesis	FROM _____ TO _____	1987 December	105

16. SUPPLEMENTARY NOTATION

17. COSATI CODES			18. SUBJECT TERMS (Continue on reverse if necessary and identify by block number)
FIELD	GROUP	SUB-GROUP	
20	11		Crack Growth, Finite Elements, Viscoplasticity, Cracks at Notches
12	01		

19. ABSTRACT (Continue on reverse if necessary and identify by block number)

TITLE: CYCLIC CRACK GROWTH EMANATING AT A ROUND NOTCH CONSIDERING VISCOPLASTICITY

Thesis Chairman: Dr Anthony N. Palazotto
Professor of Aeronautics and Astronautics

Approved for public release: IAW AFR 190-1.
LYNN E. WOLAVER 31 Dec 87
Dean for Research and Professional Development
Air Force Institute of Technology (AU)
Wright-Patterson AFB OH 45433

20 DISTRIBUTION/AVAILABILITY OF ABSTRACT	21. ABSTRACT SECURITY CLASSIFICATION
☒ UNCLASSIFIED/UNLIMITED ☐ SAME AS RPT ☐ DTIC USERS	UNCLASSIFIED

22a NAME OF RESPONSIBLE INDIVIDUAL	22b. TELEPHONE (Include Area Code)	22c OFFICE SYMBOL
Dr A Palazotto, Professor	513-255-2998	AFIT/ENY

DD Form 1473, JUN 86 — Previous editions are obsolete. — SECURITY CLASSIFICATION OF THIS PAGE: UNCLASSIFIED

Box 19:

A finite element investigation was conducted to analyze a crack growing from a round (large radius) notch under cyclic conditions at 1200° F. The results of the finite element analysis were compared to previously published results obtained for a crack emanating from a blunt notch and a single-edge-cracked specimen.

The finite element program used was a two-dimensional materially and geometrically nonlinear finite element code called SNAP. The program has the capability to release fixed nodes to allow crack growth and the ability to simulate crack closure under cyclic conditions. Constitutive equations set forth by Bodner and Partom were used to account for the nonlinear, viscoplastic material behavior exhibited by IN-718 at 1200° F. The load spectrum included loading under a positive load ratio (R= 0.1) and loading under a negative load ratio (R= -1.0).

Finite element analysis of a crack growing from a round notch under cyclic loading provided crack opening profile information, opening and closing loads, stress and strain profiles and plastic zone estimations.

Crack closure was seen to develop over a longer distance for the round notch than that for a blunt notch. The elastic stress intensity influence on the round notch was found to be within one radius of the notch. In general, the crack growth trends observed for the round notch are similar to those seen in the blunt notch and single-edge-cracked studies.